



CLASSIFICATION:

Open

**OSLO METROPOLITAN UNIVERSITY**  
STORBYUNIVERSITETET

**Department of Civil Engineering and Energy Technology – Energy and Environment**

*Postal address:* P.O.box 4 St. Olavs plass, N-0130 Oslo, Norway

*Visiting address:* Pilestredet 35, Oslo

*Website:* [www.oslomet.no](http://www.oslomet.no)

# MASTER'S THESIS

TITLE:  <b>Transient flow analysis of opening hinged/sliding door.</b>	SUBMISSION DATE:
	NO OF PAGES & APPENDICES:
AUTHORS:  Øystein Formo Hermansen	SUPERVISOR:  Arnab Chaudhuri

DONE IN COLLABORATION WITH:	CONTACT PERSON:
-----------------------------	-----------------

ABSTRACT:

In this work numerical simulations are performed with the CFD tool STAR CCM+ to solve coupled mass, momentum and energy transport equations. The overset mesh was used for moving rigid boundaries and two-equation turbulence models towards understanding the effects of door opening speed and time, thermal effects, and turbulence models. Simulations were run for three different types of doors: a hinged door, a sliding door and an elevator door. The effect of temperature difference and door opening time was also investigated.

KEYWORDS (one per line):

Turbulence  
CFD  
Door-motion



## **Preface**

This master thesis represents the end of the degree "Energi og miljø i bygg – sivilingeniør" at Oslo Metropolitan university - storbyuniversitet. The work for this thesis has been done in the spring of 2021.

First of all I have to thank my supervisor Arnab Chaudhuri. Without your effort this would not have been possible. We have had regular meetings from the start, and you have helped me and guided me through the process. You have taught me a lot about fluid mechanics and you have always been patient and motivating. I will always be grateful.

My family and closest friends also need a thank you for motivating me through this process.

This semester has provided a lot of challenges but I have also learned a lot and really challenged myself. I come out on the other side a more competent and more confident engineer.

## Summary

Most people spend the majority of a day indoors where temperature and air quality have a big impact on their work performance, comfort and health. To be able to control the spread of diseases in indoor environments it is crucial to understand the indoor air flows. An important part of this is to look at the different factors which effects the way the air moves. Understanding of air flow and mass exchange by the opening of a door is beneficial for estimation of pollutant transport and this makes us able to better predict and control desired indoor environment. In this thesis Numerical simulations were performed to solve coupled of mass, momentum and energy transport equations. The focus of this work was the usage of the overset mesh for moving rigid boundaries and two-equation turbulence models towards understanding the effects of door opening speed and time, thermal effects, and turbulence models. This work is also very relevant to the present pandemic situation. The simulations involve three different types of doors. One hinged, one sliding and one elevator door. In addition to the different door types, it has also been performed simulations with different opening times and thermal effect. Besides how the door moves the geometry and boundary conditions are the same for each case. To track the air exchange between the two rooms sulfur hexafluoride (SF<sub>6</sub>) tracer gas was used.

To verify the CFD methods used in the thesis a test case that is similar in both physics and geometry to the simulations previously reported by the other researchers in the literature have been reproduced. When reviewing the flow field and the velocity It is evident from the comparison that the solutions from the reproduced model agree well with the literature. The comparison of the opening and closing door motions times for the hinged and the sliding door shows that the total time of the motion affects the airflow. Lower opening time creates a higher velocity and more exchange between the two rooms.

For the non-thermal simulations visual comparison was done by monitoring the mass fraction of SF<sub>6</sub> in a scalar scene and the velocity with the use of the Line Integral Convolution (LIC) in the vector scene. The results clearly shows that the hinged door creates most exchange of air and creates the most velocity in the airflow. The sliding door and the elevator door has less effect. The cumulative mass of SF<sub>6</sub> exchanged through the door opening was also monitored and showed that the hinged door has the biggest impact. Time snaps at different timesteps of velocity and mass flux shows the same trend with the biggest effect from the hinged door.

For the thermal cases is also shown that the hinged door creates most exchange of air and creates the most velocity in the airflow. Still the sliding door and the elevator door seems to be most affected by the temperature. Meaning that these cases show a clearer difference compared to the non- thermal case. The cumulative mass of SF<sub>6</sub> exchanged through the door opening is also closer to hinged door. The time snaps at different timesteps shows the same trend with the most change in velocity and mass flux for the elevator and the sliding door. The hinged door is also seen the dominant force for the thermal case but it is seen clearly that the temperature difference effects the airflow.

It can be concluded that STAR CMM+ is a powerful tool and that the overset mesh works well for the purpose of simulating solid movements. Using the overset mesh is a demanding process in the start-up phase, but this type of CFD simulations provide valuable information for estimation of pollutant transport and prediction of desired indoor environment. The results are also relevant for energy use, the thermal simulations of the cold storage room in particular.

## Summary in Norwegian

De fleste tilbringer mesteparten av dagen innendørs der temperatur og luftkvalitet har stor innvirkning på arbeidsytelse, komfort og helse. For å være i stand til å kontrollere spredning av sykdommer i innemiljøer er det avgjørende å forstå innendørs luftstrømmer. En viktig del av dette er å se på de ulike faktorene som påvirker måten luften beveger seg på. Forståelse av luftstrøm og masseutveksling ved å åpne en dør er gunstig for estimering av luft forurensing og dette gjør oss i stand til bedre å forutsi og kontrollere ønsket innemiljø. I denne oppgaven ble det utført numeriske simuleringer for å løse koblet av ligninger mellom masse, momentum og energitransport. Fokuset for dette arbeidet var bruken av det «overset mesh» for å flytte solide grenser og to-ligningsturbulensmodeller for å bedre kunne forstå effekten av døråpningshastighet og -tid, termiske effekter og turbulensmodeller. Dette arbeidet er også veldig relevant for den nåværende pandemisituasjonen. Simuleringene involverer tre forskjellige typer dører. En hengslet, en glidende og en heisdør. I tillegg til de forskjellige dørtypene er det også utført simuleringer med forskjellige åpningstider og termisk effekt. Foruten hvordan døren beveger seg, er geometrien og grensebetingelsene de samme for hvert tilfelle. For å spore luftutvekslingen mellom de to rommene ble det brukt svovelheksafluorid (SF<sub>6</sub>) som sporgass.

For å verifisere CFD-metodene som ble brukt i oppgaven, er en test simulering som er lik i både fysikk og geometri. Dette blir gjengitt av simuleringene som tidligere er rapportert av de andre forskerne i litteraturen. Når vi gjennomgår strømningsfeltet og hastigheten, fremgår det av sammenligningen at løsningsene fra den gjengitte modellen stemmer godt overens med litteraturen. Sammenligningen av åpning og lukking av bevegelsestider for hengslet og skyvedør viser at den totale bevegelsestiden påvirker luftstrømmen. Lavere åpningstid skaper høyere hastighet og mer utveksling mellom de to rommene.

For de ikke-termiske simuleringene ble visuell sammenligning gjort ved å overvåke massefraksjonen av SF<sub>6</sub> i en skalar scene og hastigheten ved bruk av «Line Integral Convolution (LIC)» i vektorscenen. Resultatene viser tydelig at den hengslede døren skaper mest luftutveksling og skaper mest hastighet i luftstrømmen. Skyvedøren og heisdøren har mindre effekt. Den kumulative massen av SF<sub>6</sub> som ble byttet ut gjennom døråpningen ble også overvåket og viste at den hengslede døren har størst innvirkning. Tidsklipp på forskjellige tidspunkter av hastighet og masseflyt viser den samme trenden med den største effekten fra den hengslede døren.

For de termiske tilfellene er det også vist at den hengslede døren skaper mest luftutveksling og skaper mest hastighet i luftstrømmen. Likevel ser skyvedøren og heisdøren ut til å være mest påvirket av temperaturen. Dette betyr at disse tilfellene viser en klarere forskjell i forhold til ikke-termisk tilfelle. Den kumulative massen av SF<sub>6</sub> som utveksles gjennom døråpningen, er også nærmere hengslet dør. bilder ved forskjellige tidspunkt viser den samme trenden med mest endring i hastighet og massestrøm for heisen og skyvedøren. Den hengslede døren er også sett på som den dominerende kraften for den termiske saken, men det sees tydelig at temperaturforskjellen påvirker luftstrømmen.

Det kan konkluderes med at STAR CMM + er et kraftig verktøy og at «overset mesh» fungerer bra med det formål å simulere solide bevegelser. Å bruke det overskuddsnett er en krevende prosess i oppstartsfasen, men denne typen CFD-simuleringer gir verdifull informasjon for estimering av transport av forurensende stoffer og forutsigelse av ønsket innemiljø. Resultatene er også relevante for energibruk, spesielt de termiske simuleringene av kjølerommet.

# Contents

Preface.....	iii
Summary.....	iv
Summary in Norwegian .....	v
Contents .....	vi
1 Introduction.....	1
1.1 Background.....	1
1.2 Definition of the Problem .....	10
1.3 Aim and objective.....	11
1.4 Research scope and limitation .....	11
1.5 Audience.....	11
2 Methods and Materials .....	12
2.1.1 Governing equations .....	12
2.1.2 RANS (Reynold-averaged Navier-Stokes equations) .....	13
2.2 Method for the simulations.....	19
Volume control.....	26
3 Verification CFD methods.....	40
3.1 Verification case setup .....	40
3.2 Results verification case .....	42
4 Problem setup .....	46
5 Results & Discussion .....	50
5.1 Different door motions.....	50
5.2 Thermal effects.....	64
6 Conclusions.....	84
7 References [17].....	86
Figures .....	89
Appendices .....	94
Appendix A Residuals .....	95

Appendix B Matlab .....	97
Appendix C Hinged 4s temperature .....	101
Appendix D Flux of SF6 non thermal .....	104
Appendix E Thermal flux of SF6 and heat flux.....	106
Appendix F Excel.....	109
Appendix G Running time.....	111

# 1 Introduction

## 1.1 Background

Most people spend the majority of a day indoors where temperature and air quality have a big impact on their work performance, comfort and health. To be able to control the spread of diseases in indoor environments it is crucial to understand the indoor air flows. An important part of this is to look at the different factors which effects the way the air moves. In certain specialist environments, such as hospital isolation rooms and clean rooms, understanding the processes by which pollutants can be transferred is particularly important. To understand the role of airflow exchange between spaces, it is crucial to be able to describe the processes of mixing and transport of substances. This is driven by air motion and this is why it is essential for evaluating indoor air quality.

In healthcare settings isolation rooms are used to contain infectious patients or to protect vulnerable patients from infection. This is an important part of the facility and helps to protect patients and staff against the risk of infection by airborne pathogens. There have been relatively few published studies on the effect door-opening motions have on the integrity of containment in hospital isolation rooms. Even fewer of these include the effects of a healthcare worker moving through the doorway. Tang et al. [1] described a clinical situation where a severe case of adult chickenpox (VZV, infection) was managed in a negative pressure isolation room, with no adjacent anteroom. This caused an infection of a VZV-susceptible nurse whose only contact with the patient was when he stood outside the room. The door to the isolation room was a standard single hinged door that opened into the room. The non-immune nurse developed chickenpox 10 days later. It was confirmed that it was the same virus between the patient and the nurse. The negative pressure difference across the doorway was measured to be only 3 Pa. Each time the door was opened to receive the supplies it was postulated that the pressure was easily reversed. It is clear from this incident that this was an insufficient amount of pressure to maintain the containment during a door-opening motion.

Flow visualization studies were performed to exam the effect the hinged door opening motion had on the airflow across the doorway. Tang, Julian W., et al. [2] make the point that the most important implication from this study is that whatever door design is used, there is likely to be some leakage across the doorway to a lesser or greater degree as a human figure moves through the door at a reasonable walking speed. This is a strong argument that supports the requirement for anterooms for isolation rooms.

Physical isolation of airborne contaminant sources is another strategy that can be considered as very efficient in controlling the diffusion of infections. In some cases, it is still not sufficient to prevent contamination from airborne sources of infection like virus, bacteria and fungal spore. With very small diameters variable in a range between 0.02  $\mu\text{m}$  and 100  $\mu\text{m}$  these types of particles remain suspended in



the air for long periods [3]. Several studies have been conducted aiming to evaluate the performance of pressurization-depressurization areas regarding the maintenance of differential pressure across doors when closed. For example, Rice et al. [4] performed a measurements campaign that lasted two seasons, measuring differential pressure values in 18 different rooms. This included standard rooms, isolation rooms (infectious patients) and protective rooms (patients with low immune defense system). The measurements showed variations especially in protective rooms.

Multiple coupled interactions, involving heat-mass momentum transfer and phase change of constituent components play important roles during the operating condition of a cold storage room in such applications. The key parameters for optimal operation and energy consumption are temperature and moisture control. Among several other factors, infiltration of hot and moist air through open doors become crucial for the infiltration load and the performance of the rooms. It is often a big difference in temperature to the adjacent room, and this increases the effect of the door opening. Therefore, it can be very valuable to be able to reduce the amount of air that is exchanged when the door to the cold room opens. In the past it has been few detailed numerical studies dealing with infiltration via doors in cold storage setups. Ayarmal [5] carried out a numerical study of hot, moist air exchange through a sliding door in a cold storage room. It was observed that, the energy transport and the cooling of the product load was affected by a fan in the room and by the doorway. An analysis with a transient sliding door setup for a scaled room with one cycle of opening and closing was performed. Without the fan, the air exchange appeared almost identical during the opening and closing phase of the sliding door at 55% opening. It was found a lower air exchange rate when a fan was included. In the future it will be interesting to do a more detailed study where more realistic condensation of the moist air will be considered, which includes an intake within the framework of a full scale cold storage room with a transient sliding door.

Relatively few studies have been conducted, that assesses the effect of the door opening and healthcare worker behavior on pressure and airflows regime. In fact, a pressure difference between adjacent rooms can only be obtained if the door separating the rooms is closed and airtight, so that the disequilibrium air flow can produce a large pressure drop while passing through the door. When the door is opened, the pressure loss through the door is weakened, and the previously induced pressure differences are strongly reduced and become negligible. In most cases including mechanical ventilation very small variations of the room pressure, slightly modifies the air flows and their disequilibrium. This makes it possible to ensure an air flow in the wanted direction, but at very low velocities. In these types of conditions, the kinetic energy induced by the door opening can overcome the one of the air flux due to the air flow rates disequilibrium. This can cause the two rooms air mixing which leads to neutralizing the contamination control action. Fontana et al [3] experimentally and quantitatively investigated the door operation effect on air transfer,

and consequent airborne contamination with a two-room scale model. This was also done in the presence of unbalanced supply-extraction flows and consequent differential pressurization, as well as applying a door movement law deducted from full scale experiments. The results confirmed that the door operation is able to produce a dirty air transfer in the clean room. The transferred volume entity was almost independent on the differential pressure and on the flow rate imbalance, at least for the experimentally tested values. It still appeared to be strongly related to the air volume displaced in the door opening operation and had the same order of magnitude of it.

The effect of door motion is not only relevant for special rooms. It is also very relevant in for example educational and office buildings. Wherever there are many people gathered there is important to be able to control and predict the airflow. Both to achieve best possible indoor air quality and to prevent airborne pollution.

Hathway et al [6] performed field measurements and laboratory experiments to characterise door operation and to quantify its influence on air volumes exchanged between rooms due to door motion. The field study was conducted to identify typical total door cycle times in single person offices. The laboratory experiments were conducted in a scale model to investigate the exchange flow between two generic rooms. They found out that with ventilation rates for a medium air quality the risk of infection is low, but the probability of infection quickly rises with lower ventilation rates. It is suggested that there is discrepancy in the literature about the air exchanged across doorways due to the door opening, and the relative importance of door speed and hold open time. Therefore, there is a need to generate more experimental data of door opening and to evaluate the potential risk this poses to infection transfer as much as indoor air quality.

#### 1.1.1 Door opening motion and experimental work

Understanding of air flow, mass exchange by the opening of a door is beneficial for estimation of pollutant transport and this makes us able to better predict and control desired indoor environment. When a hinged door is opened it leads to mass exchange between the two rooms that are separated by the door. The fluid enters as a rotating cloud into the room which the door opens. The rotating cloud spreads around the walls of the room and causes significant mixing of the air in the space. [7] The airflows through the doorway are mainly driven by either pressure gradients across the doorway, or air being dragged in the wake of people or objects moving through the doorway. The pressure gradients are influenced by large scale effects because of temperature differences or ventilation and local influences such as pressure changes when a door is opened and closed.

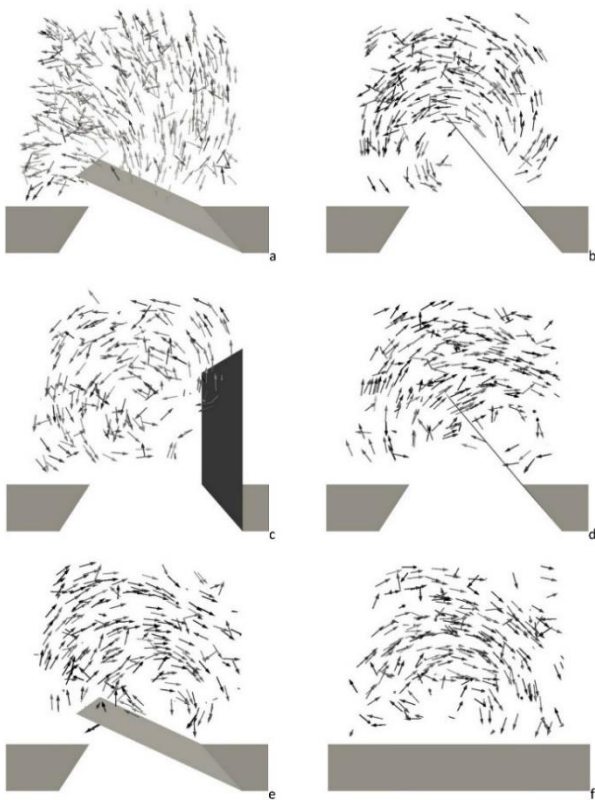


*Figure 1 Effect of opening a hinged door.*

Figure 1 above is taken from the work of Papakonstantis et al. [7] and shows indicative images of the instantaneous velocity fields generated from the door motion in the zone surrounding the region the door moves through. The general flow patterns and the directionality changes of the flow field are also highlighted in the figure. The indoor air flow and mass exchange induced by the rotating motion of a hinged door separating two rooms was investigated. The flow visualizations showed the transport mechanism associated with the opening and closing phases of the door motion. In the room which the door is opened a large-scale vortex is formed during opening, which is advected along the walls. In the adjacent room, a volume of fluid spread both longitudinally and transversely.

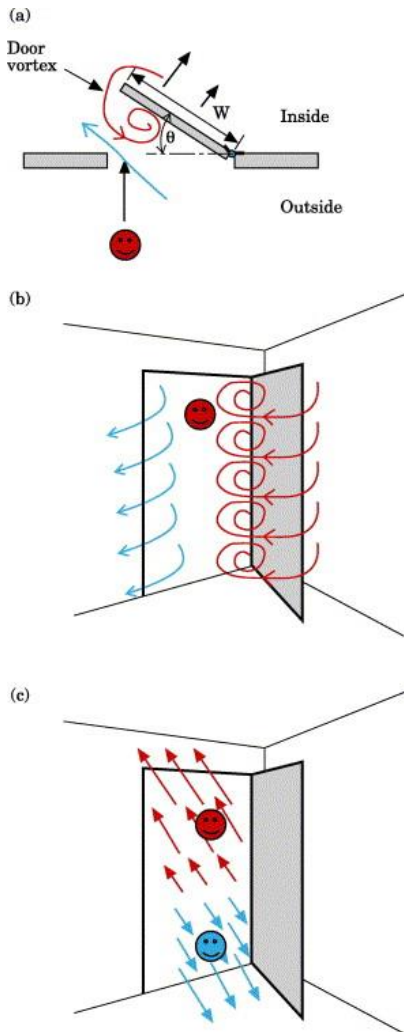


Figure 2 Airflow across an open doorway induced by door opening motion.

Figure 2 is taken from Tang et al. [1] and is another illustration of the effect door opening has on the airflow. It was made after the video footage of the model water tank presented in their study was analysed. The simple water tank and food dye model showed that movement of air from opening the door could have resulted in the exposure of a person standing outside the room. a) and b) show how the predicted airflow currents when a door is opened. An inward air current flowing into the room from outside illustrated by blue, light arrows. The vortices of possibly infected air from inside are illustrated by red, dark arrows and is seen circulating around the open door. This means that a person walking into this area of air circulation would be exposed to and may inhale infectious air emerging from the isolation room even though the person has not entered the room. c) show the same view from inside the room as illustrated in b) but is showing the possible airflow trajectories considering the temperature and density differences between cooler air outside in the corridor and warmer air inside a hypothetical isolation room. It is a simple illustration but gives a good idea of how the door motion effects the air flow.

Several studies show that a door opening motion generates notable air exchange and airborne contaminant transfer across a doorway. This effect is especially notable for a hinged door. [7] [8] Studies also show that the effect is larger when a person is passing through the doorway. [9] Door hold open time and temperature difference also effects the amount of contaminant transfer. [7] [10] Possible solutions can for example be to use sliding doors or an airlock which can create a barrier between the two areas you want separated. Still, when there is passage you can see notable amount of air being transferred in both cases. [9]

Tung et al. [11] investigated air exchanges between an isolation room and the anteroom through numerical studies. This was done in presence of mechanical ventilation with differential pressurization. When the communication door was open, they found that to obtain an air flow direction completely from the anteroom to the room a significant amount of air changes was needed. A minimum of 24 air changes per hour air flow rates was needed from the anteroom to the room.

Adams et al. [12] investigated by releasing fluorescent microspheres as contaminant into the isolation room. The airborne concentration inside the room, in the anteroom and corridor, was measured. The results showed differential pressures ranging from 2.5 to 20 Pa, and conditions of null or high care provider traffic. They found that operating the doors and provider traffic have a big effect on the containment. Kiel and Wilson [13] have presented measurement results, along with theoretical analysis of the fluid volume that is exchanged through an external doorway. They concluded that the exchanged volume is almost constant with hold open time, which is the time a door is held open at an angle of 90°. They also observed that the exchanged volume increased linearly with the door speed for a laminar flow and independently from the speed for fully turbulent flow conditions.

Earlier studies have also from visual observations concluded that hinged doors allow more fluid to be exchanged than sliding doors. Tang, Julian W., et al. [2] is clear on the fact that for general infection control purposes, sliding doors (single or double) offer some obvious advantages over the more conventional hinged-door design. This shows in the amount of air exchanged across isolation room doorways each time they are opened. This was tested with different sliding and hinged doors to study the flow induced by the door motion. It was also tested in the combination with a manikin. They concluded that the images and videos obtained clearly demonstrates that sliding doors induce much less airflow across the doorway than hinged doors. It is also seen that single doors cause less disturbance than double doors. This is assuming that the single doors are smaller than the double doors. The movement of a single healthcare worker through the doorway in either direction induces additional airflow movement, thereby increasing the amount cross-contamination across the doorway. Still the motion of a hinged door is seen to be more important for the exchange than the motion of a manikin. This study showed that the motion of a hinged door has a big impact on the air exchange in the room. The observations were also validated using experiments conducted in a full scale model by Kalliomäki et al. [10] [9].

It is important to improve the understanding of the mechanisms responsible for exchange of air in everyday environments. This can contribute in the understanding and control of infection outbreaks. This can also assist in describing the indoor environment during indoor air-quality studies.

The draft that is created in busy environments may also interact with low-speed ventilation devices, and this will influence the user comfort. This is why it can be valuable to also consider the movement of air during door motion in a non-pressurized environment. The development of numerical models attempting to incorporate the effect of door motion of indoor air flows, shows that it is a clear need to improve the current understanding of the mass exchange and flow patterns that are generated during door movement [7].

Tang et al. [1] used a scale model of an isolation room without differential pressure, with water to simulate air and food dye to simulate infectious aerosols. The door and dye motions were captured by a video camera. The experimental tests showed that there was a clear fluid exchange between the isolation room and the clean room. The authors suggested that this effect could persist also in presence of a differential pressurization if the door opening motion was fast enough.

Eames et al. [14] estimated motion and diffusion of a contaminant in an isolation room, in absence of differential pressure. They showed that there was a fluid exchange between the rooms caused by the opening and closing of the door.

As recent as 2019 Kalliomäki et al. [15] investigated the effectiveness of the directional airflow across an isolation room doorway in limiting air and airborne contaminant escape out of a hospital isolation room. Laboratory experiments were performed measuring the air migration induced by the opening of the hinged door, passage through the doorway and temperature difference. They concluded that the studied directional airflows limited air escape from the isolation room in all cases. Both in the case of hinged door opening, passage and temperature difference induced air escape it was seen a notable difference. The method in use was found to be promising but should be studied in more detail in the future to find the optimal parameters in limiting the doorway airflows.

### 1.1.2 Computational fluid dynamics and numerical work

Alongside the experimental work there has also been growing interest in representing effects of human movement, door motion and ventilation in Computational fluid dynamics (CFD) models. The development of dynamic and moving meshes has made this possible. CFD simulations have been used increasingly in design, optimization of ventilation systems, and the prediction of air movement in ventilated spaces. In this thesis the effect of door opening motion is going to be investigated. Numerical simulations will be performed to solve coupled of mass, momentum and energy transport equations for this task. The

numerical simulations will be done by using STAR CCM+ which is a CFD modelling program. STAR-CCM + uses the Finite volume method and solve Navier-Stokes equations to perform the calculations numerically. Regarding environmental engineering CFD can for example be used for looking at distribution of pollutants and effluents which is very relevant for the case of door opening. To use such a program, it is important that the person using it have competence and understands the numerical physics that underlies the simulations. The results generated by the CFD code are at best as good as the physics and chemistry embedded in it and at worst as good as its operator. When CFD is used it is often a question about if it is possible to simplify something, so it becomes less demanding in both time and computational power. Papakonstantis and Hathway [16] presented a pilot study to develop a door momentum source for use in CFD that could represent the air flow generated by a door motion. The results even with a coarse mesh showed good qualitative agreement to experimental results but the coarse mesh still over-predicted the velocities. They concluded that further work is required to investigate finer meshes and the related improvement in simulation versus computational time.

The focus of the simulations in this work will be the usage of the overset mesh for moving rigid boundaries and two-equation turbulence models towards understanding the effects of door opening speed and time, thermal effects and turbulence models. Overset mesh is a technique that allows the calculation program STAR CCM + to simulate movable objects. Overset meshes are used to discretize a computational domain with several different meshes that overlap each other in an arbitrary manner. This will be a central concept regarding the simulation of the door opening motion.

**Error! Reference source not found.** below presents a mesh scene from an initial test case. Here the overset mesh has been used to be able to simulate the motion of a hinged door.

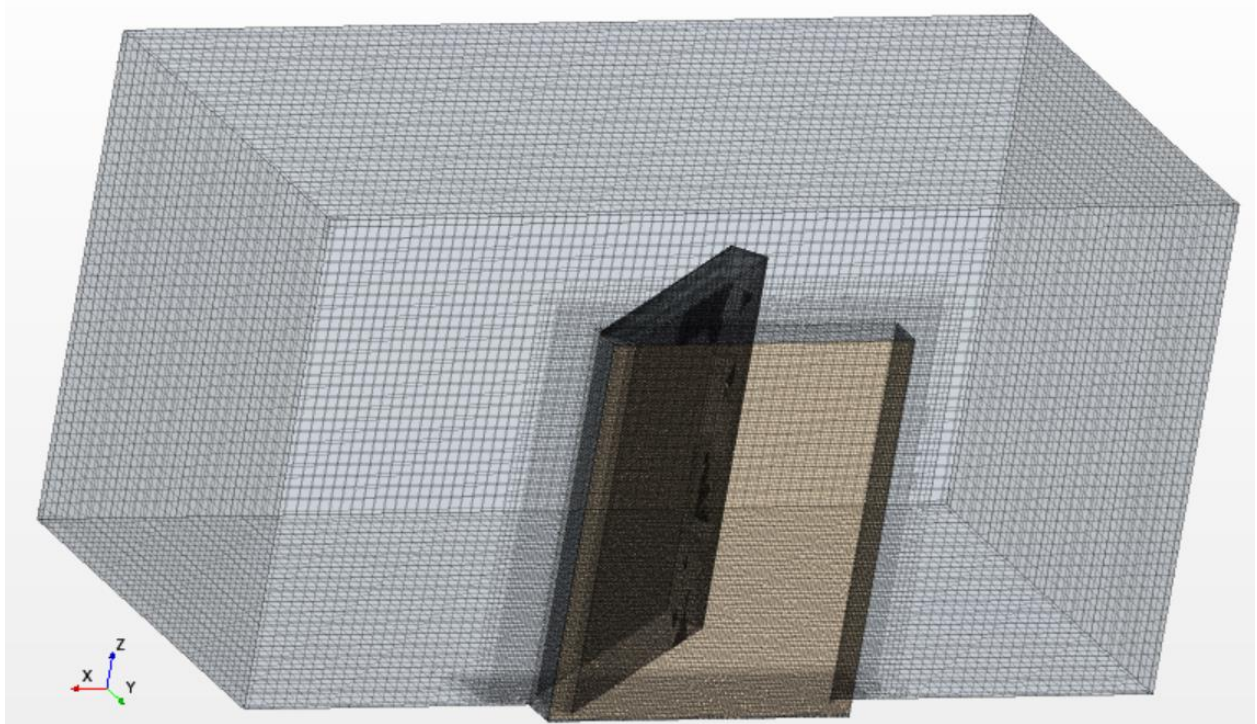


*Figure 3 Mesh scene from initial test case with hinged door*

A few investigations conducted using CFD simulation with dynamic mesh techniques have indicated that transient events such as object movements play important roles in indoor dynamic airflows and contaminant dispersion. For example, Tung et al. [11] used dynamic grid deformation approaches to generate the computational mesh around a moving body in an isolation room.

Chang et al. [8] studied the leakage flow induced by door opening and closing to determine the total leakage volume. They used a simulation and experiment method involving tracer gas and an inner-outer room model. The air in outer rooms was treated as unfiltered air and marked with tracer gas sulfur hexafluoride (SF<sub>6</sub>). In this way the leakage could be easily monitored. It was adopted in an unsteady CFD simulation with a dynamic mesh technique in which the door was the moving object. This was followed by a full-scale experiment to validate the total leakage volume. Among the results it was found that the leakage flow rate always was positive, which implies that leakage occurs throughout the door rotating process.

Lee et al. [17] looked at the difference between a swinging and a sliding door separating an air-contaminated room and a corridor in an office building. The CFD model was developed using the moving mesh technique and was validated by comparing the results of various simulation cases with full-scale measurements. The results suggested that a sliding door is more useful than a swing door in decreasing the



contaminant leakage from a room. The CFD including the moving mesh model was found to be very useful in evaluating the effects of door opening on the rate of transport of indoor air pollutants.

When investigating the airflow induced by door motion it is important to understand the role of the Reynolds-averaged Navier–Stokes equations (RANS equations). RANS equations are time-averaged equations of motion for fluid flow, where the idea behind the equations is Reynolds decomposition. You take an instantaneous quantity and decompose it into its time-averaged and fluctuating quantities. The RANS equations are primarily used to describe turbulent flows. These equations can be used with approximations based on knowledge of the properties of flow turbulence to give approximate time-averaged solutions to the Navier–Stokes equations. [18]

The literature that is mentioned in this literature study demonstrates that developments in numerical modelling of moving objects, and the resulting impact on airflow, are progressing at an impressive rate. This has been an important part of being able to better understand the turbulence effect of a door motion. Together with the experimental work this contributes in the growing understanding of the mechanisms involved. It seems to be the general opinion that hinged doors is a greater risk regarding potential pollutant transport via the air flow. This is shown in the results achieved both in experiments and in numerical simulations. Most hospital isolation rooms today still use a more traditional hinged-door design. It is possible that this is because of the space requirements and the practicalities of higher installation and maintenance costs. It can also be a factor that where air-tight containment facilities are required, it is much easier to ensure an airtight seal around a hinged-door than a sliding-door. [2]

It has been done a lot of great work that have benefitted in the understanding of the effect door opening and closing have on air flow and mass exchange. One thing even the most recent studies suggest is that more work needs to be done. In this thesis different types of door motions is going to be investigated. This includes a “new” type of elevator door, that to our best knowledge has not been simulated before. This is going to be performed by numerical simulations to solve coupled of mass, momentum and energy transport.

## **1.2 Definition of the Problem**

Understanding of air flow, mass exchange by the opening of a door is beneficial for estimation of pollutant transport and predict/control desired indoor environment. Numerical simulations are to be performed to solve coupled of mass, momentum and energy transport equations for this task. The focus of this work will be the usage of the overset mesh for moving rigid boundaries and two-equation turbulence models towards understanding the effects of door opening speed and time, thermal effects, and turbulence models. This work is also very relevant to the present pandemic situation. Different types of doors are going to be investigated and compared. A classic hinged door is going to be compared with a sliding door. An elevator door that opens from both sides is also going to be investigated. To our best knowledge this is

something that has not been done before, so this provides a new angle. The effect of different opening times and temperature differences are also going to be investigated.

### **1.3 Aim and objective**

The aim and objective with this work is to get a better understanding of how different types of door motions effect the air flow, as this is a possible threat regarding airborne contamination and is also relevant for energy use. A room is going to be modelled in STAR CCM+ where different types of door are going to be tested. Another objective for this work is to validate some of the experiments that have been done previously that have investigated door opening motion. The experiments are going to be validated by recreating them in a CFD simulation with realistic input. This is also going to be done in STAR CCM+.

### **1.4 Research scope and limitation**

This work focusses on turbulence in the airflow created by door motion and work related to this. A clear limitation for this work is the CFD simulations where STAR-CCM + is being used. The program uses the Finite volume method and the Navier-Stokes's equations to perform the calculations numerically. To do simulations in STAR CCM + one is dependent on relatively large computing power to be able to carry out the calculations. When you include more parameters or more grid points you need more computing power and processor performance. The time is also a limitation as complicated simulations is very time demanding. This is related to the computing power that is available. Especially Large eddy simulations is something that is very time consuming and is something that is possible to investigate more detailed in the future. With a better processor performance, it is possible to perform more complicated simulations in much less time. This a clear limitation when the mesh was created.

### **1.5 Audience**

The audience for this work is everyone who is interested in understanding the effect the door motion has on the air flow and mass exchange between two rooms. There has been a growing interest in representing effects of human movement, door motion and ventilation in CFD models. The development of dynamic and moving meshes has made this possible. CFD simulations have been used increasingly in design, optimization of ventilation systems, and the prediction of air movement in ventilated spaces. Understanding of how the door motion affects the airflow and how this connected to ventilation is something that can be valuable for many. This includes for example people working with energy and environment in buildings where ventilation is an important factor both when it comes to energy and air quality. Regarding the understanding on how pollutants move in an indoor environment this work will also be relevant for the current pandemic situation. Moreover, to benefit from this work it is a clear advantage that the reader has some knowledge with engineering and fluid dynamics.

## 2 Methods and Materials

In this section the method for the thesis will be presented. This involves an introduction of the tool used for the simulations and a description of the method. Here the most essential features will be explained in more detail. A presentation of the governing equations of the fluid flow is also included.

### 2.1.1 Governing equations

The physical model that is defined when performing the simulation is based on solving governing equations that describes the fluid flow. Compressible Navier-Stokes equations are solved together with the mass and the energy conservation equations. Continuity equation:

$$\frac{\partial \rho}{\partial t} + \nabla \cdot (\rho \mathbf{u}) = 0$$

$\rho$  is the density,  $\mathbf{u}$  is the velocity vector and  $t$  is the time. This equation is three-dimensional and unsteady for a compressible fluid.

The momentum equation is defined as the momentum of the flow depending on the forces that are acting on the fluid. This is defined as:

$$\frac{D(\rho \mathbf{u})}{Dt} = -\frac{\partial p}{\partial \mathbf{x}} + \nabla \cdot (\mu \nabla \mathbf{u}) + S_M$$

Here  $p$  is the pressure,  $\mu$  is the dynamic viscosity and  $S_M$  is the source term, that for example can be gravity. When applying the first law of thermodynamics on a control volume, we can write the conservation of energy as:

$$\frac{D(\rho E)}{Dt} = -p \nabla \cdot \mathbf{u} + \nabla \cdot (k \nabla T) + S_e + \Phi$$

$E$  is energy,  $k$  the thermal conductivity of the fluid,  $T$  the temperature,  $S_e$  is energy source term and  $\Phi$  is dissipation term due to deformation work.

The working fluid is air which can be treated as ideal gas, with equation of state.

$$p = \rho RT$$

Where  $p$  is pressure,  $R$  is ideal gas constant,  $\rho$  is density and  $T$  is temperature.

The governing equations written above, equation (1), (2) and (3), can be written in a general form called the transport equation. This can be written for any conserved property as:

$$\frac{D(\rho\phi\mathbf{u})}{Dt} = \nabla \cdot \Gamma \nabla \phi + S_\phi$$

$\phi$  is some scalar property,  $\Gamma$  is diffusion coefficient. The governing equation involves advection term in left hand side and the terms on the right-hand side signify the diffusion term and the generation term respectively.

It is possible to write the governing equations in a more compact form which is called the material derivative or the advective derivative. It describes the time rate of change for some property  $\phi$ . This can be extended to:

$$\frac{D(\rho\phi\mathbf{u})}{Dt} = \frac{\partial(\rho\phi)}{\partial t} + \nabla \cdot (\rho\phi\mathbf{u})$$

This junction involves the transient term of the governing equation and the convective term. This is a more compact way to write the governing equations. In general, CFD techniques can solve these equations. For turbulent flows, Reynolds averaged Navier-Stokes can be used.

## 2.1.2 RANS (Reynold-averaged Navier-Stokes equations)

Indoor airflow is generally turbulent. There are three numerical flow simulation methods available when you want to look at turbulent flow. DNS (Direct Numerical Simulation), LES (Large Eddy Simulation), and RANS (Reynolds Averaged Navier–Stokes). The application of DNS and LES to unsteady flow fields with door rotating demands extensive computer memory and rapid computer calculation speed. RANS method offer the most economic approach for computing complex turbulent flows in terms of accuracy, computing

efficiency, and robustness for modeling an indoor environment [8]

The Navier-Stokes equations are based on Newton's second law, also called the impulse rate, which describes the relationship between change in a particle's momentum and the resultant force. The equation is applied to each fluid volume in three dimensions. It consists of four parts, where the first two describe the acceleration while the last two describe the forces acting on the element. The acceleration is derived from the principle of continuity and Bernoulli's law which describes that when the fluid flow rate increases, the pressure decreases, while the forces acting on the fluid element are compressive forces acting on the surface, shear stresses and normal voltages. The difference between Navier- Stokes equations and the closely related Euler equations is that Navier–Stokes equations take viscosity into account while the Euler equations model only inviscid flow. As a result, the Navier-Stokes are parabolic equations which means that they have better analytic properties. The Navier-Stokes equation, in modern notation, is

$$\frac{\partial \mathbf{u}}{\partial t} + \mathbf{u} \cdot \nabla \mathbf{u} = -\frac{\nabla P}{\rho} + \nu \nabla^2 \mathbf{u}$$

The Reynolds-averaged Navier–Stokes equations are time-averaged equations of motion for fluid flow. The idea behind the equations is Reynolds decomposition. You take an instantaneous quantity and decompose it into its time-averaged and fluctuating quantities. This idea was first proposed by Osborne Reynolds. The RANS equations are primarily used to describe turbulent flows. These equations can be used with approximations based on knowledge of the properties of flow turbulence to give approximate time-averaged solutions to the Navier–Stokes equations. [18]

Usually, CFD omit solves time-averaged properties for the flow, which means they solve mean velocity mean stresses and mean pressures. Therefore, turbulent flow is mostly simulated with Reynolds-Averaged Navier-Stokes equations or RANS. This takes the governing equations as described in the previous section, where flow properties is replaced with the sum of the mean and a fluctuating component such as:

$$\mathbf{u} = \mathbf{U} + \mathbf{u}'$$

$$u = U + u'$$

$$v = V + v'$$

$$w = W + w'$$

$$p = P + p'$$

The continuity becomes :

$$\frac{\partial \bar{P}}{\partial t} + \text{div}(\bar{\rho} \bar{\mathbf{u}}) = 0$$

RANS equations:

$$\frac{\partial(\bar{p}\tilde{U})}{\partial t} + \text{div}(\bar{p}\tilde{U}\tilde{u}) = -\frac{\partial\bar{P}}{\partial x} + \text{div}(\mu \text{grad } \tilde{U}) + \left[ -\frac{\partial(\overline{\bar{p}u'^2})}{\partial x} - \frac{\partial(\overline{\bar{p}u'v'})}{\partial y} - \frac{\partial(\overline{\bar{p}u'w'})}{\partial z} \right] + S_{Mx}$$

$$\frac{\partial(\bar{p}\tilde{V})}{\partial t} + \text{div}(\bar{p}\tilde{V}\tilde{u}) = -\frac{\partial\bar{P}}{\partial y} + \text{div}(\mu \text{grad } \tilde{V}) + \left[ -\frac{\partial(\overline{\bar{p}u'v'})}{\partial x} - \frac{\partial(\overline{\bar{p}v'^2})}{\partial y} - \frac{\partial(\overline{\bar{p}v'w'})}{\partial z} \right] + S_{My}$$

$$\frac{\partial(\bar{p}\tilde{W})}{\partial t} + \text{div}(\bar{p}\tilde{W}\tilde{u}) = -\frac{\partial\bar{P}}{\partial z} + \text{div}(\mu \text{grad } \tilde{W}) + \left[ -\frac{\partial(\overline{\bar{p}u'w'})}{\partial x} - \frac{\partial(\overline{\bar{p}v'w'})}{\partial y} - \frac{\partial(\overline{\bar{p}w'^2})}{\partial z} \right] + S_{Mz}$$

Scalar transport equation:

$$\frac{\partial(\bar{p}\tilde{\Phi})}{\partial t} + \text{div}(\bar{p}\tilde{\Phi}\tilde{u}) = \text{div}(\bar{p} \text{grad } \tilde{\Phi}) + \left[ -\frac{\partial(\overline{\bar{p}u'\phi'})}{\partial x} - \frac{\partial(\overline{\bar{p}v'\phi'})}{\partial y} - \frac{\partial(\overline{\bar{p}w'\phi'})}{\partial z} \right] + S_{\phi}$$

In the equations above, the overbar indicates a time-averaged variable, and the tilde indicates a density-weighted or Favre-averaged variable. [18] To be able to calculate RANS equations, turbulence modelling is needed. This is since number of unknowns in the above equation exceeds the number of equations. Therefore it is needed additional equations, which we get from turbulence modelling. This is presented in the next section.

### 2.1.3 Turbulence modell

As mentioned in the previous section, turbulence modelling is needed to solve RANS equations. There are many different turbulence models out there but depending on the problem a suitable model must be chosen. For good prediction of air flows in a door opening motion its needed to choose a model that can describe the air flows behavior well. To describe if the flow is either turbulent or laminar, the dimensionless number Reynolds number (Re) is used, see 2.1.5 Reynolds number. When the Reynolds numbers of the flow is high it can be stated to be turbulent, where the flow is chaotic, and the motion appears random. Then we need a turbulence model in CFD software to be able to describe this behaviour. [18]

In this thesis it has been worked with a Relizable Two-Layer K-Epsilon turbulence model. The K-Epsilon model has been proven effective for various engineering applications, but certain characteristics of inleakage flow, such as the creation of regions with very low velocities and thus low Reynolds numbers, particularly in near-wall regions, could not be accurately predicted by standard k-ε.

The standard Two-Layer K-epsilon model and the Relizable Two-Layer K-Epsilon model still offer the most mesh flexibility. It is possible to use both with the same meshes as the high Reynolds number versions. They give good results on fine meshes, and also produce the least inaccuracies for intermediate meshes which make them favourable to work with. If there is uncertainty conserving which turbulence model to use in a given situation, then the Relizable Two-Layer K-Epsilon model is a reasonable choice. The Realizable Two-Layer K-Epsilon model combines the Realizable K-Epsilon model with the two-layer approach. The coefficients in the models are identical, but the model gains the added flexibility of an all-y+ wall treatment. If the mesh is coarse, it provides results that are quite close to the version without the two-layer formulation. If the mesh is fine enough to resolve the viscous sublayer, the results will be similar to a low Reynolds number model. [19] This is why it was chosen to work with the Realizable Two-Layer K-Epsilon model as it offers the most mesh flexibility.

#### 2.1.4 Near wall treatment

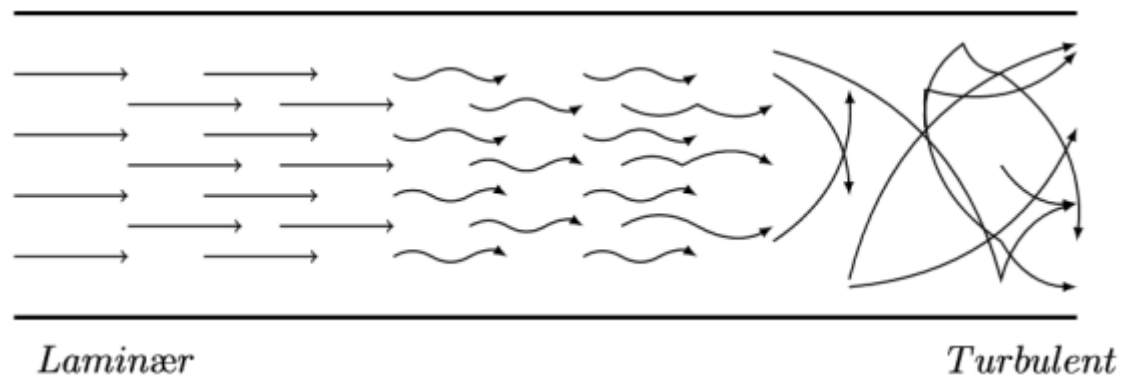
The Turbulence near the walls plays an important role in CFD. Since the flow is interacting with a solid surface instead of being free turbulent flow, the flow will behave differently, and models to describe this is needed. If a Reynolds number is formed with a distance,  $y$ , from the wall we get the formulation:

$$Re_y = \frac{U_y}{\nu}$$

Where  $\mu$  is kinematic viscosity,  $U$  is velocity and  $y$  is the distance from the wall. This tells us that closer to the wall, the Reynolds number will be lower. This will cause the viscous effects to be more dominant. [18] A suitable  $y +$  wall treatment was chosen in the simulations in this thesis.

#### 2.1.5 Reynolds number

We divide flow into two category's, turbulent or laminar flow. Between these you have a transition region, see the figure under



To be able to decide if the flow is turbulent or laminar its needed to define a dimensionless number called the Reynolds number (Re). This is the ratio between inertia forces and viscous forces and the definition of this is:

$$Re_L = \frac{uL}{\nu}$$

Where  $u$  is the velocity of the fluid,  $L$  is the characteristic length and  $\nu$  the is kinematic viscosity. For example large Reynolds number above 2900 you will have turbulent flow for pipe flow, and for low numbers below 2300 you will have laminar flow for pipe flow.

### 2.1.6 Computational Fluid Dynamics (CFD)

CFD or Computational fluid dynamics is the analysis of system involving fluid flow, heat transfer and associated phenomena such as chemical reactions by means of computer-based simulation. CFD spans a wide range of industrial and non-industrial application areas. Some examples are aerodynamics, hydrodynamics and power plant, and electrical, chemical and environmental engineering. Regarding Environmental engineering CFD can for example be used for looking at distribution of pollutants and effluents which is very relevant for the case of door opening. All CFD codes are structured around the numerical algorithms that is able to tackle fluid flow problems. All commercial CFD packages include sophisticated user interfaces to input problem parameters and to examine the results, in order to provide easy access. Computers have evolved and have become better and more powerful in recent years. The program is in step with this development able to process difficult and more demanding problems than before. A CFD program uses advanced mathematical models and equations that are solved numeric. To use such a program, it is important that the personnel have competence and understands the numerical physics that underlies the simulations. The results generated by the CFD code are at best as good as the physics and chemistry embedded in it and at worst as good as its operator. [18]



In this thesis the program Star CCM+ is used. The main steps in a process of solving a problem with CFD are the three phases: Pre-processor, solver and Post-processor.

In the Pre-processor phase the computational domain is defined. This involves setting up the geometry of the problem setup with a working mesh. The mesh is the control volumes we divide a problem setup into, where governing equations are solved for properties of interest. A good prediction of a problem demands a good quality mesh, where its representative to real physics. This involves having finer mesh in regions where there is larger variations in the properties from point to point

The next part is the solver where most of the CFD tools uses the finite volume method (FVM) based solver. This involves integrating the governing equations inside a control volume, taking the resulting equations into a system of equations. this is usually solved with an iterative method. Different type of solvers can be used, depending on the problem, such as different turbulence models, models for near wall treatment etc. [18]

The last process is the Post-processor. When results are obtained, the results must be analyzed and/or visualized. This can be in form of XY-plots, vector/scalar plots, streamlines etc. There are many ways to analyze a problem, depending on the intention of a study. In this thesis, when running turbulent simulations in Star-CCM+ a second order implicit coupled flow solvers was used.

### 2.1.7 STAR CCM+

STAR-CCM+ is a CFD modeling program produced by CD-adapco which in 2016 was acquired by Siemens digital Industries Software. The program bases its calculations on numerical algorithms. You can use the CAD tool to define advanced physical models and it is also possible to customize the division of geometry. STAR-CCM + uses the Finite volume method and the Navier-Stokes equations to perform the calculations numerically. To do simulations in STAR CCM + one is dependent on relatively large computing power to be able to carry out the calculations. When you include more parameters you need more computing power and processor performance. STAR-CCM+ is a Computational Aided Engineering (CAE) solution for solving multidisciplinary problems in both fluid and solid continuum mechanics, within a single integrated user interface. The program provides the world's most comprehensive engineering physics simulation inside a single integrated package. STAR-CCM+ is not just a CFD solver, but an entire engineering process for solving problems involving flow (of fluids or solids), heat transfer, and stress. It provides a suite of integrated components that combine to produce a powerful package that can address a wide variety of modelling needs.

Amongst other things STAR CCM+ can amongst other things be used to: Generate different types of meshes, import and create geometries, solve the governing equations, analyse results, utomize the simulation workflows for design exploration studies. Is also possible to Connect to other CAE software for co-simulation analysis. [19]

## 2.2 Method for the simulations

When making a CFD model, it is important to have a clear overview of the situation that is going to be simulated. It is important to know the physical properties, type of medium as well as the geometry. The task is to look at different type of door motions and see how the airflow is affected. To be able to monitor the airflow in a better way the simulation involves tracer gas in the form of Sulfur hexafluoride (SF<sub>6</sub>). The tracer gas is being used to see how much potential contamination that is going into the room and how much that stays in the room after the door motion.

The simulations involve three different types of doors. One hinged, one sliding and one elevator door. In addition to the different door types, it has also been looked at different opening times and thermal effects. Besides how the door moves the geometry and boundary conditions are the same in each case. For the three different door types it has also been investigated how a temperature difference effect the airflow. This has been done by making the inner room a cold storage room. That means changing the initial conditions so there is a temperature difference between the two rooms. This chapter describes the methodology for important parts of the modelling in STAR CCM+.

### 2.2.1 Geometry

The geometry in STAR-CCM + can be drawn using 3D-CAD which is a CAD tool implemented in the program. It is also possible to import geometries from other programs such as Revit. In this simulation, all geometries were constructed in the desired plane with the Sketch function, and then extruded with "Extrude" to get a volume referred to as Body.

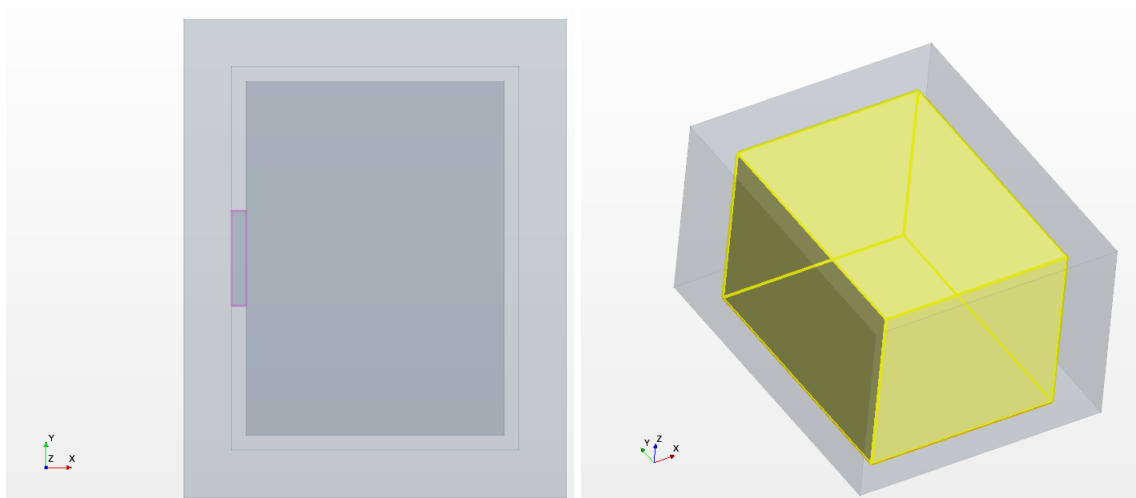


Figure 4 Draw and extrude

Initial it was 4 different body's. three bigger rectangle and one smaller was draw as shown in Figure 4 to represent respectively the inner room, the walls around the inner room, the outer room and the doorframe. To create the walls between the inner and the outer room the "Boolean operations" have been used. "Subtract" was used to remove the space between the inner and outer room and this worked ass walls. In the thermal cases there was assumed no heat loss through the walls.

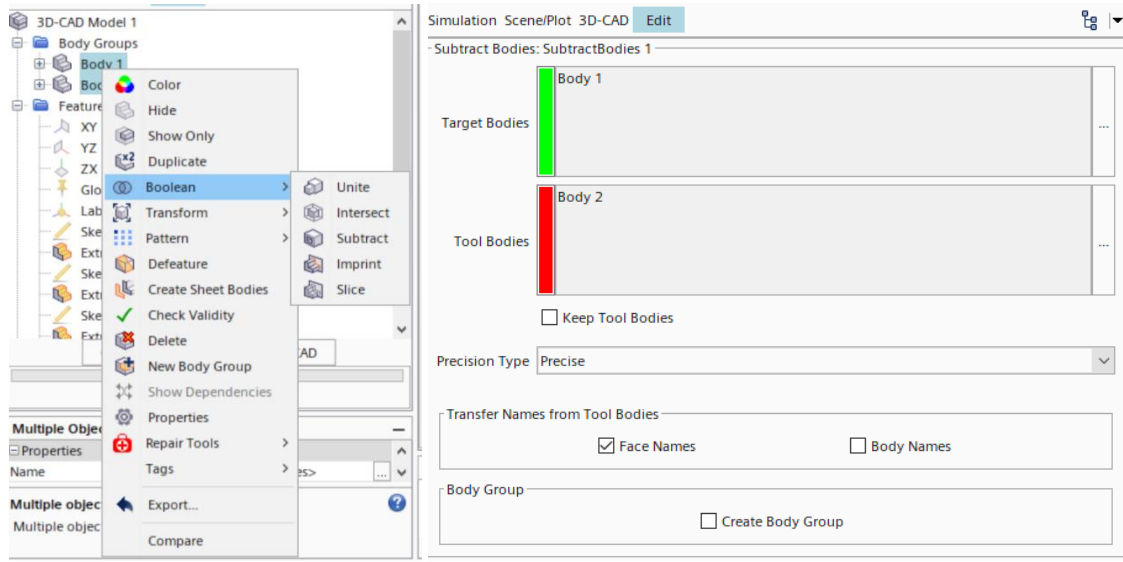


Figure 5 Boolean operations

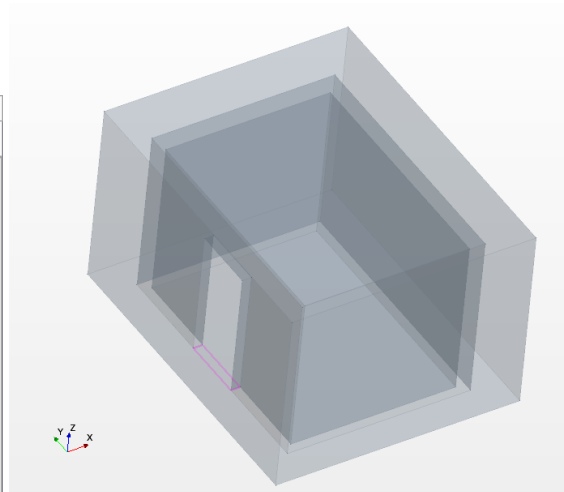
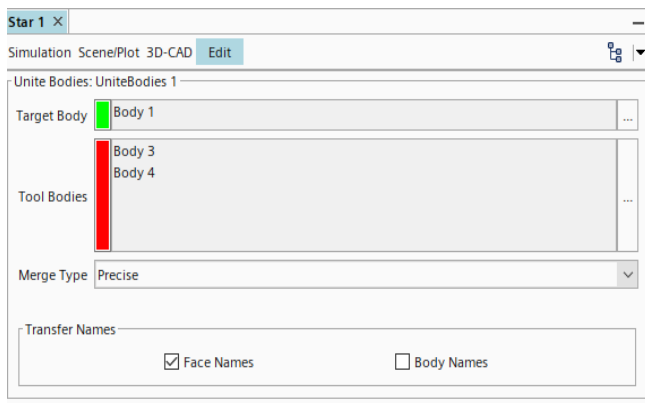


Figure 6 Unite bodies

After the subtract was used, "Unite" was used to combine the remaining parts in to one part. The body 1 was then as shown in Figure 6 over. The only remaining thing was to draw the door which became body 5.

Then you had two bodies to work with. After several test cases it was seen that it was beneficial with a small gap when simulating the door motion to make the simulation run smoothly. “Translate bodies” was used and the door was moved 0.01 m in Z-direction. From the start it was also added a small gap on each side and on the top of the door. After the geometry was finished the parts could be created and the surfaces named with “Split by patch”.

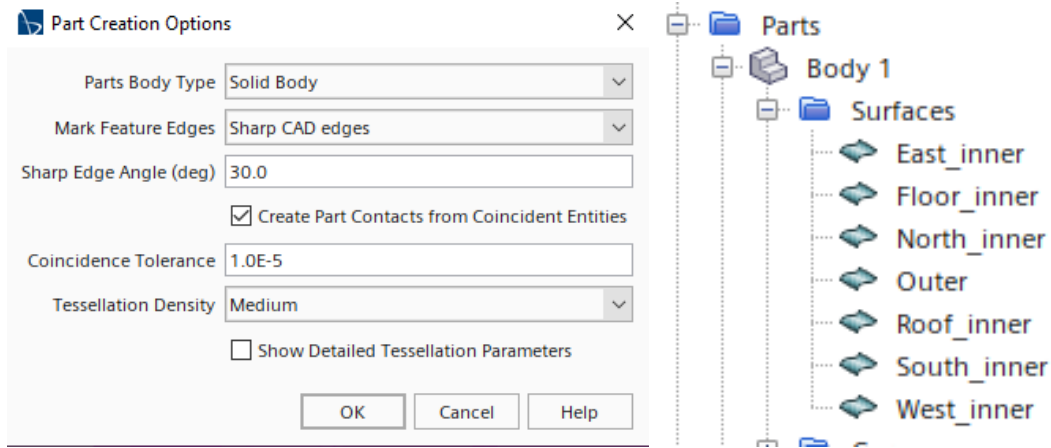


Figure 7 Create parts and split by patch

The next face was to create new shape parts called “blocks”. This was done mainly for two purposes:

- To create the interface that becomes the overset mesh (explained in Overset Mesh)
- To create volume control for the meshing (explained in mesh)

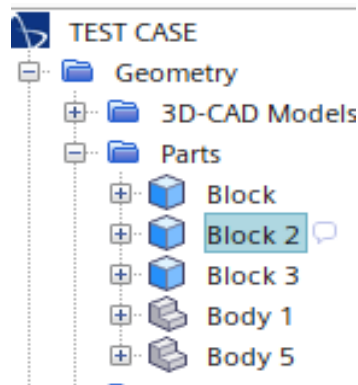


Figure 8 Creating Blocks

For the purpose of working as the overset region the intersect is created by the following steps:

- 12. Mark body 5 (the door) and the block surrounding the door and make a subtract. Right click – Boolean – Subtract

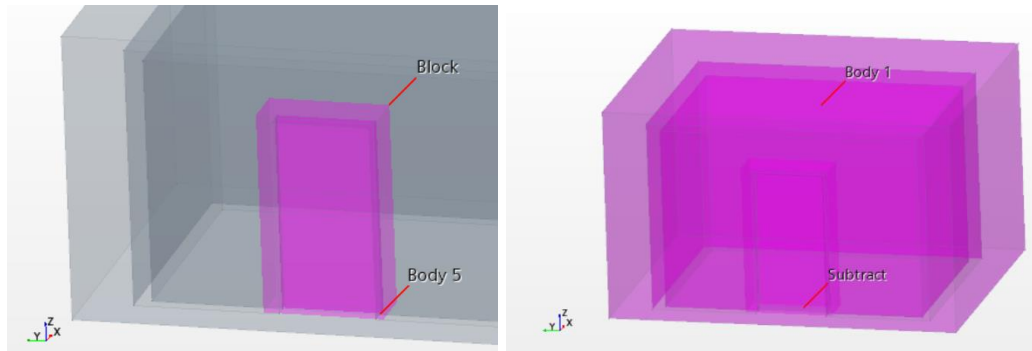


Figure 9 Boolean subtract

- Combine this subtract and body 1( background ). Mark body 1 and subtract, right click – Boolean - Intersect
- This intersect as shown in figure x will work ass the overset region

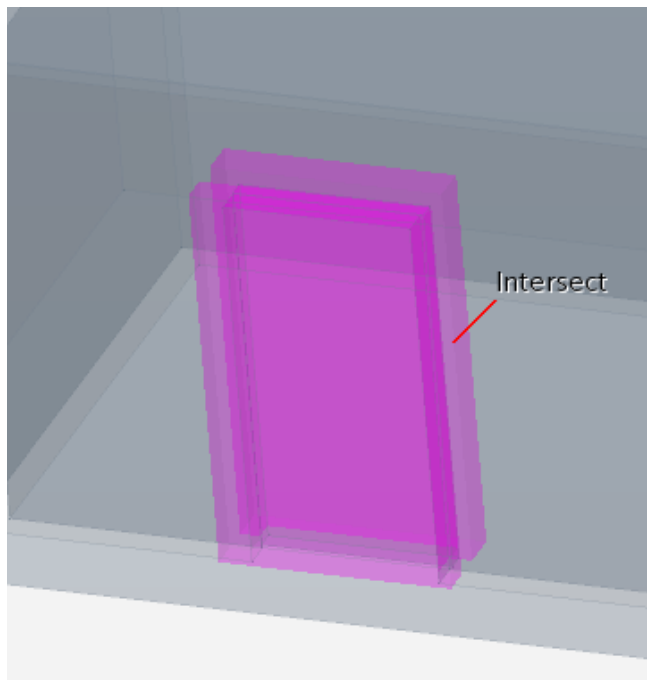


Figure 10 Intersect working as the overset region

These are the most important steps when creating the geometry and parts for this task. The next step is to Assign parts to region and then set the boundary conditions. Other important things from the creation of the simulation files will be explained in separate parts.

## 2.2.2 Boundary conditions

After the regions are created, the boundary conditions can be fixed. A boundary can be one or more objects connected to one boundary condition. Under boundary conditions, one can choose the type of boundary.

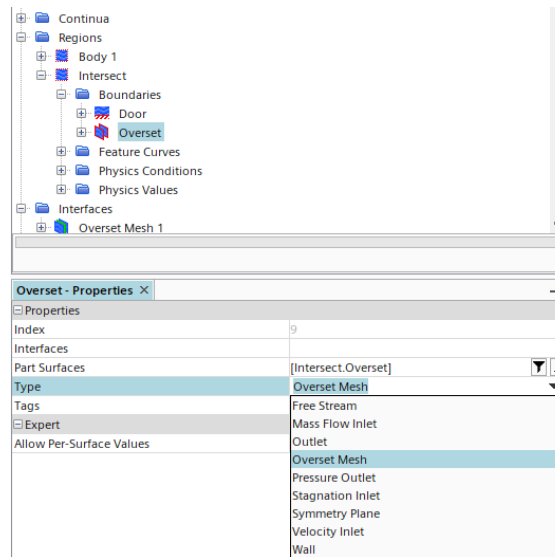


Figure 11 Setting Boundary Conditions

When the type of boundary is selected, it is possible to specify the physics of the boundary. This can be done in Physics Conditions. The boundaries that were used for the simulations are shown in Table 1.

Table 1 Boundary conditions for the simulations

Boundary	Used for
Wall	Used at impermeable limits for non-viscous flows and viscous flows with adhesion condition. It can also be used for fixed material limits where temperature or heat flux is specified. This was used for all everything besides the overset region.
Overset mesh	Used for the overset region

As there was no inlet or outlet in the simulation the wall and the overset mesh boundaries was the only boundaries that was needed.

### 2.2.3 Mesh

A mesh is a discretized representation of a geometric domain. This domain can include real-world geometry, its content, and its surrounding environment. The physical space that you want to solve within is called the simulation domain. Generating a mesh typically involves creating a suitable simulation domain. There are two types of flows that require different approaches when creating the simulation domain: internal flow for example in a pipe, and external flow, such as the flow around and through a car. In this thesis it is internal flow that is the case.

Parts Based Mesher will be used when creating the mesh. PBM detaches the meshing from the physics and provides a flexible and repeatable meshing pipeline. This can be enabled by applying an Automated Mesh operation in the Parts tree and selecting “Per Parts Meshing” in the Properties menu. The meshing models that were used was:

- Trimmed Cell mesher
- Surface Remesher
- Prism Layer Mesher, which will be used to properly capture near wall boundary layers.

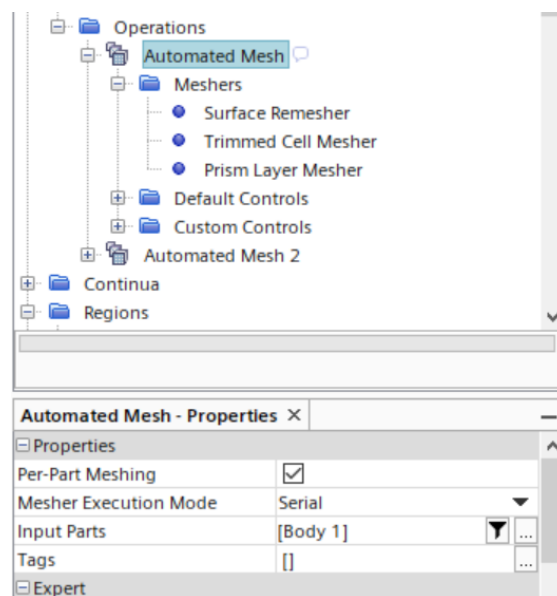


Figure 12 Meshing models

#### Trimmed cell Mesher

The reason Trimmed Cell mesher was chosen over the Polyhedral, was due to computational limitations. The polyhedral cells that are created typically have an average of 14 cell faces. In contrast, trimmed cells have only 4. In general, the memory requirements for meshing are:

- Trimmed mesh: About 0.5 GB / million cells.
- Polyhedral mesh: About 1GB / million cells.

The downfall of the trimmed cell mesher, is that near surfaces the cells collapse from polyhedral to tetrahedral or hexahedral. This means that when a Volumetric Control is applied on a trimmed cell mesh, the abrupt change in cell size will cause the Cell Quality to drop near that surface area. However, this can be combated to a certain degree by enabling the Run Post Mesh Optimizer setting.

### Surface Remesher

The Surface Remesher can be used to retriangulate the surface. This option improves the overall quality of an existing surface mesh and optimises it for the volume meshing. It also aids the subsurface generator when the prism mesher option is selected. The quality of an overall mesh is first of all dependent on the surface meshing performed. The following options in the Surface Remesher dialog was chosen:

- Meshing Method as Triangle
- Perform Curvature, Proximity & proximity Refinement
- Minimum Face Quality 0.05

### Prism Layer Mesher

The Prism layer mesher is required to efficiently resolve the wall boundary layers and improve the accuracy of the flow solution. Prism layers allow the solver to resolve near wall flow accurately, which is critical in determining the forces on the wall. Accurate prediction of these flow features depends on resolving the velocity and temperature gradients normal to the wall. These gradients are much steeper in the viscous sublayer of a turbulent boundary layer than would be implied by taking gradients from a coarse mesh. The quality of the Prism layer can be viewed in a mesh scene, by making sure the layers created capture the surface of the geometry effectively.

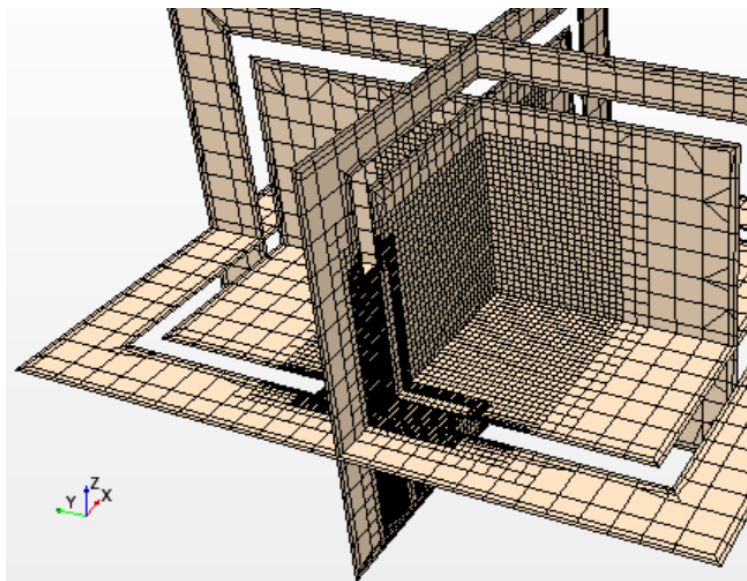


Figure 13 Mesh shown with plane sections



## Custom Mesh Controls

Custom controls override any default controls for the surface and volume meshers. This facility allows you to refine or coarsen the mesh for part curves, part surfaces, geometry parts, and specified volumes. The following types of custom mesh controls are available: Curve Controls, Surface Controls, Part Controls and Volumetric Controls. Surface controls specify alternative surface mesh and prism layer settings for part surfaces, geometry parts, and composite parts. If a part surface belongs to several controls, the following hierarchy determines the surface control that takes precedence. This hierarchy depends on how you apply the part surface to the control. For this task, the volume control has been the preferred custom control.

### Volume control

You use a volumetric control to specify the mesh density in a specific zone for both surface and volume meshes. You can define the mesh refinement zone using volume shapes and geometry parts. For geometry parts, the control takes its definition from the Root description only. You can apply each volumetric control to any combination of meshing models. Therefore, you can set specific cell sizes within the zone for each mesh generation stage. Volumetric controls can overlap and extend outside the region boundary definition. Volumetric controls can also overlap from one region to another, but the effect is only included if the region belongs to the same mesh continuum as the volumetric control. If two or more volumetric controls overlap, the smallest user-defined cell size takes priority.

Volumetric controls affect each meshing model in a different way. The three meshing models that were used for the volume control was:

- Surface Remesher — Refines the surface size.
- Trimmed Mesher — Refines with either an isotropic or anisotropic cell size. If you specify both options, the smallest cell size in each coordinate direction takes priority.
- Prism Layer Mesher — Refines the number of prism layers, prism layer stretching, and prism layer thickness. To include the prism layer, the extent of the volumetric control must exceed the boundary.

The values that was specified for the volume control was:

*Table 2 Volume controll settings*

Property	Value
Custom size	0.08m
Number of prism layers	5

For the simulations in this thesis the volume control was prioritized to be used. For each of the different door motions a different volume control was created. The figures under shows an example of how the volume control was used a finer mesh in the crucial areas. For the case of the hinged door in Figure 14 the finer mesh is created to cover all of the motion of the hinged door and the area where it is expected to have most turbulence. In the case of the elevator door an additional block was added as seen in Figure 15.

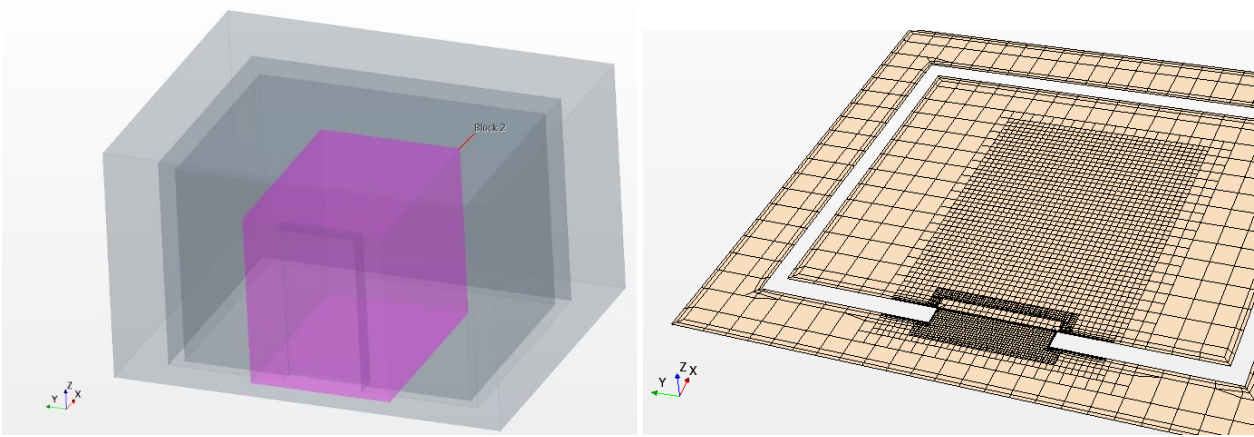


Figure 14 Volume control for the hinged door

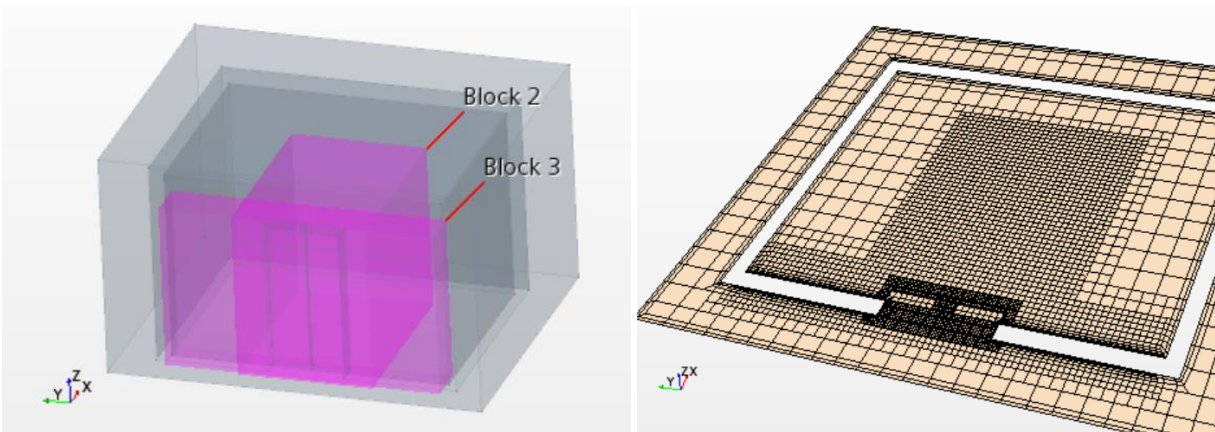


Figure 15 Volume control for the elevator door

#### 2.2.4 Physics

The physical model defines what type of medium the calculation should work with. Under Continua it is possible to choose the physical models for the simulation. Every region needs a physical model. Several regions can have the same physics model, and this is the case in all the simulations. A physical model was

created for the simulation where it was used by all regions. Figure 16 shows the models chosen for the simulations. The only difference between the thermal and the non-thermal simulations was that gravity was added for the thermal case.

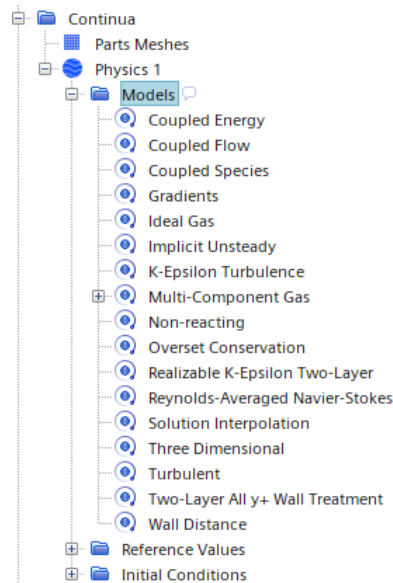


Figure 16 Physics Continua

The time model must also be chosen. These models use different methods for calculating the overall transport size ( $\varphi$ ) and the equations will be discretized differently by the different time models. As a time model in for this task, Implicit unsteady is selected, since transient calculations must be calculated. The overset mesh technique can only be used for transient calculations.

When using implicit unsteady for each physical time step, a certain number of internal iterations are calculated to converge the solution within the time step. When using this model, one must specify the size of the physical time step and the total time the simulation passes. Internal iterations per time step also needs to be set.

In this thesis, it has been chosen to have 10 internal iterations per time step. This is because this gives a more accurate result compared to having for example 5 internal iterations. The size of the physical time step and the total time the simulation runs is only a few seconds and then 10 internal iterations is prioritized.

In the physical model, one must choose what kind of material the region consists of. In this task a multicomponent gas is chosen. The multicomponent gas mixture consists of air and SF6(tracer gas).

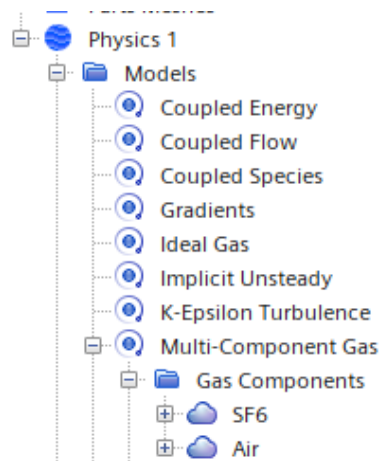


Figure 17 Multi-Component Gas

The amount of air and SF6 in each room was set by fixing the initial conditions with the help of field functions. This is explained further in Field Functions.

The Coupled Flow model solves the conservation equations for mass and momentum simultaneously using a pseudo-time-marching approach. One advantage of this formulation is its robustness for solving flows with dominant source terms, such as rotation. This is very relevant for our case. Another advantage of the coupled solver is that CPU time scales linearly with cell count. That means that the convergence rate does not deteriorate as the mesh is refined, which is an advantage.

For this task, an eddy viscous method has been used, since the flow is turbulent. The K-epsilon model is one of the most common turbulence models and is chosen to be used for the simulations. It is an equation model, which means that two additional transport equations are used to represent the turbulent flow properties. The choice of turbulence model is explained in "Turbulence model".

### 2.2.5 Motion

In Simcenter STAR-CCM+, motion is applied on a region basis. The following method outlines the steps for selecting motion models and assigning them to regions.

1. Expand the "Tools – Motions" node.

By default, the simulation contains the "Stationary" motion, which is automatically assigned to all regions. Setting a region to use a motion model other than "Stationary" results in movement of the mesh vertices during the simulation.

To add a motion model to the simulation:

2. Right-click the "Motions" node, select "New" and choose the appropriate motion model.

There are several options to choose from but for the motions is this thesis “Rotation and Translation” have been used for the hinged door and “Translation” have been used for the sliding door and the elevator door.

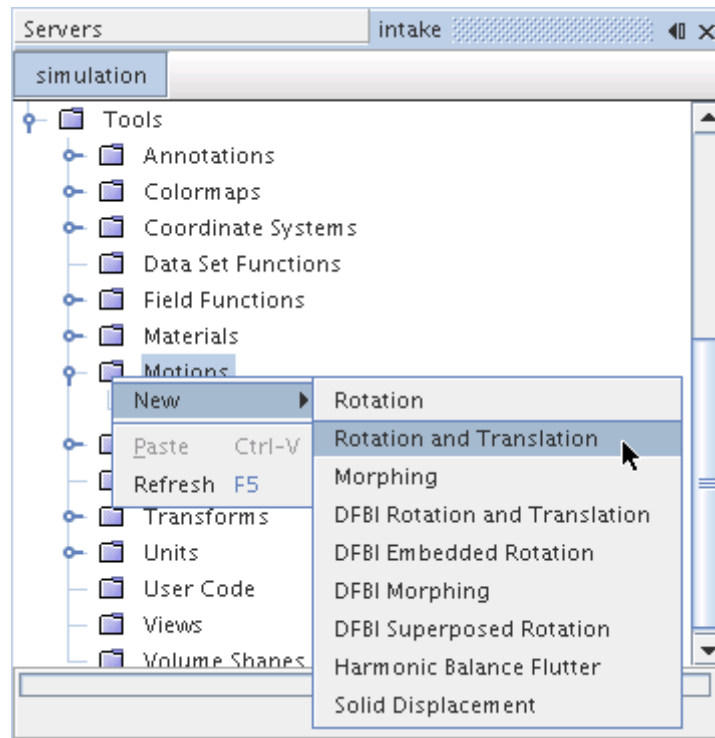


Figure 18 Rotation and Translation

After the motion is set you need to assign the motion model to a region:

3. Select the “Regions > [Region] > Physics Values > Motion Specification” node and set “**Motion**” to the relevant motion model. For this case the motion is assigned to the door within the intersect(overset) region.

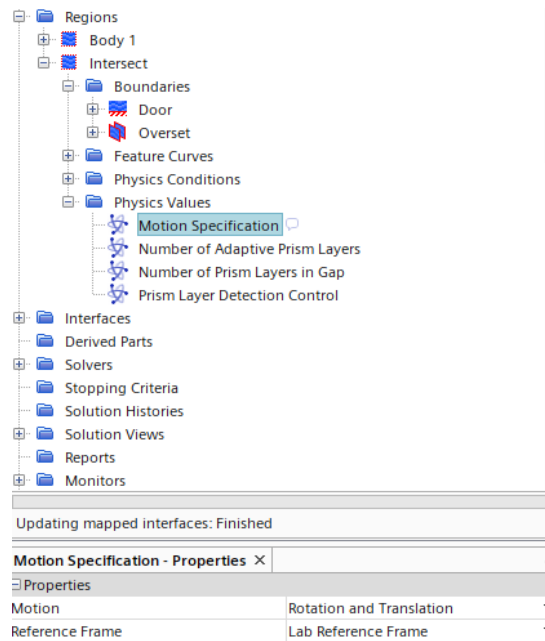


Figure 19 Motion Specification in the Region

After the motion is created and have been assigned to a region there are still some things to consider. Amongst them you have:

- Axis Direction - Specifies the direction vector that defines the axis of rotation, with respect to the selected Coordinate System.
- Axis Origin - Specifies the position vector that defines the origin of the axis of rotation, with respect to the selected Coordinate System.
- The rotation rate around the axis (entered as a scalar quantity using either a constant value or a space-invariant expression). Here field functions have been used to set the wanted motion for the different simulations. This will be explained in Field functions.
- Cordiante system – As a default the coordinate system is set as the one used when drawing up the geometry. For our case we want the origin to be where the door is rotating as shown in Figure 21 under. A new cartesian coordinate system is created for this cause.

Rotation and Translation - Properties	
Properties	
Axis Direction	[0.0, 0.0, 1.0]
Axis Origin	[0.0, 0.0, 0.0] m
Rotation Rate	\$_{RR}\$
Translation Velocity	[0.0, 0.0, 0.0] m/s
Coordinate System	Laboratory->Cartesian 1
Managed Coordinate Systems	[]
Tags	[]

Figure 20 Rotation and Translation Properties

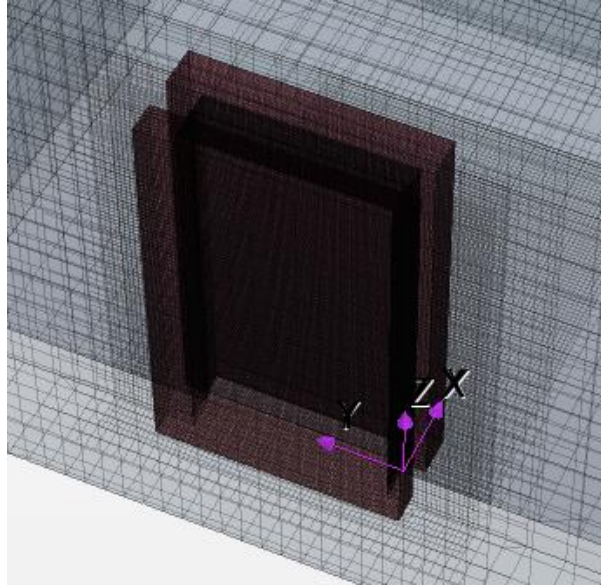


Figure 21 Cartesian Coordinate system

Lastly it is wanted to move the door at a certain speed within a specified time interval. This can be done by creating a “Field Function”.

## 2.2.6 Field functions

Field functions allow you to access fields (scalar or vector data that are evaluated at cells, vertices, or boundary faces) in Simcenter STAR-CCM+. You can use field functions to visualize the computed fields, to specify boundary and region values, or to define initial conditions. It can also be used to fix a motion at wanted speed and time. For this task, the field functions have been used for three different cases:

- Fixing the opening and closing motions for the different types of doors
- Fixing the initial conditions of the mass fraction of the SF6
- Fixing the initial conditions of the temperature for the thermal cases

### 2.2.6.1 Door opening and closing motion

It was chosen to look at a total opening and closing time of 4 seconds and 8 seconds. For the case of the hinged door with a 4 s opening time the following field function was used:

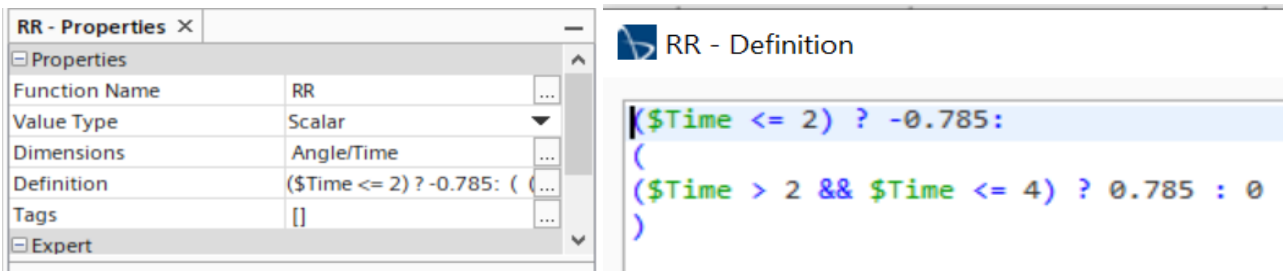


Figure 22 Field function: Rotation Rate

RR(Rotation Rate) is defined to make the door move at wanted speed within a time interval. This means that the door moves with a speed of the -0.785 rad/s in 2 seconds until it is fully open(At this point the door was perpendicular to the wall). Then it will turn with a speed of 0.785 rad/s without stopping until  $t = 4s$  and the door is fully closed again The door opening and closing times was inspired by Chang et al [8]. The reasoning for this can be found in the verification chapter. In the case of 8 second opening time the same principle was used, only the speed and the time was adjusted.

For the sliding motion a new field function called Slide was created. The same principal was adopted here but the speed needed to be adjusted to a sliding speed of m/s instead of rad/s.

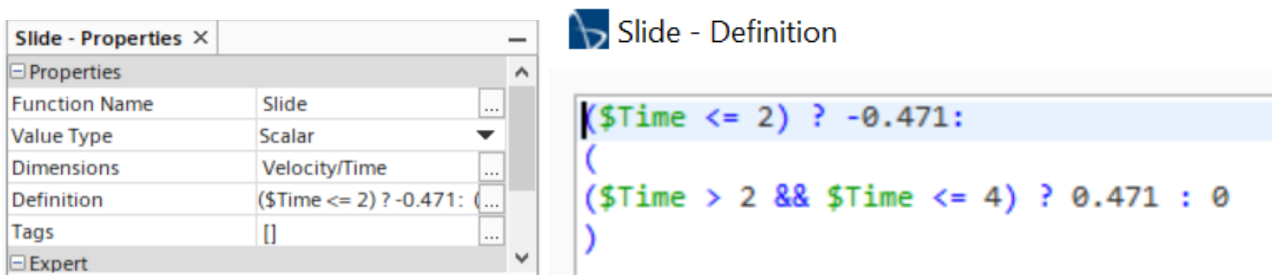


Figure 23 Field function: Slide

In the final case of the Elevator an additional Slide function was created to be able to make the two bodies move in opposite direction at the same time.

### 2.2.6.2 Multicomponent gas

To be able to fix a wanted mass fraction of SF<sub>6</sub> in the outer room two field functions was created. This was done by fixing the inner room to be just air and the rest with a mass fraction of 0.000058 which equals to a concentration of 706.2 mg/m<sup>3</sup>.



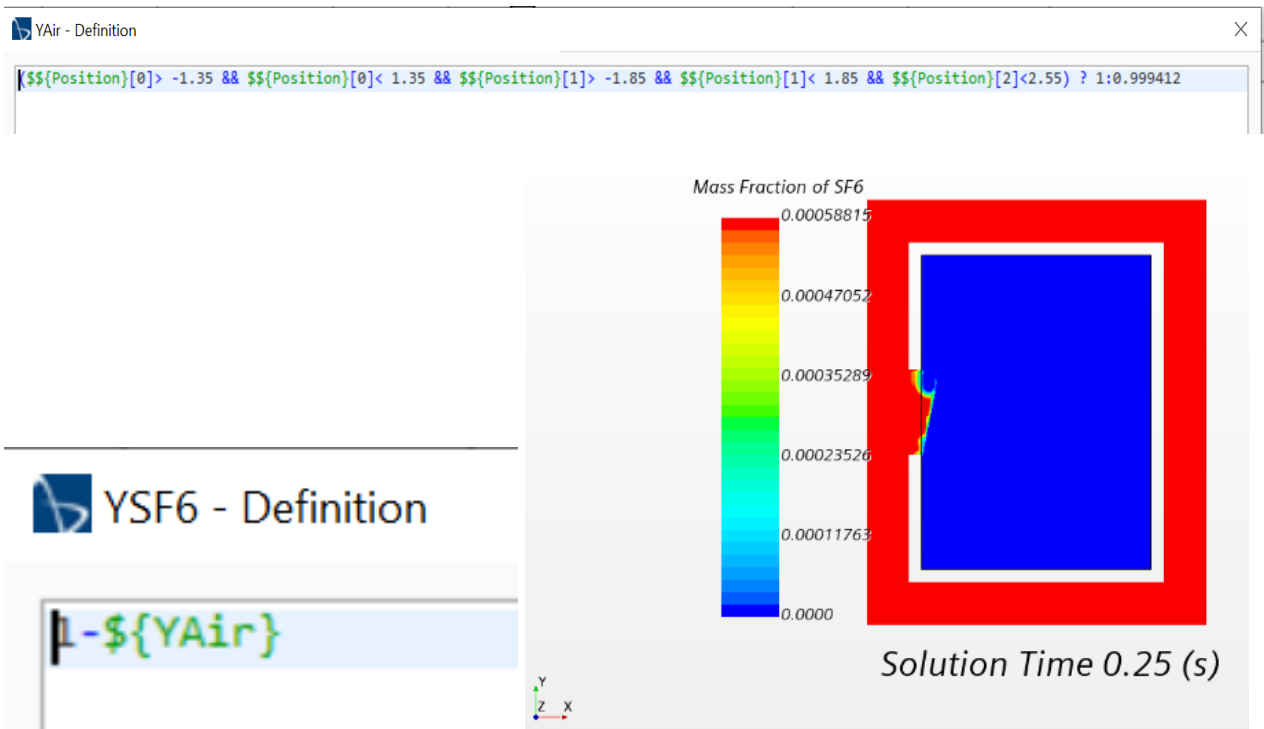


Figure 24 Field function for fixing the mass fraction of SF6 and a scalar scene showing the Mass Fraction of SF6

After the field functions are created the method can be set in “species mass fraction” within the Initial conditions. See Figure 25.

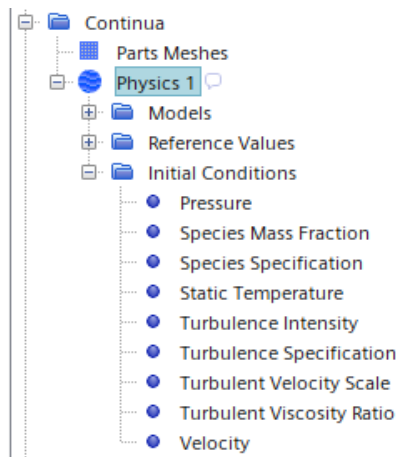


Figure 25 Species mass fraction

To fix the temperature for the thermal case the same method was used.

## 2.2.7 Presentation grid

The presentation grid part samples data from regularly spaced intervals on a finite plane in a region.

This part is similar to a plane section, the difference being that the output points of a presentation grid are sampled on a regular grid. The points from the plane section are based on the topology and discretization of the underlying mesh. Simcenter STAR-CCM+ allows the creation of a presentation grid part from parent parts consisting of regions and boundaries only. The finite plane can be defined by specifying a point for the origin, and two other points which, together with the origin define two axes for the plane. An explicit plane tool is available to assist with positioning the plane graphically. The presentation grid can be useful for extracting data at structured intervals in a region. For this task the presentation grid is used to extract transient data of relevant flow-field variables. velocity, mass flux, temperature and heat flux.

When creating a rectangular grid it is needed to choose the X resolution and the Y resolution as well as origin and two points as shown in Figure 26. When creating the presentation grid, the X resolution and Y resolution must be set as reasonable values. If the presentation grid is too coarse with a low resolution the interpolated solution may appear as data with low resolution. If you have too few points much information will be missed. To know which resolution you want it is needed to know how much distance you can have between each point. A good way to choose this is by reviewing the mesh size in this part. A good rule is that  $\Delta x$  and  $\Delta y$  (distance between the points in x and y direction) should not be bigger than 2\*the mesh size. A mesh size of 0.02 m makes a choice of  $\Delta x=0.04$  m and  $\Delta y=0.04$  m reasonable but it would have been even better with a finer resolution like the actual mesh. With the doors measurements of 2m\*1m this equals to a X resolution of 25 and Y resolution of 50. Which still provide some good results.

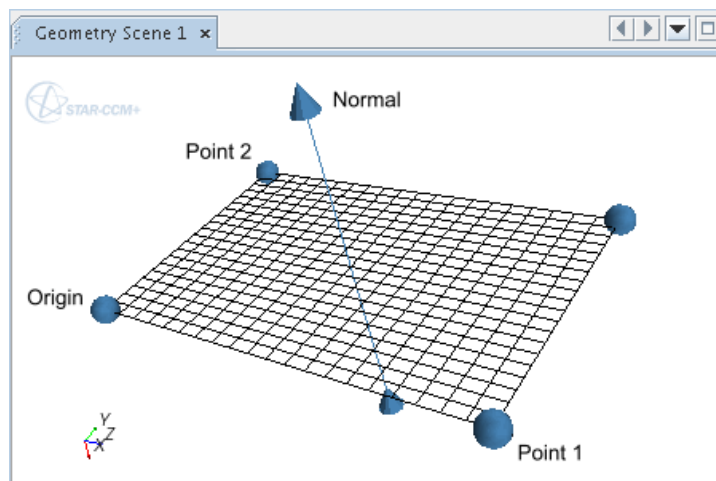


Figure 26 Drawing of the grid

When setting the origin and the two points it is important to remember to go 0.02 m in from the edge (the mesh size). That is why the points and the origin for example is placed at a Y-value of -0.48 and 0.48 instead of -0.50 and 0.50 where the door starts and stops in Y-direction. If the points are placed at -0.50 and 0.50 the points will also extract information from 0.02 m of the solid wall.

Presentation Grid - Properties X	
[- Properties	
Parts	[Body 1, Intersect] <span>▼</span> <span>...</span>
Normal	[-1.0, -4.62592926927...E-16, 0.0] m, m, m <span>...</span>
Origin	[-1.5000000000000002, 0.48, 0.02] m, m, m <span>...</span>
Point 1	[-1.4999999999999998, -0.48, 0.02] m, m, m <span>...</span>
Point 2	[-1.5000000000000002, 0.48, 2.02] m, m, m <span>...</span>
Coordinate System	Laboratory <span>▼</span>
X Resolution	25
Y Resolution	50
Tags	[] <span>...</span>

Figure 27 Presentation Grid properties

This gives us a grid looking like shown in Figure 28 . figure x show the velocity through the grid at t=4s for a non thermal and a thermal simulation of the elevator door.

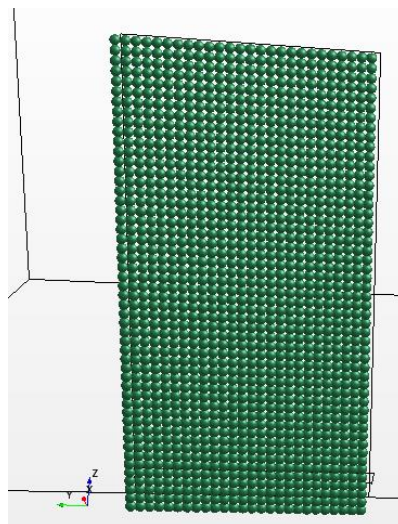


Figure 28 Presentation Grid

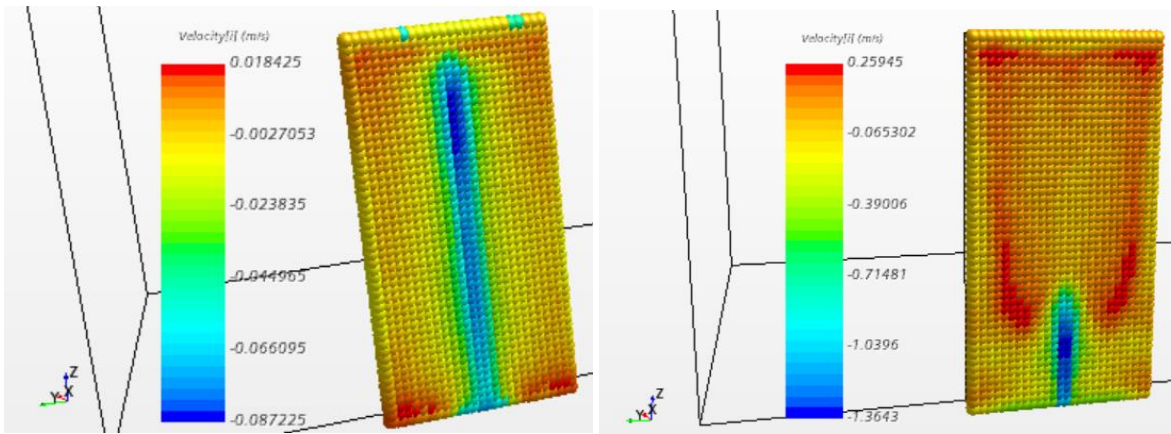


Figure 29 Velocity through the grid at t=4s for a non-thermal case and thermal case

To be able to store the desired information from the presentation grid the XYZ Internal table is created and recorded. The presentation grid is chosen as a part and the wanted information I chosen to be extracted. This is stored in a excel file by choosing to “save to file”. Example files for both the non-thermal case and the thermal case can be found in appendix F.

XYZ Internal Table - Properties	
Extracted	[Mass Fraction of SF6, Velocity[i], Density, Area...
Scalars	[Mass Fraction of SF6, Velocity[i], Density, Ar...
Parts	[Presentation Grid]
Coordinate System	Laboratory
Data on Vertices	<input type="checkbox"/>
Representation	Volume Mesh
Tags	{}

Update - Properties	
Enabled	<input checked="" type="checkbox"/>
Auto Extract	<input checked="" type="checkbox"/>
Trigger	None
Save To File	<input checked="" type="checkbox"/>
Output Directory	C:\Users\loys_h\Dropbox (Master 2021)\STAR-...
Base Filename Append Tag	table

Figure 30 Extracting information with XYZ Internal Table

To extract the information that is stored in the excel files, Matlab has been used. 4 different scripts were created:

- 1. A script for the non-thermal cases that could plot the cumulative mass of SF6 exchanged through the door during the simulation.
- 2. A script for the thermal cases that could plot the cumulative mass of SF6 exchanged through the door, as well as the cumulative energy and the cumulative mass of the gas mixture exchanged during the simulation.
- 3. A script for the non-thermal cases that could show time snaps of velocity, mass flux and flux of SF6.
- 4. A script for the thermal cases that could show time snaps of velocity, mass flux, flux of SF6 as well as temperature and heat flux.

Figure 31 shows a part of script number 2 used for the thermal cases.

```

1  clear all; close all; clc;
2
3  dt = 0.005; % time step (s)
4  dx = 0.04; % length of the presentation grid (m)
5  dy = 0.04; % length of the presentation grid (m)
6  A = dx * dy; %Area m^2 of the presentation grid
7              % corresponding to each grid point
8
9  n = 800;      % Total number of files
10 m = n+1;
11
12 E = zeros(m,1);
13 Mmix = zeros(m,1);
14 M = zeros(m,1);
15 part1 = 'XYZ_Internal_Table_table_';
16 part3 = '.csv';
17 count = 1;
18 cp = 1003.5 ; %J/kg*K
19
20
21 for i = 1:n
22     part2 = num2str(i, '%d');
23     filename = [part1 part2 part3 ]
24     Data = readtable(filename);
25     mydata = table2array(Data);
26     mdot = A * mydata(:,1) .* mydata(:,2) .* mydata(:,3); %kg/s of SF6
27     totalm = mdot * dt; %kg of SF6
28     count = count + 1;
29     M(count) = sum(totalm);
30     totale = cp * A * mydata(:,2) .* mydata(:,3) .* mydata(:,6)* dt %joule
31     E(count) = sum(totale);
32     mdotmix = A * mydata(:,2) .* mydata(:,3); %kg/s of SF6
33     totalmmix = mdotmix * dt;
34     Mmix(count)=sum(totalmmix);
35 end

```

Figure 31 Matlab script for presenting cumulative mass and Energy

The usage of matlab to extract information gave some interesting results. These are shown and discussed in Results&Discussion. Snapshots from the other scripts that was used can be found in Appendix B.

The following integral is calculated for the whole area of the grid over a chosen amount of timesteps. This is how the cumulative values can be found.

$$\varphi(t) = \left[ \iint_A (\rho \phi \vec{V} \cdot \vec{n} dA) \right] dt$$

Here  $\rho$  is density,  $\vec{V} \cdot \vec{n}$  is the normal velocity and  $\phi$  can be different depending of what information that is wanted. For example:

$\phi = 1$  for mass

$\phi = Y_{SF6}$  (mass fraction of SF6) for mass of SF6

$\phi = C_p T$  for Energy

### 3 Verification CFD methods

To verify the CFD methods used in this thesis we have chosen a test case that is similar to the simulations that is going to be performed. It is similar in both physics and geometry. Chang et al [8] looked in to control room contaminant inleakage produced by door opening and closing. This was done with the help of dynamic simulations and experiments. This involves looking at different rotating times and how this effect the spreading of SF6 traces gas into the room. The dynamic simulations were done by using a commercial CFD program, Ansys FLUENT 15.0. The method and input are well explained so it is possible to recreate a similar test case in STAR CCM+.

#### 3.1 Verification case setup

This 3D test case consists of a turbulent coupled flow created by the motion of a hinged door. The RANS model with RNG k- $\epsilon$  was adopted in this study. The hinged door was the only moving object that opens and closes during the simulation. To improve numerical accuracy the second-order upwind scheme was used for discretizing pressure, density, momentum, tracer gas, and energy in the governing equation.

The model consists of an inner room, an outer room, and a hinged door. The dimensions of the inner room is 2.55 m (L)  $\times$  2.11 m (W)  $\times$  2.55 m (H) as shown in Figure 32 the dimensions of the inner room are the same as those of the Main Control Room (MCR) hallway. Since the hallway is the key and vulnerable area for door inleakage, the inner room is set as the hallway. As shown in Figure 32 the outer room encloses the inner room entirely. The dimensions of the outer room are 3.80 m (L)  $\times$  3.60 m (W)  $\times$  3.00 m (H).

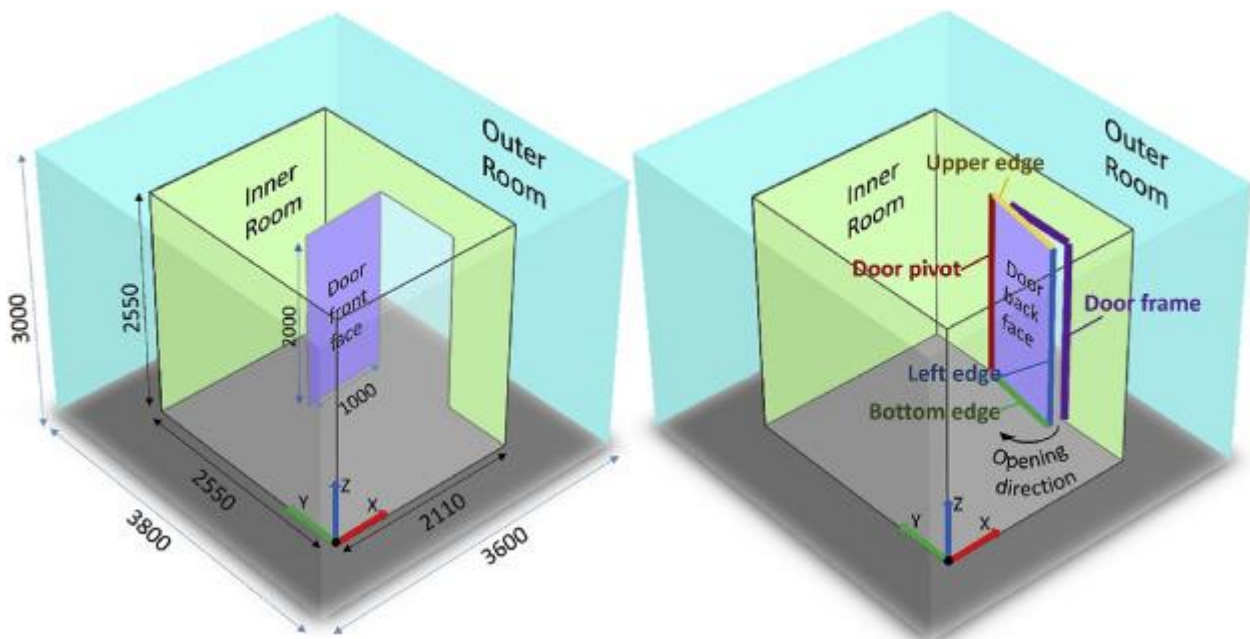
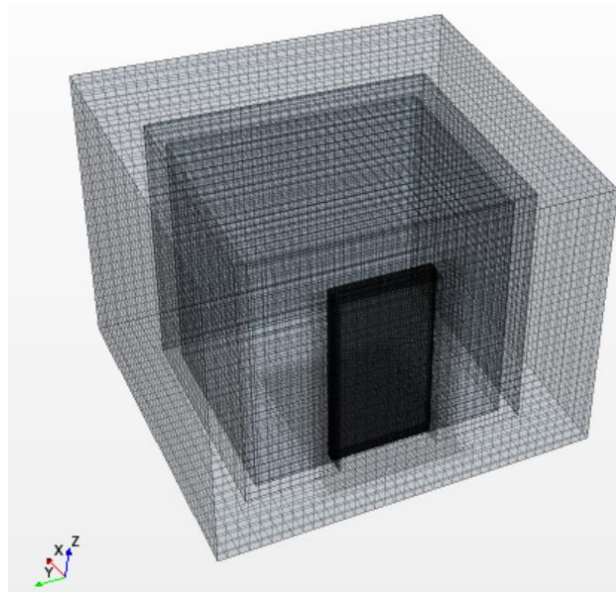


Figure 32 Geometry test case

On the wall of the inner room, there is a 2.00 m × 1.00 m hinged door. Each part of the door is illustrated and labelled in Figure 32. The door is hinged along one side to allow the door to pivot away from the doorway. The door can only be pushed inwards, and this type of door is adopted in MCR engineering. The outer room represents the MCR ambient environment, and the inner room represents the MCR indoor environment. Since the study concerns inleakage solely from the ambient environment into the inner room, the outer room encompassing the inner room was chosen as the most appropriate setup. This is because all the air that leaks into the inner room originates solely from the outer room without any interference from other sources. Air inleakage through the door was detected using sulfur hexafluoride (SF6) tracer gas.



*Figure 33 Mesh scene showing the geometry in STAR CCM+*

### **Set up for dynamic simulation**

#### **boundary conditions**

- All the walls, the ceiling and the surfaces of the door was set as solid wall.
- The overset region was set as overset mesh
- There was no inlet or outlet for either room.

#### **Initial conditions:**

- The initial pressure of the inner and outer rooms was set at 101.325 kPa
- The temperature of both rooms was set at 22 °C.



- At  $t = 0$ , the initial SF6 concentration of the outer room was  $706.2 \text{ mg/m}^3$ , and the initial SF6 concentration of the inner room was zero. This model focused only on the inleakage induced by door rotating, which meant the inleakage caused by temperature difference or initial pressure difference was not taken into consideration. One difference between the verification test case and the actual setup is that in the article they only look at the SF6 inleakage. The simulations in STAR CCM+ also shows how the air goes out of the inner room and mixes with the air in the outer room. A mass fraction of 0.000588 equals to a concentration of  $706.2 \text{ mg/m}^3$  which is the concentration of SF6 in the outer room when the simulation starts.

The hinged door was initially parallel to the wall with a small gap between the door and the doorframe. When the simulation began, the door began to rotate at a given constant angular velocity until the door was fully opened. At this point the door was perpendicular to the wall. Without stopping, the door then rotated back until it was totally closed in its initial position. In the article it was chosen to look at six test cases with different rotating times in the range of  $T = 3.0 \sim 8.0 \text{ s}$ . was chosen based on the actual situation. In practice, it was found that when  $T < 3.0 \text{ s}$  for normal opening and closing, the angular velocity is too fast for most people; and when  $T > 8.0 \text{ s}$ , the process of door opening and closing became too slow and abnormal. It was chosen to look at the 8 s simulation and compare the results at three different times. This was done by comparing the vector and scalar scenes. Each time step was set to 0.005 s.

### 3.2 Results verification case

To compare the results from The STAR CCM+ simulations with the results from the verification case it was chosen to compare the mass fraction of SF6 and the velocity in a scalar scene and a vector scene at different times. This is a good way to visualise the results. The comparison is shown for  $t = 1.5 \text{ s}$ ,  $3.5 \text{ s}$  and  $7.9 \text{ s}$  for both scenes.

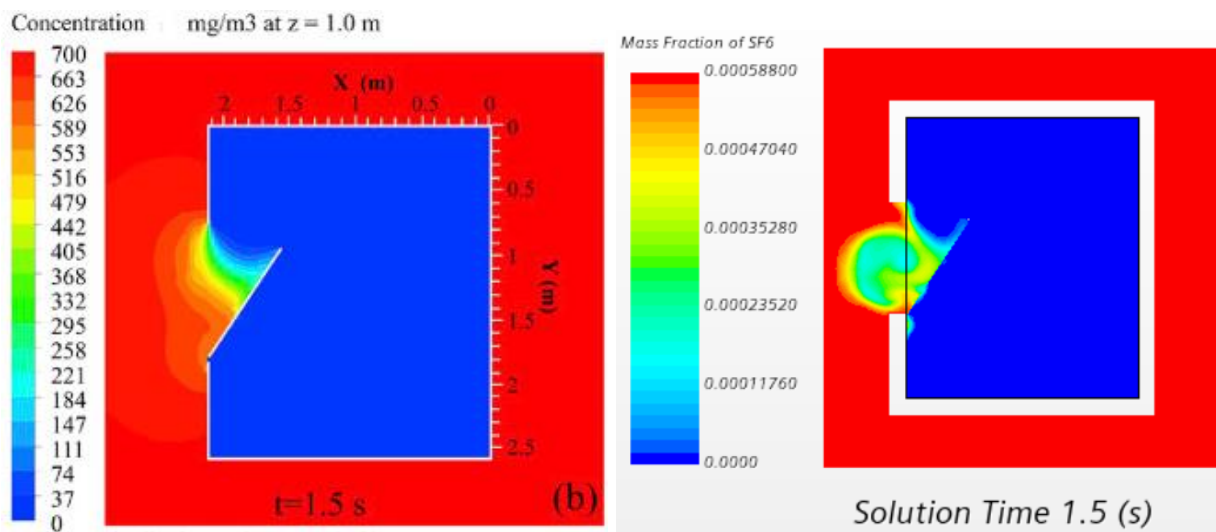


Figure 34 Comparison of Mass fraction of SF6 at  $z=1\text{m}$ ,  $t=1.5 \text{ s}$

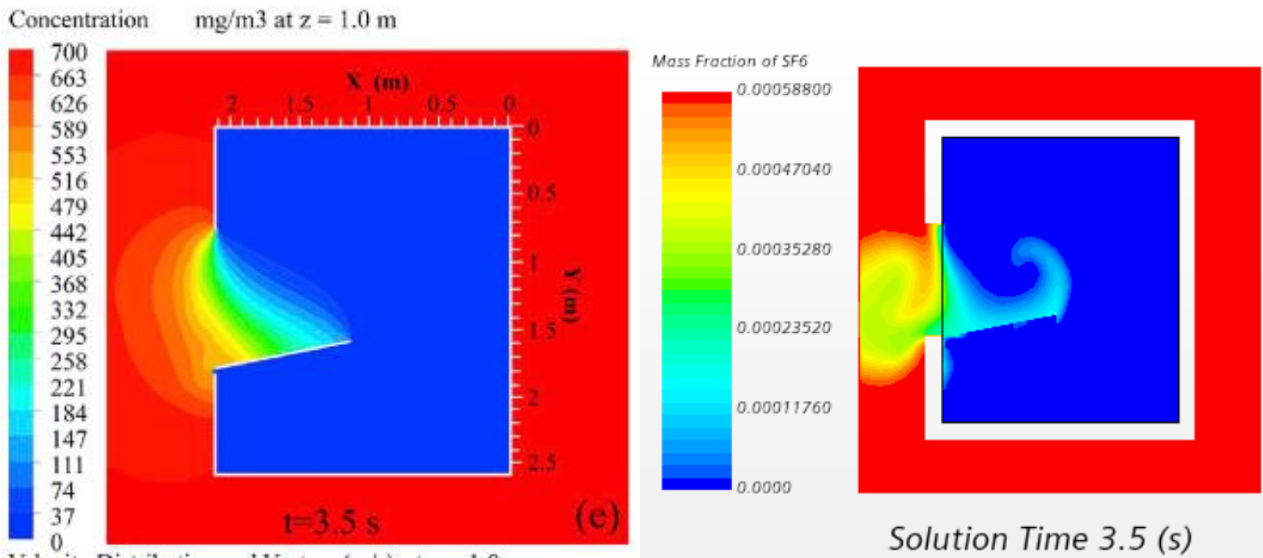


Figure 35 Comparison of Mass fraction of SF6 at z=1m, t=3.5 s

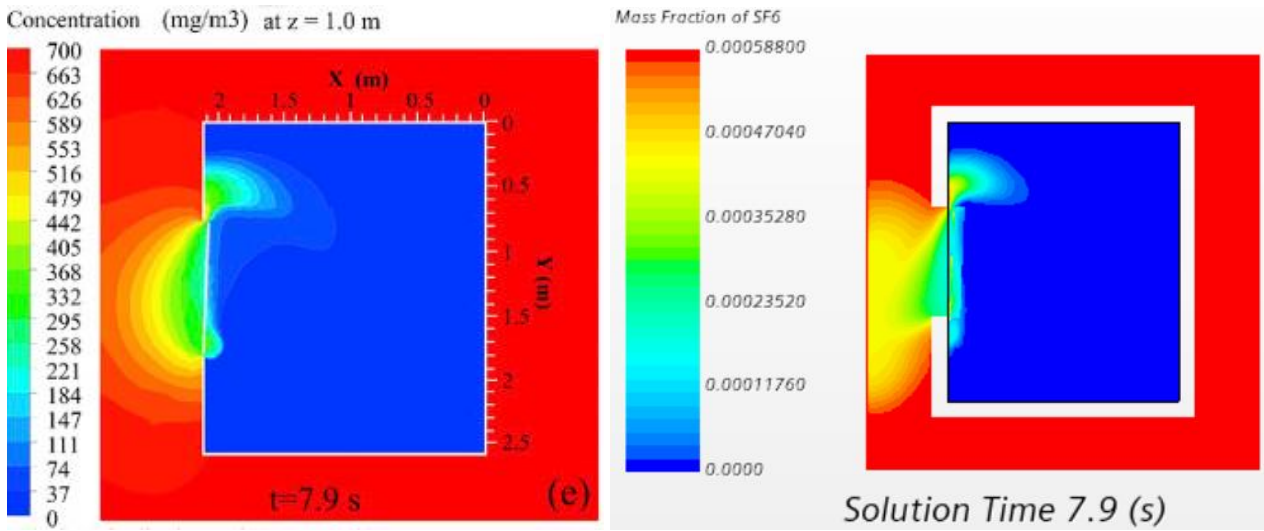


Figure 36 Comparison of Mass fraction of SF6 at z=1m, t=7.9s

The scalar scenes show a very similar trend. At t=1.5 and t=7.9 it is clearly seen, while at 3.5 s it looks a little more different. This can be due to a lot of different factors like for example meshing or how they fixed the constant concentration of the SF6 in the outer room.

Lee et al [17] also looked at the motion of a hinged door. The visualized airflow at different times during door opening and closing and the results of the CFD simulation are shown in Figure 37. The standard  $k-\epsilon$  turbulence model was also used here. The picture after 4 seconds of running time in Figure 37 under is seen to have very similar characteristic as seen from the scalar scene at 3.5 seconds.

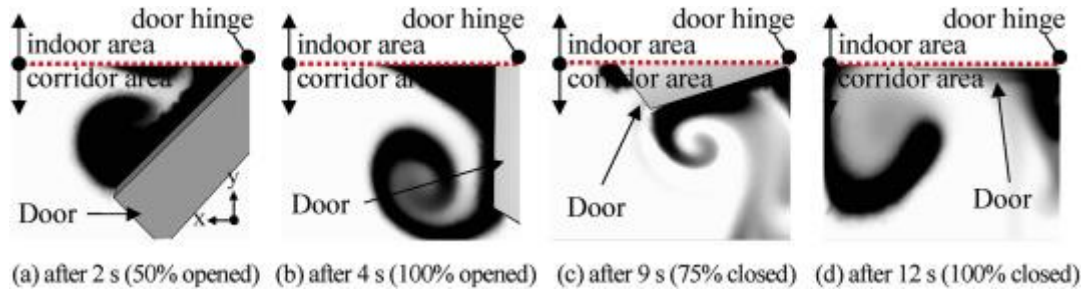


Figure 37 visualized airflow at different times

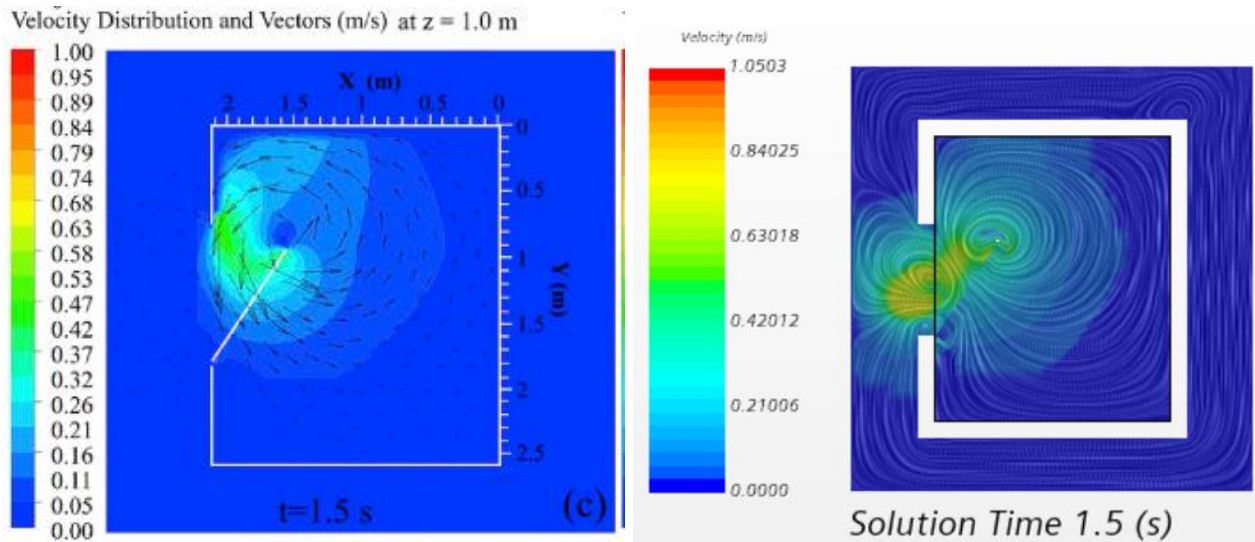


Figure 38 Comparison of velocity at  $z=1m$ ,  $t=1.5s$

Velocity Distribution and Vectors (m/s) at  $z = 1.0$  m

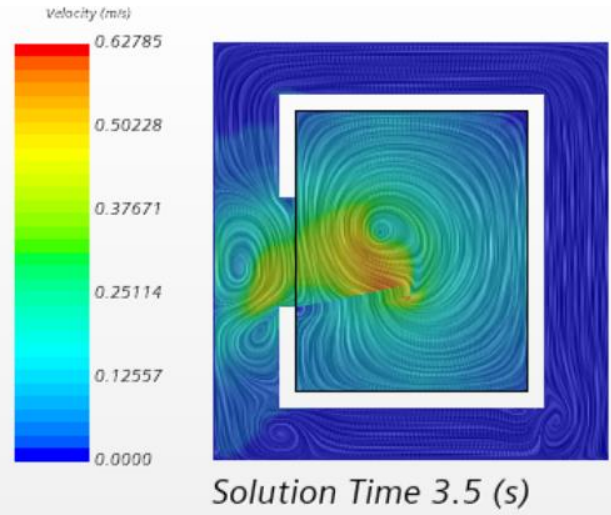
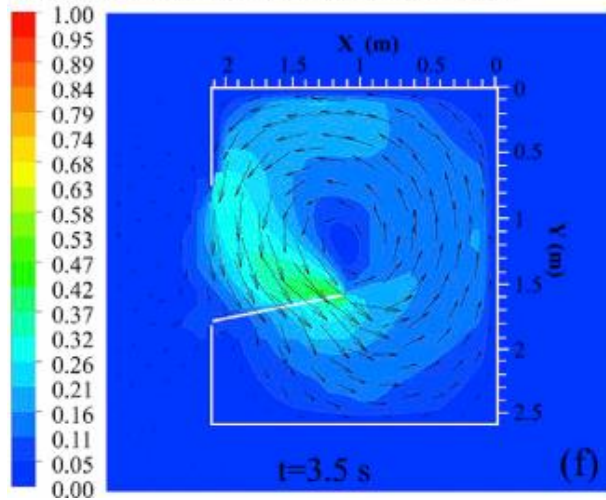


Figure 39 Comparison of velocity at  $z=1m$ ,  $t=3.5s$

Velocity Distribution and Vectors (m/s) at  $z = 1.0$  m

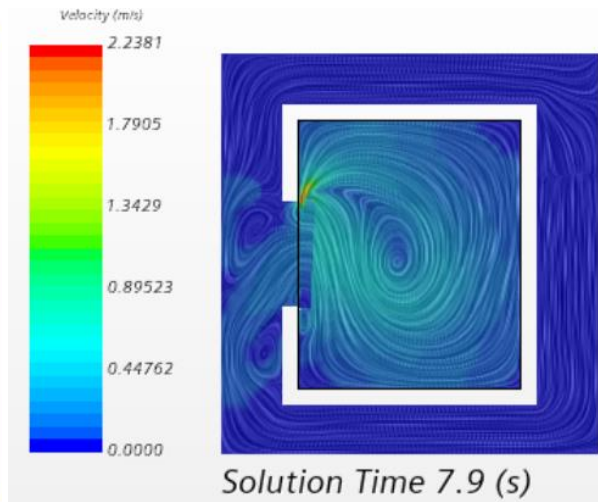
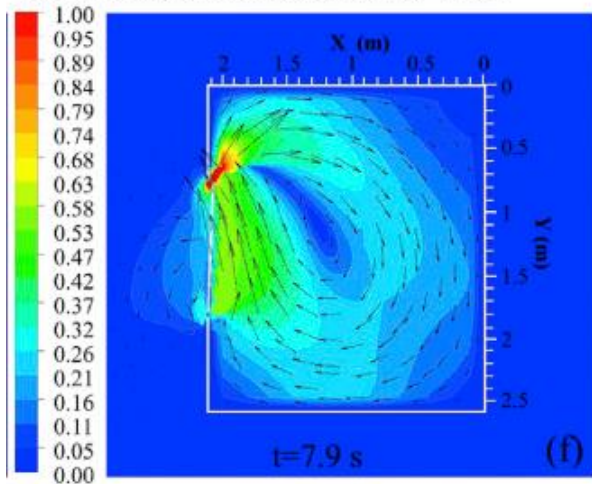


Figure 40 Comparison of velocity at  $z=1m$ ,  $t=7.9s$

The Line Integral Convolution (LIC) for the vector scenes also looks similar. When reviewing the flow field and the velocity at different places it is seen to be in very good agreement. At  $t=1.5$  seconds it is seen a higher speed in about the same place and the general flow looks to be going in the same direction. At  $t=3.5$  s and  $7.9$  s it is also seen that the velocity is increasing in the same areas. It is evident that from the figures of the comparison that the present solutions agree well with the literature.



## 4 Problem setup

In this part the problem setup for the simulations is presented. The simulations will consist of three different types of doors. One hinged, one sliding and one elevator door. In addition to the different door types it has also been looked at different opening times and thermal effect. Besides how the door moves the geometry and boundary conditions are the same in each case. For the three different door types it has also been investigated how a temperature difference effect the airflow. This has been done by making the inner room a cold storage room. That means changing the initial conditions so there is a temperature difference between the inner and the outer room. The geometry problem setup for the simulations in this thesis is inspired by the verification case. Only the measurements are altered. The bigger room makes it possible to have the sliding door and the elevator door fully open without a problem.

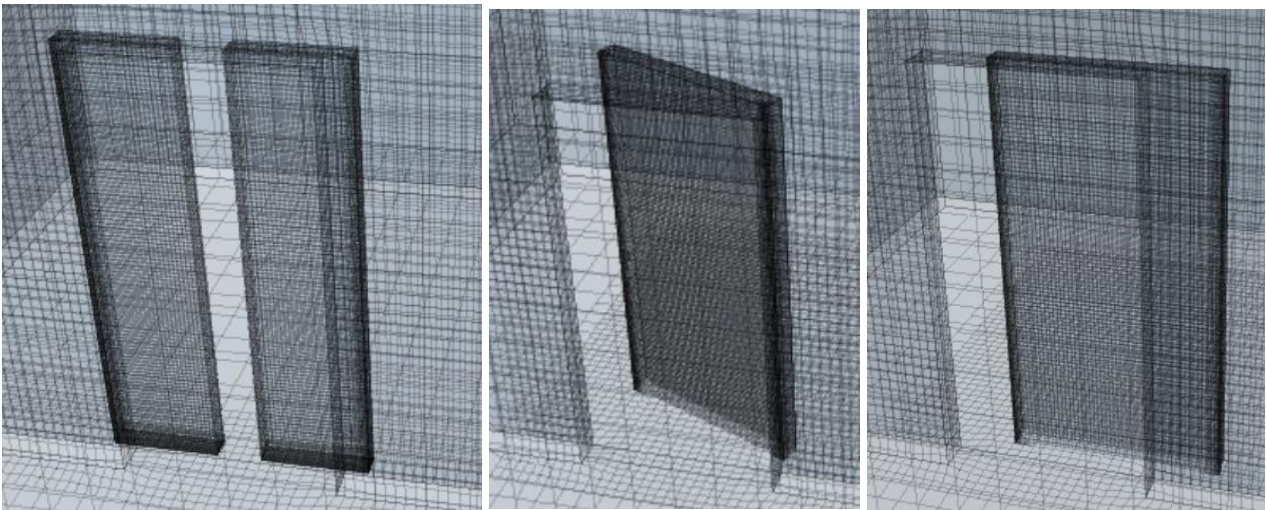


Figure 41 Elevator door, Hinged door and Sliding door

The geometry for the problem setup is the same as for the validation case. The only difference is the measurements.

Table 3 Measurements for the problem setup

	H (z direction) mm	W (x direction) mm	L (y direction) mm
Outer room	3000	4000	5000
Inner room	2550	2700	3700
Door	2000	150	1000

Table 4 Wall, roof and door thickness

Part	Thickness (m)
Walls( Inner room)	0.15
Roof( Inner room)	0.15

Door	0.15
------	------

**Mesh generation**

Automated mesh in Star-CCM+ was used to generate the mesh. The method for generating the mesh is explained in more detail in the method. For each of the three simulations it was a different number of cells. This is because of the different motions required a finer mesh in different areas. The settings for the background region in Table 6 and overset region in Table 7 was the same for each case.

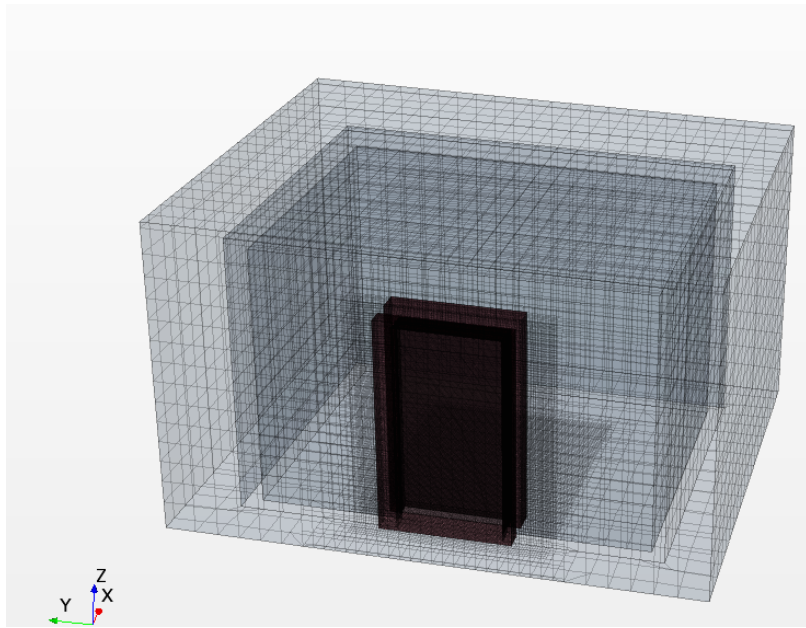


Figure 42 Mesh scene displaying the mesh

Table 5 Number of cells for the simulations

<i>Simulation</i>	<i>Number of cells</i>
<i>Hinged</i>	317901
<i>Sliding</i>	351290
<i>Elevator</i>	344141

Table 6 background region mesh

<i>Property</i>	<i>Value</i>
<i>Base size</i>	0.2m

<i>Target surface size</i>	100%=0.2 m
<i>Minimum surface size</i>	10%=0.02
<i>Surface growth rate</i>	1.3
<i>Number of prism layers</i>	2
<i>Prism layer stretching</i>	1.5
<i>Prism layer total thickness</i>	33.33%=.0.066
<i>Maximum cell size</i>	100%=0.2m
<i>Post mesh Optimisation</i>	Enabled

Table 7 Overset region mesh

<i>Property</i>	<i>Value</i>
<i>Base size</i>	0.02m
<i>Target surface size</i>	100%=0.002 m
<i>Minimum surface size</i>	10%=0.02
<i>Surface growth rate</i>	1.3
<i>Number of prism layers</i>	2
<i>Prism layer stretching</i>	1.5
<i>Prism layer total thickness</i>	33.33%=.0.0066
<i>Maximum cell size</i>	100%=0.02m
<i>Post mesh Optimisation</i>	Enabled

## Initial conditions

Table 8 Initial conditions for the problem setup

<i>Pressure</i>	Constant 0.0 Pa
<i>Species Mass Fraction</i>	Fixed with Field Function
<i>Species Specification</i>	Mass Fraction
<i>Static Temperature</i>	Non-Thermal: Constant 295 K for Thermal: Field function
<i>Turbulence Specification</i>	K + Epsilon
<i>Turbulence Dissipation Rate</i>	Constant 1.0E-6 m <sup>2</sup> /s <sup>3</sup>
<i>Turbulent Kinetic Energy</i>	0.001 J/kg

The turbulence model, physics models and the boundary conditions are explained in the method.



## 5 Results & Discussion

Simulations for three different types of doors were performed. The results are divided in to two parts:

### **Different door motions:**

The first round of simulations involved comparing the effect of different type of doors. a Hinged door, a sliding door and an elevator door was investigated. The time for the opening and closing of the door was fixed at 4s and the effects on the airflow was compared. It was also tested how the opening time effects the airflow for the hinged and the sliding door. In this case a run with a total run time of 8s was also performed.

### **Thermal effects:**

Thermal case. The inner room was looked at as a cold storage room and the temperature was fixed at -20 °C. The outer room had a temperature of 22 °C and it was investigated how this temperature difference effects the airflow and the exchange of SF<sub>6</sub>.

In the end the results are compared and discussed.

### 5.1 Different door motions

In this first part of the results only the door motion is in focus. The hinged door, sliding door and elevator door will be compared. First a visual comparison will be done. This will be done by monitoring the mass fraction of SF<sub>6</sub> in a scalar scene and by monitoring the velocity with the use of The Line Integral Convolution (LIC) in a vector scene. The cumulative mass of SF<sub>6</sub> exchanged through the door opening will also be compared with the help of a prestation grid. The presentation grid also provides time snaps at different timesteps, so it is possible to compare velocity, mass flux and mass of SF<sub>6</sub> at different times of the simulation.

### 5.1.1 Hinged door

Figure 43 and Figure 44 shows the mass fraction of SF6 at  $z=1\text{m}$  in two different simulations of a hinged door. The difference between the two figure shows that the opening time effects the spread of SF6 in the room and how much air that is exchanged between the two rooms.

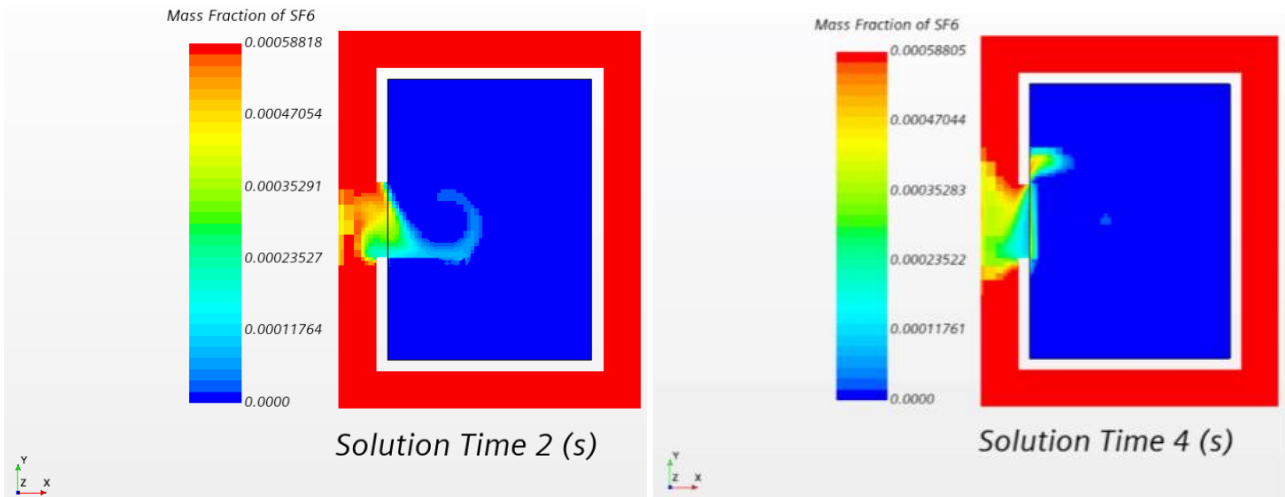


Figure 43 Hinged door 4 s opening time, Mass fraction of SF6 at  $z=1\text{ m}$

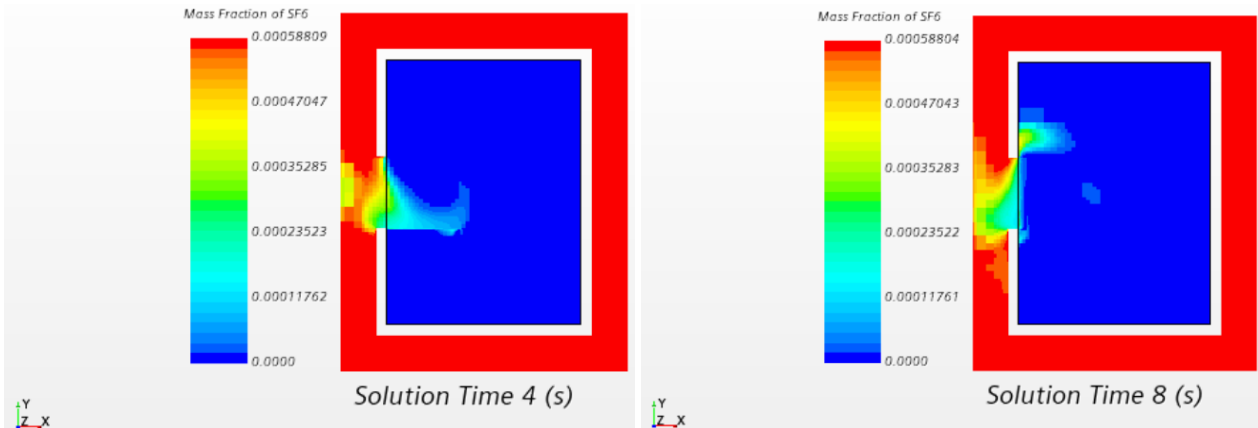


Figure 44 Hinged door 8 s opening time, Mass fraction of SF6 at  $z=1\text{ m}$

Figure 45 and Figure 46 shows the velocity at  $z=1\text{m}$ . With a opening motion of 4 seconds a higher air velocity in the room is created. This indicates that opening the door slower creates a lower air velocity and less mixing of the air for the hinged door.

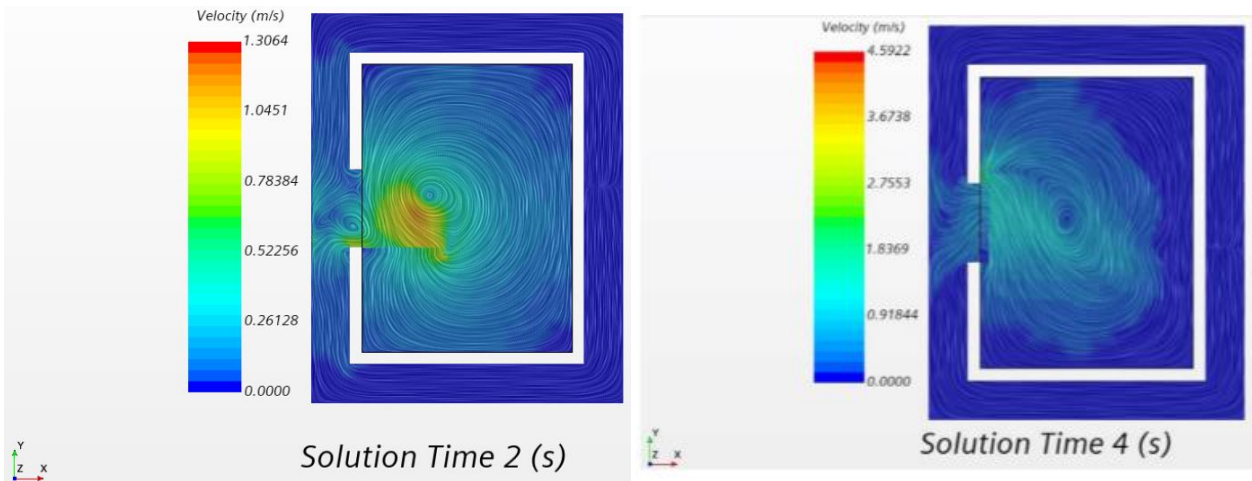


Figure 45 Hinged door 4 s opening time, velocity at z=1

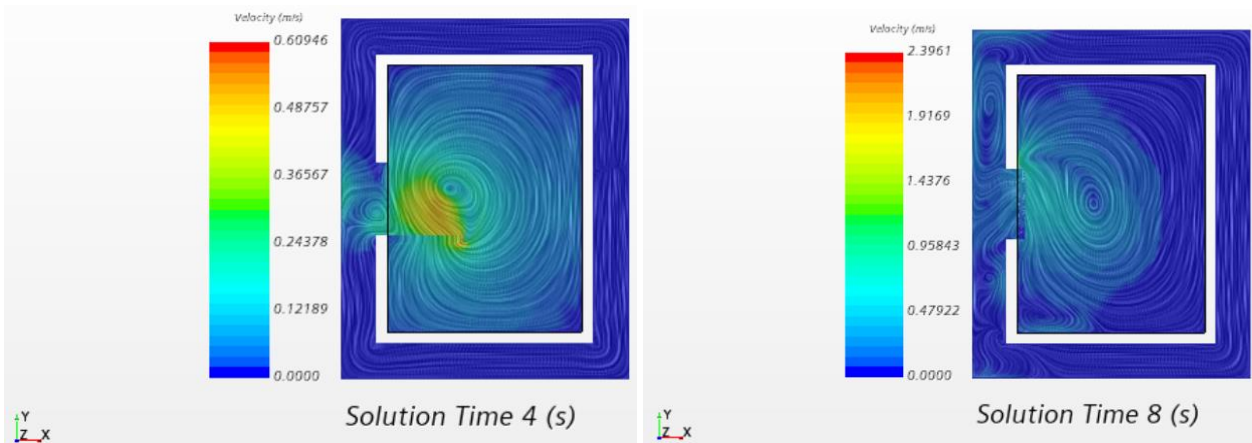


Figure 46 Hinged door 8 s opening time, velocity at z=1

The residuals for the simulations were typically similar to Figure 47. Residuals for some of the other cases can be found in Appendix A.

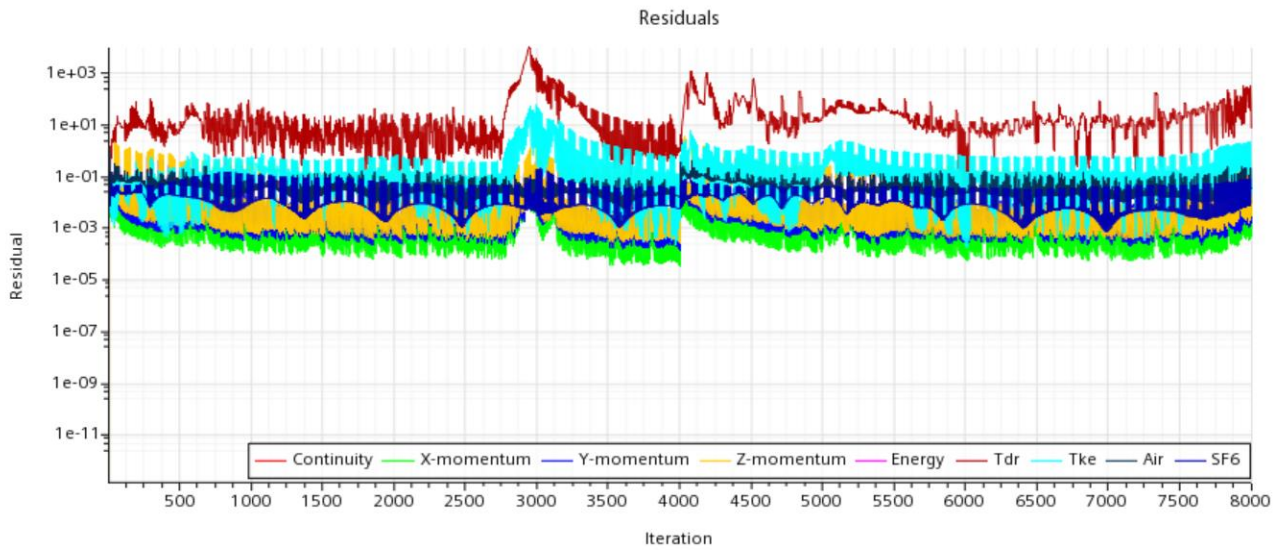


Figure 47 Residuals hinged door 4 s opening time

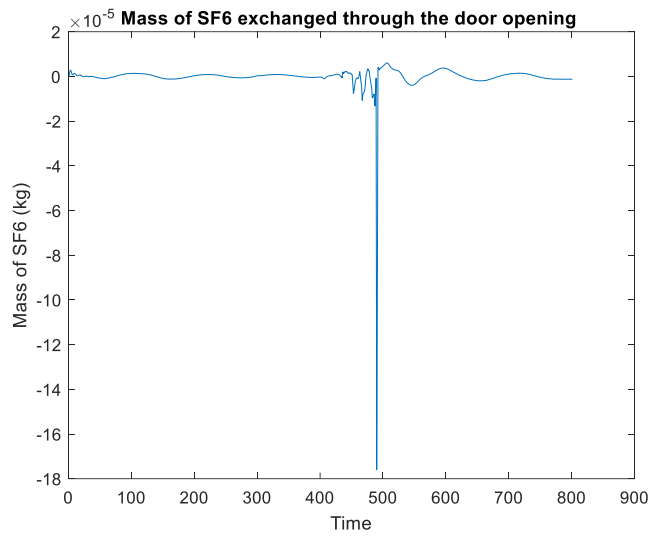


Figure 48 Hinged door, mass of SF6 exchanged through the door opening

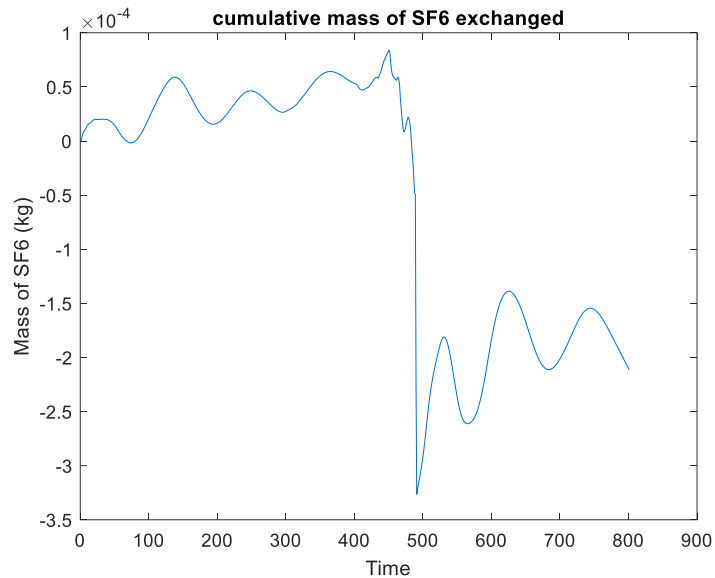


Figure 49 Hinged door, cumulative mass of SF6 exchanged through the door opening

Figure 49 show the cumulative mass of SF6 exchanged through the door opening. After the simulation is ended a negative cumulative mass of  $-2.11\text{E}-04$  kg is the result. This means by the end of the simulation 0.2 g more of SF6 is going out through the grid versus going in. It is seen in both Figure 49 and Figure 50 that it is a change right before 500 timesteps. This is likely because at 400 timesteps which equals to 2 second running time the door is fully opened and turns the other way. Some of the SF6 that has already entered is then “pushed” out by the hinged door.

### 5.1.2 Sliding door

Figure 50 and Figure 51 show the mass fraction of SF6 at  $z=1\text{m}$  in two different simulations of a sliding door. The difference between the two figure shows that the opening time effects the spread of SF6 in the room and how much air that is exchanged between the two rooms.

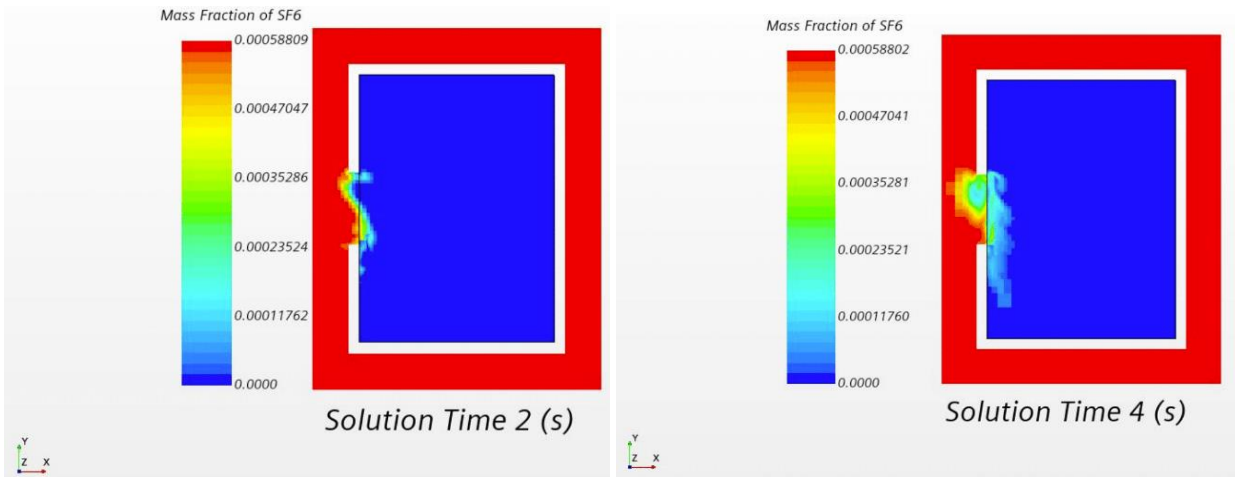


Figure 50 Sliding door 4 s opening time, Mass fraction of SF6 at z=1 m

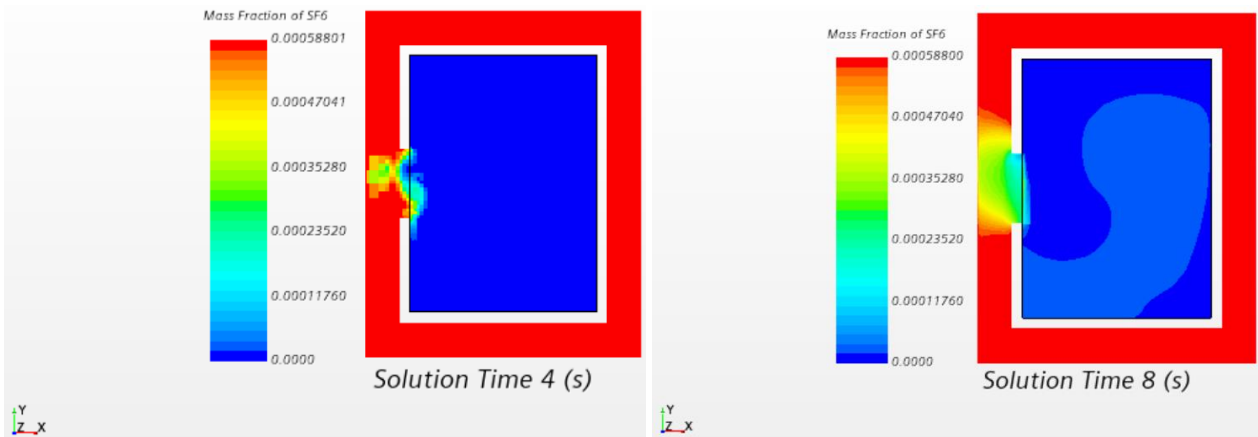


Figure 51 Sliding door 8 s opening time, Mass fraction of SF6 at z=1 m

Figure 52 and Figure 53 shows the velocity at z=1m. With a opening motion of 4 seconds a higher air velocity in the room is created. This tells us that opening the door slower creates a lower air velocity and less mixing of the air. The effect is less then of the hinged door but a differnce can still be seen.

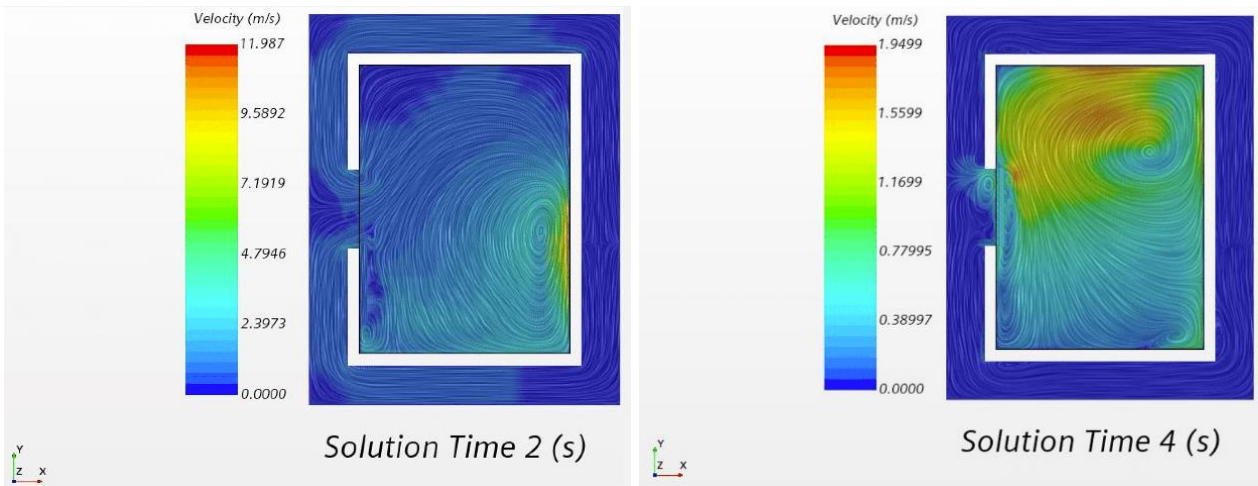


Figure 52 Sliding door 4 s opening time, velocity at  $z=1$

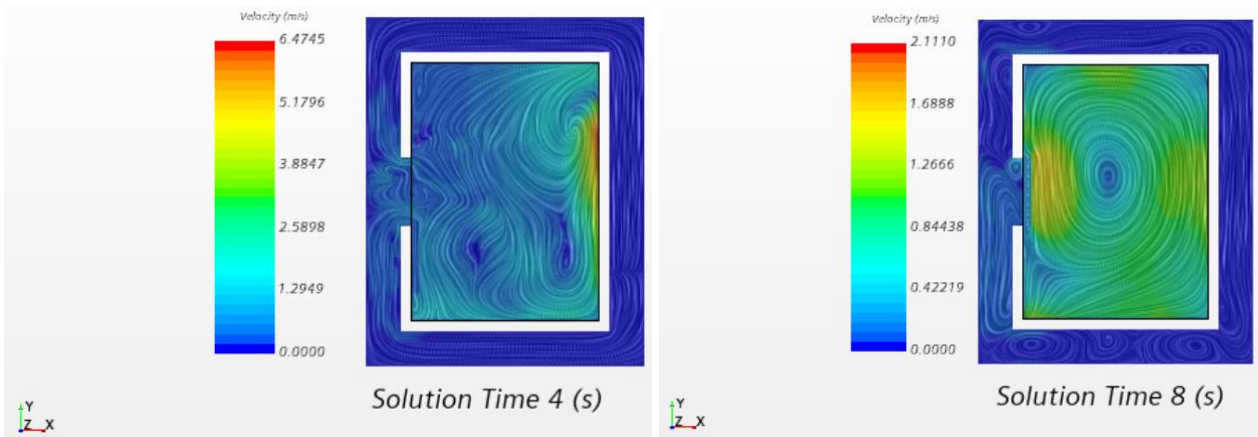


Figure 53 Sliding door 8 s opening time, velocity at  $z=1$

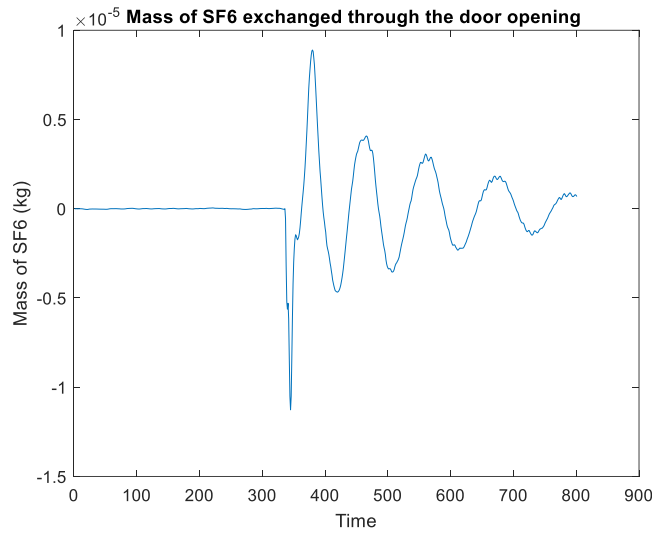


Figure 54 Sliding door 4 s opening time, mass of SF6 exchanged

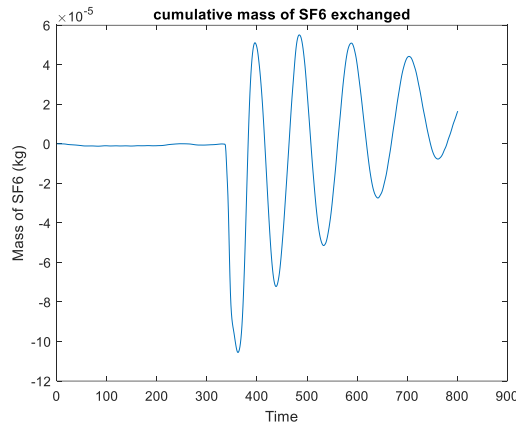


Figure 55 Sliding door 4 s opening time, cumulative mass of SF6 exchanged

Figure 55 show the cumulative mass of SF6 exchanged through the door opening. After the simulation is ended a cumulative mass of 1.6546e-05kg is the result. This means by the end of the simulation 0.016 g more of SF6 is going in through the grid versus going out. For the sliding door it is noticeable that the mass exchanged is varying at throughout the simulation. The door opening motion of the sliding door seems to have less effect on the exchange of SF6 compared to the hinged door.

### 5.1.3 Elevator door



Figure 56 show the mass fraction of SF6 at z=1m for the elevator door. It is seen that the elevator door looks to be spreading the SF6 less then the other cases.

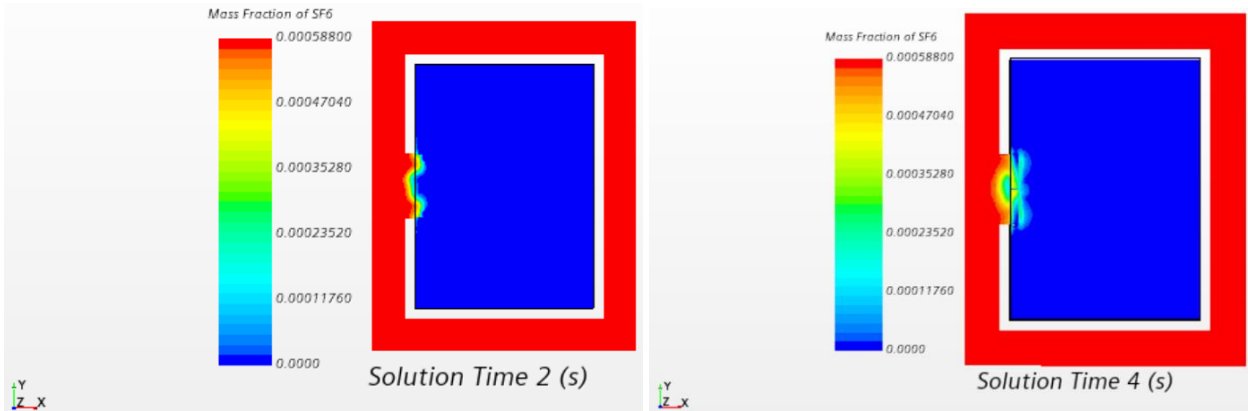


Figure 56 Elevator door 4 s opening time, Mass fraction of SF6 at z=1 m

Figure 57 shows the velocity at z=1m for the elevator door. The vector scene also shows low speeds which compares well with the scalar scene.

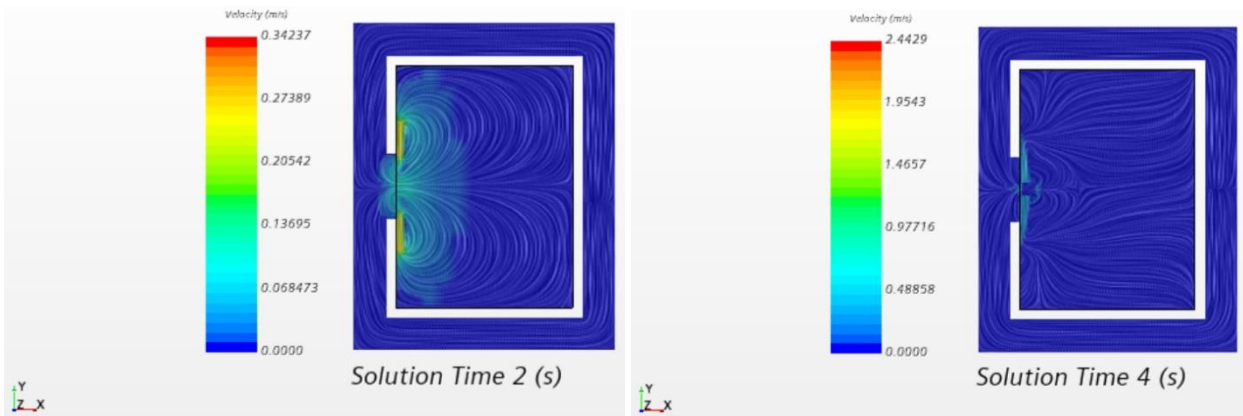


Figure 57 Elevator door 4 s opening time, velocity at z=1

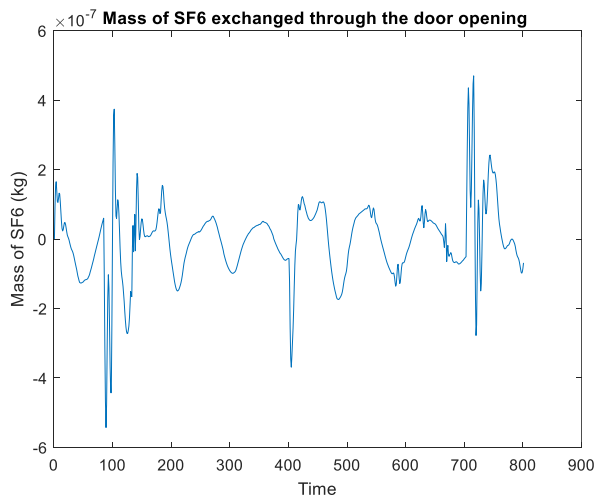


Figure 58 Elevator door 4 s opening time, mass of SF6 exchanged

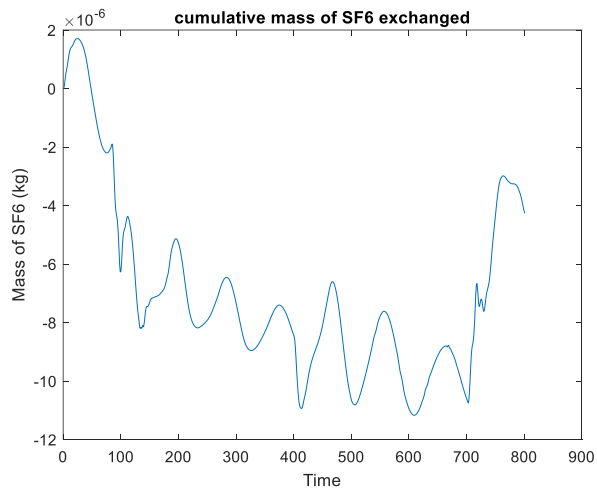


Figure 59 Elevator door 4 s opening time, cumulative mass of SF6 exchanged

Figure 59 show the cumulative mass of SF6 exchanged through the door opening. After the simulation is ended a negative cumulative mass of  $-4.2666 \times 10^{-6} \text{kg}$  is the result. This means by the end of the simulation 0,0042g more of SF6 is going out through the grid versus going in. This is a small amount and a similar trend is seen as for the sliding door. The mass exchanged is varying at throughout the simulation. The door opening motion of the elevator door also seems to clearly have less effect on the exchange of SF6 compared to the hinged door.

## 5.1.4 Comparison of velocity and mass flux

### 5.1.4.1 Velocity

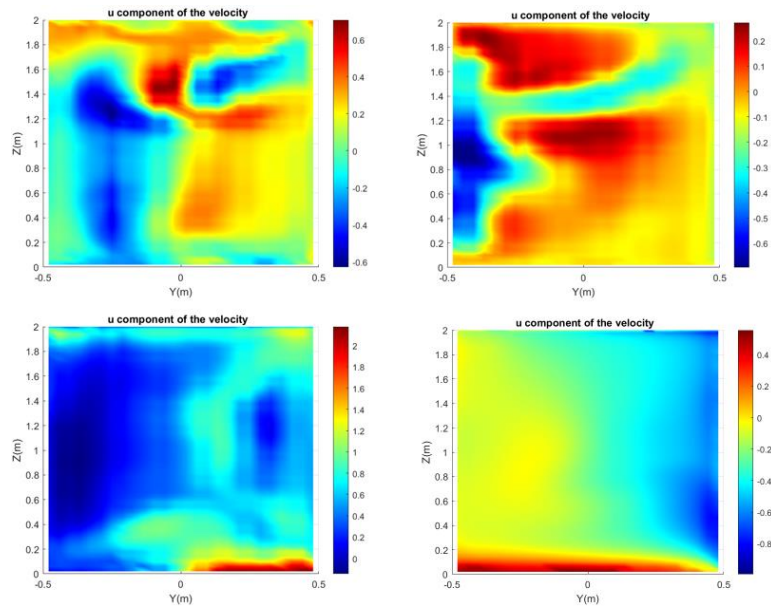


Figure 60 Hinged 4s motion, u component of the velocity at t=1,2,3, 4 s

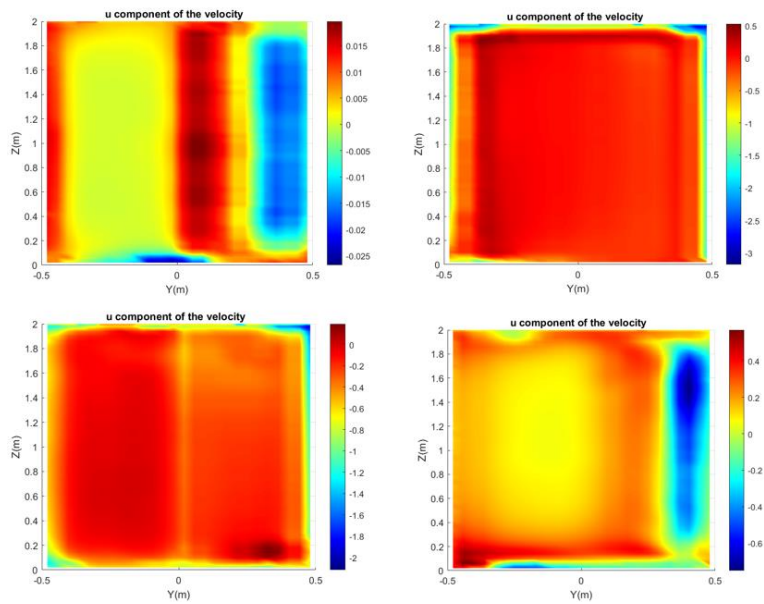


Figure 61 sliding 4s motion, u component of the velocity at t=1,2,3, 4 s

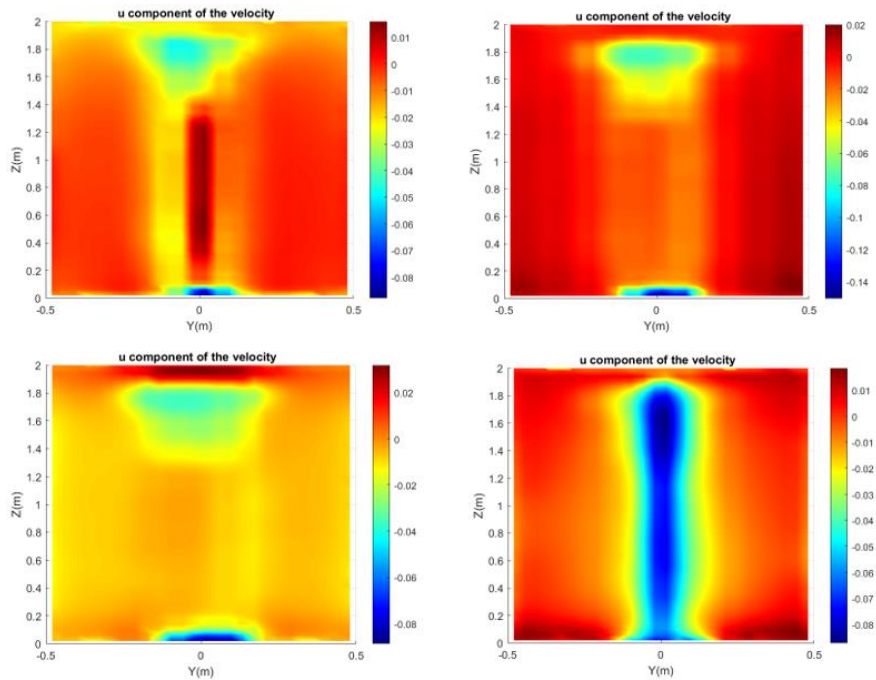


Figure 62 Elevator 4s motion, u component of the velocity at t=1,2,3, 4 s

The figures above show the u component of the velocity in m/s. A positive u velocity means the gas mixture is entering the room. It is seen that velocity is higher and more chaotic in the case of the hinged door. It is also seen that at t=3s the velocity is mostly negative which means that the air is going out again as seen in the previous part. This is likely because of the motion of the hinged door that is closing. For the elevator door and the sliding door it is less variation in the velocity. In Figure 62 it is noticeable that the elevator door also pushes the air out again in some degree when closing. It is still seen that it is without a doubt the hinged door that creates most velocity in the airflow.

#### 5.1.4.2 Mass flux

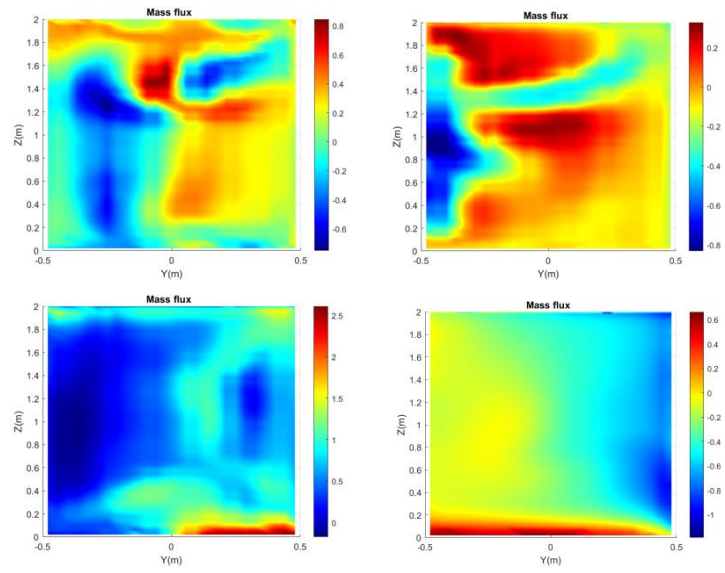


Figure 63 Hinged 4s motion, Mass flux at t=1,2,3, 4 s

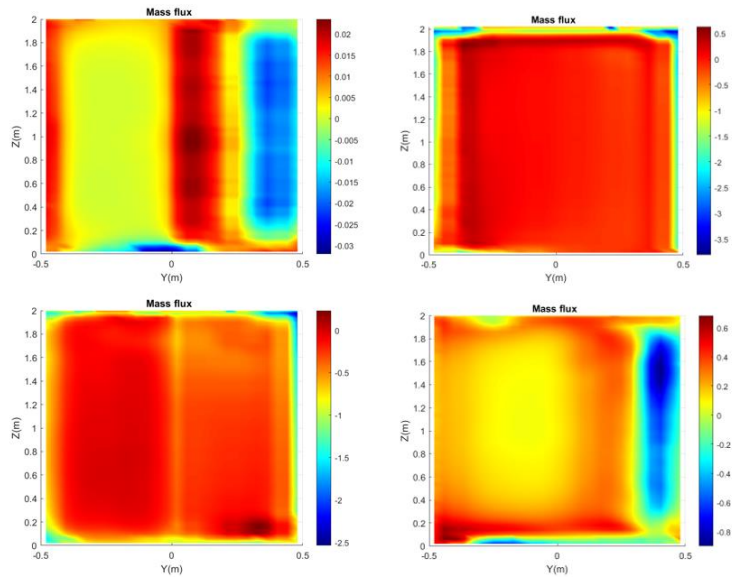


Figure 64 Sliding 4s motion, Mass flux at t=1,2,3, 4 s

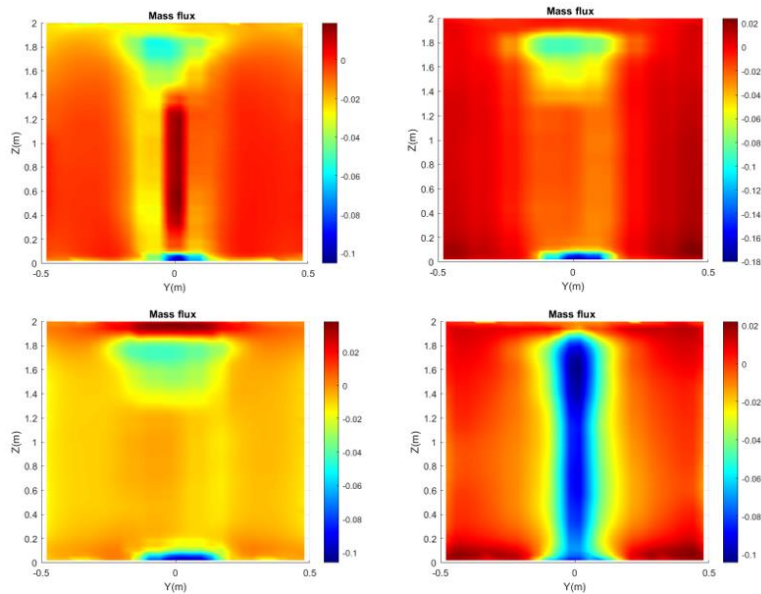


Figure 65 Elevator 4s motion, Mass flux at t=1,2,3, 4 s

The figures above show the mass flux in x direction in  $\text{kg}/\text{m}^2 \cdot \text{s}$ . It is observed a very similar trend like in the case of the velocity. The mass flux is higher and more chaotic in the case of the hinged door. It is also seen that at  $t=3\text{s}$  the mass flux is mostly negative which means that the mass is leaving the room. This is likely because of the motion of the hinged door that is closing. For the elevator door and the sliding door it is less variation in the mass flux and its most of the time a small amount that goes in. It is still noticeable in Figure 64 and Figure 65 that the sliding and the elevator door also pushes the air out again in some degree when closing. It is still seen that it is the hinged door that creates the most exchange of mass between the rooms.

### 5.1.5 Summary non thermal simulations

The visual comparison by monitoring the mass fraction of SF6 in a scalar scene and the velocity with the use of The Line Integral Convolution (LIC) in the vector scene clearly shows that the hinged door creates most exchange of SF6 and creates the most velocity in the airflow. The sliding door and the elevator door has less effect. The cumulative mass of SF6 exchanged through the door opening also shows that the hinged door has the biggest impact. The time snaps at different timesteps shows the same trend with the most velocity and mass flux created by the hinged door. The mass flux of SF6 at the different timesteps is shown in Appendix D.

Table 9 Cumulative mass of SF6 exchange non-thermal

Door type	Hinged	ELEVATOR	Sliding
Cumulative mass of SF6 exchanged	-2.11E-04 kg (- 0.2 g)	-4.2666e-06 (-0.0043 g)	1.6546e-05 (0.0165 g)

## 5.2 Thermal effects

In this first part of the results the thermal effects are taken into consideration. Besides that the method for comparison is the same for the first part. Regarding the prestaton grid, cumulative Energy and Cumulative mass of gas mixture will also be monitored in addition to the cumulative mass of SF6. The presentation grid also provides time snaps at different timesteps for the thermal cases, so it is possible to compare velocity, mass flux, mass of SF6 and also temperature and heatflux at different times of the simulation.

### 5.2.1 Hinged door

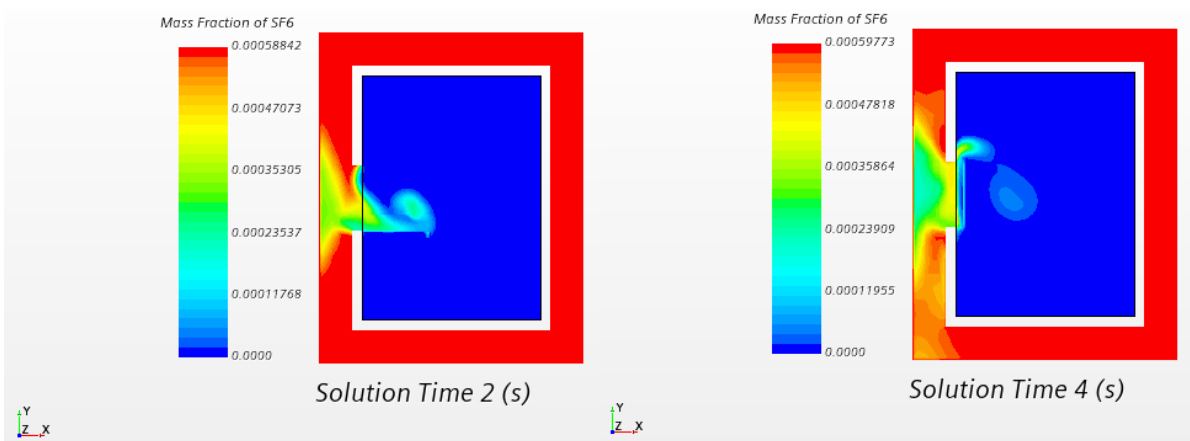


Figure 66 Hinged door 4 s opening time,  $\Delta T=42$  °C, mass fraction of SF6 at  $z=1$  m

Figure 66 show the mass fraction of SF6 at  $z=1$ m with a temperature difference of 42 °C. At  $t=2$ s the hinged door is fully opened and at  $t = 4$  the door is fully closed.

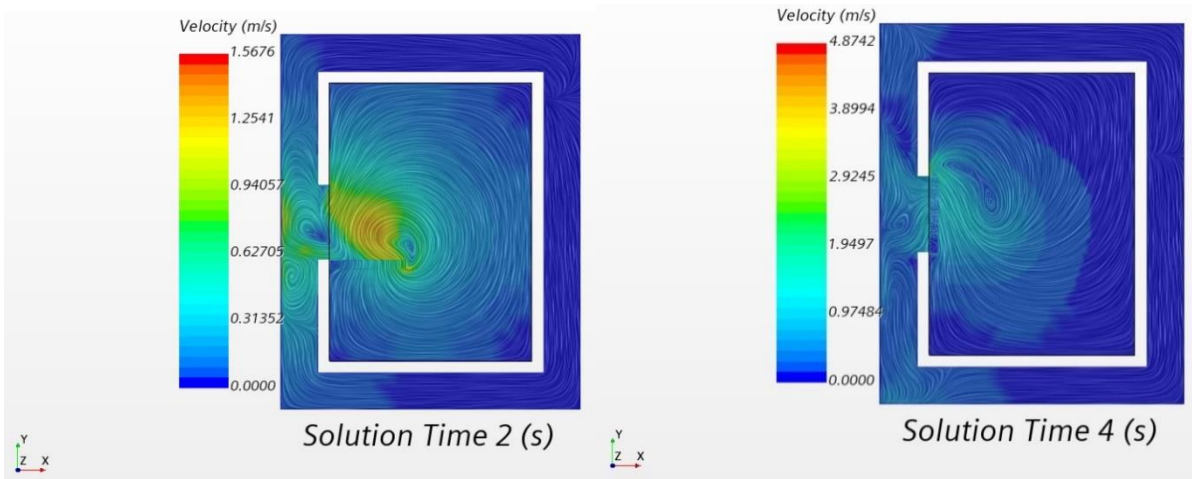


Figure 67 Hinged door 4 s opening time,  $\Delta T=42$  °C, velocity at  $z=1$

Figure 67 show the velocity at  $z=1$ m with a temperature difference of 42 °C. At  $t=2$ s the hinged door is fully opened and at  $t = 4$  the door is fully closed.

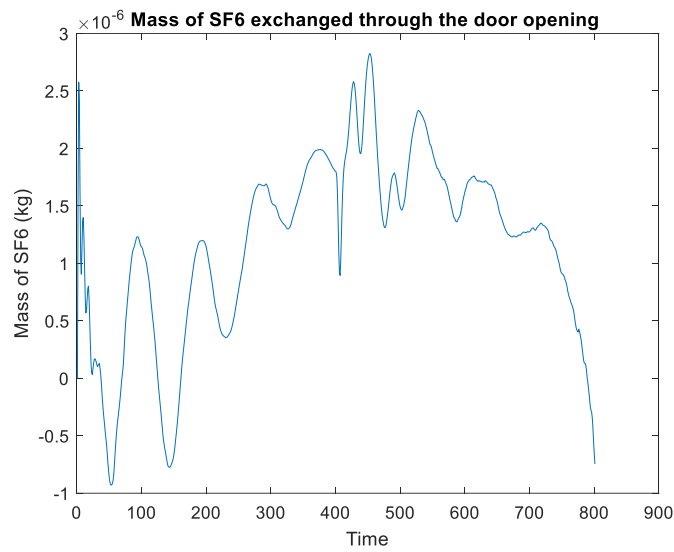


Figure 68 Hinged door,  $\Delta T=42$  °C, mass of SF6 exchanged



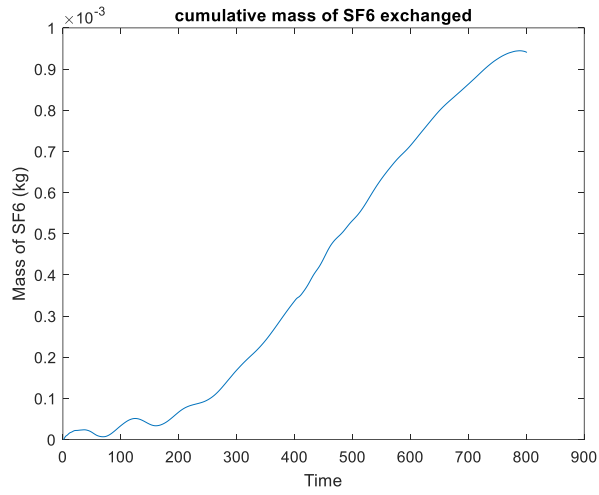


Figure 69 Hinged door,  $\Delta T=42$  °C, mass of SF6 exchanged

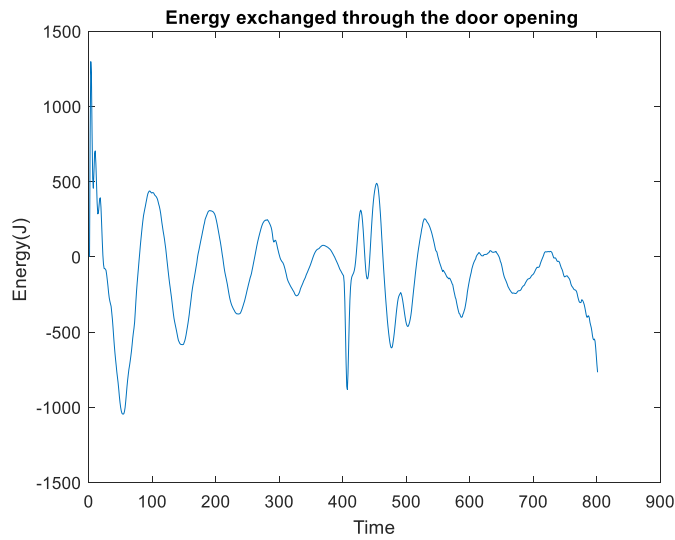


Figure 70 Hinged door,  $\Delta T=42$  °C, Energy exchanged

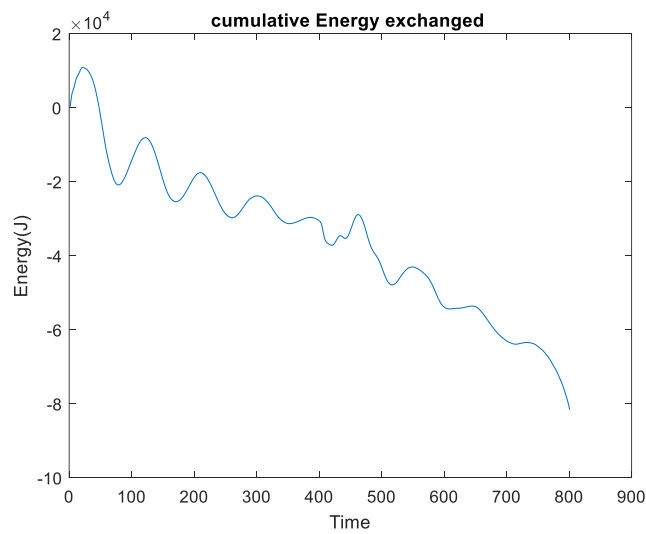


Figure 71 Hinged door,  $\Delta T=42$  °C, cumulative Energy exchanged

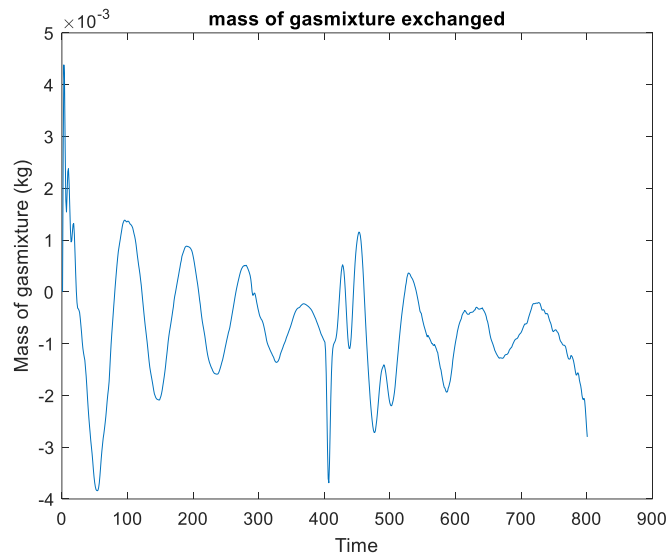


Figure 72 Hinged door,  $\Delta T=42$  °C, mass of gasmixture exchanged

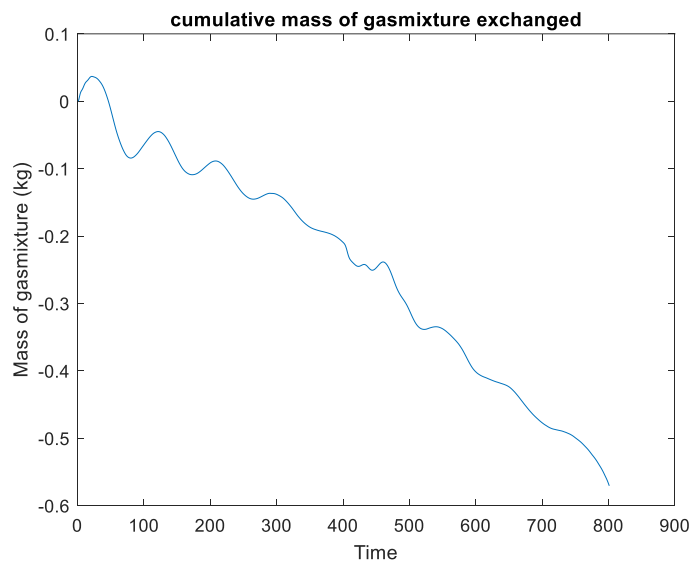


Figure 73 Hinged door,  $\Delta T=42$  °C, cumulative mass of gasmixture exchanged

Figure 69 shows that the cumulative mass of SF6 is positive which means that the mass of SF6 is mostly entering. Figure 71 shows that the cumulative energy is negative which mean that energy is leaving the room. Figure 73 shows the cumulative mass of gasmixture exchanged is negative.

Table 10 Cumulative values Hinged door thermal

	Hinged Door
Cumulative mass of SF6 (kg)	9.4035e-04 (0.9 g)
Cumulative Energy (J)	-8.16E+04
Cumulative mass of gass mixture (kg)	-0.5707 (-570 g)

### 5.2.2 Sliding door

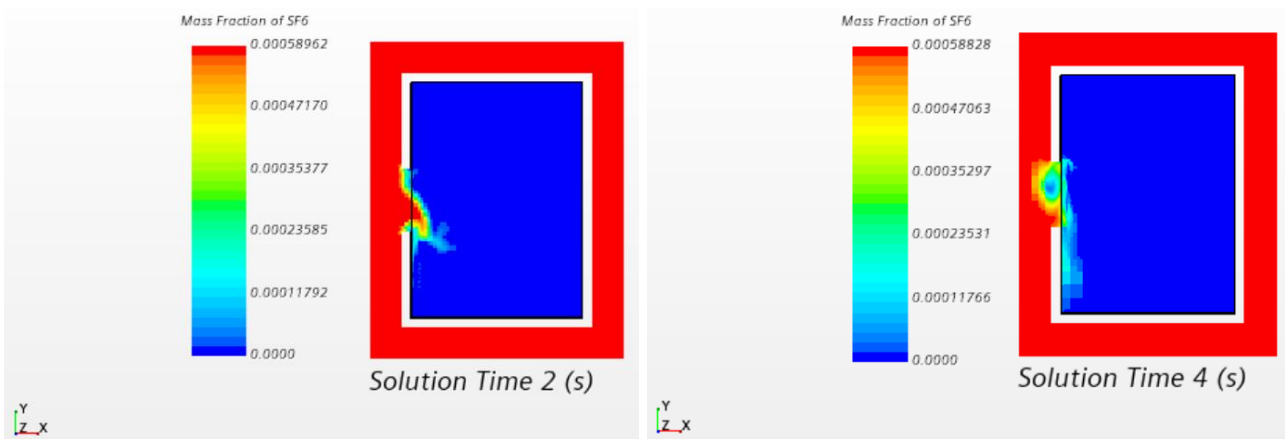


Figure 74 Sliding door 4 s opening time,  $\Delta T=42$  °C, mass fraction of SF6 at  $z=1$  m

Figure 74 show the mass fraction of SF6 at  $z=1$ m with a temperature difference of 42 °C. At  $t=2$ s the sliding door is fully opened and at  $t = 4$  the door is fully closed.

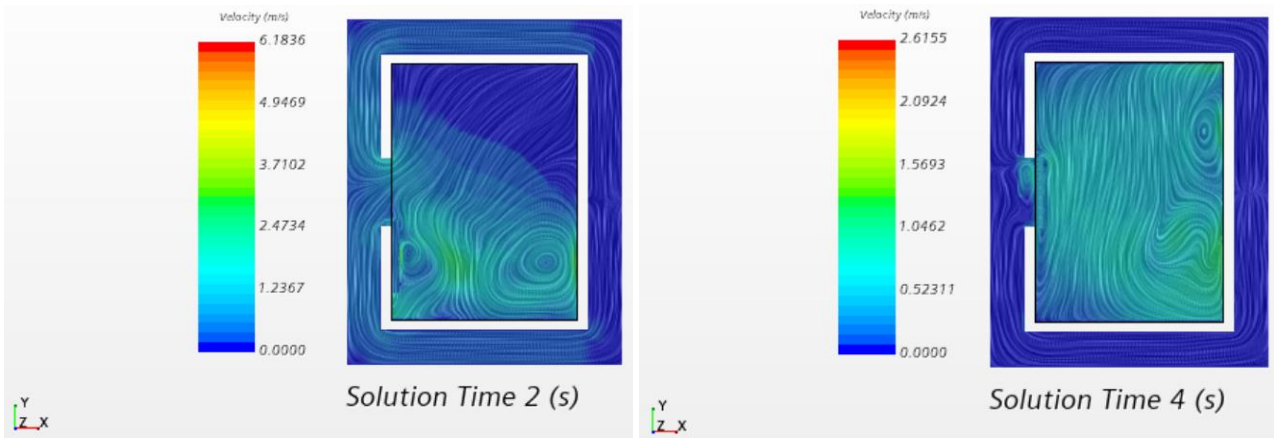


Figure 75 Sliding door 4 s opening time,  $\Delta T=42\text{ }^{\circ}\text{C}$ , velocity at  $z=1$

Figure 75 show the velocity at  $z=1\text{m}$  with a temperature difference of  $42\text{ }^{\circ}\text{C}$ . At  $t=2\text{ s}$  the sliding door is fully opened and at  $t = 4$  the door is fully closed.

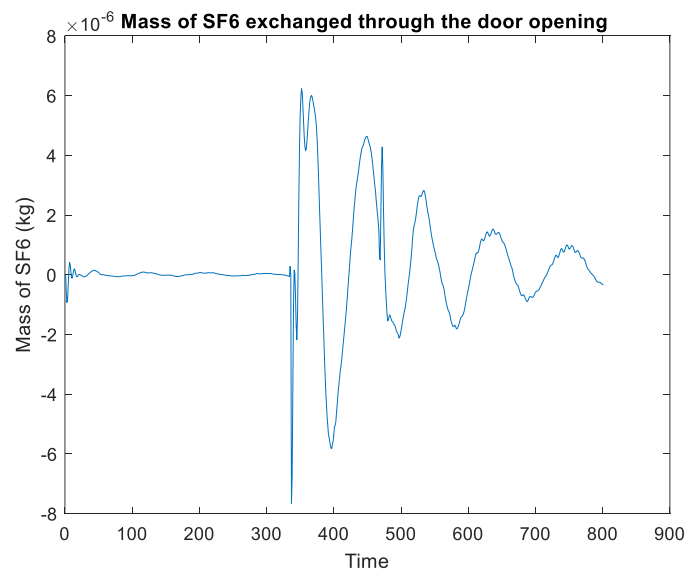


Figure 76 Sliding door,  $\Delta T=42\text{ }^{\circ}\text{C}$ , mass of SF6 exchanged

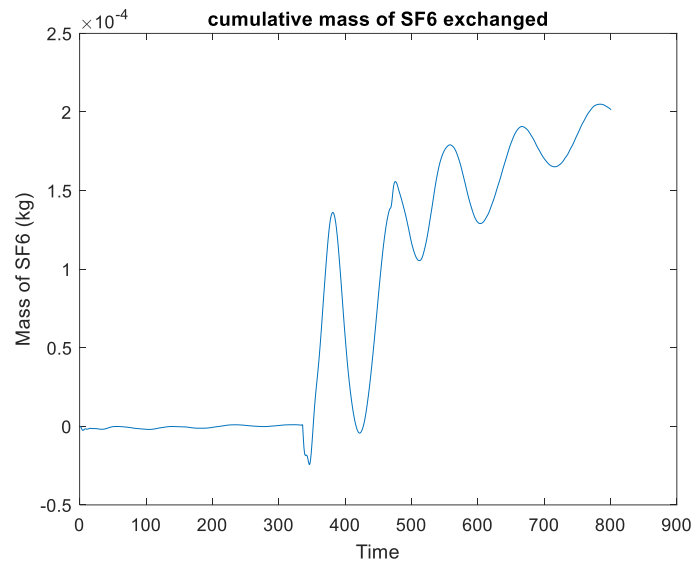


Figure 77 Sliding door,  $\Delta T=42$  °C, cumulative mass of SF6 exchanged

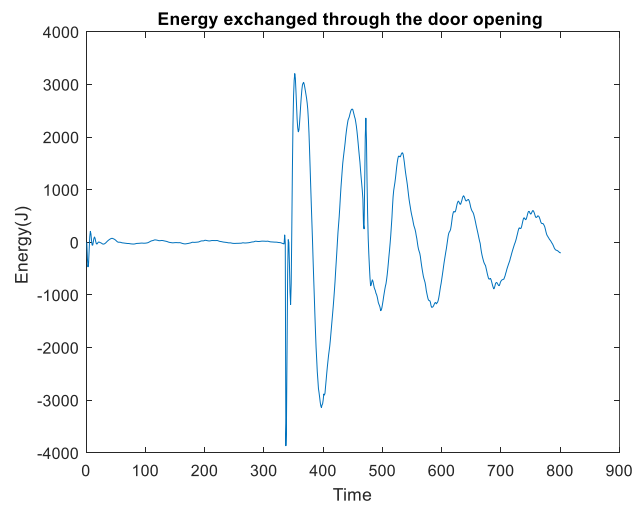


Figure 78 Sliding door,  $\Delta T=42$  °C, Energy exchanged

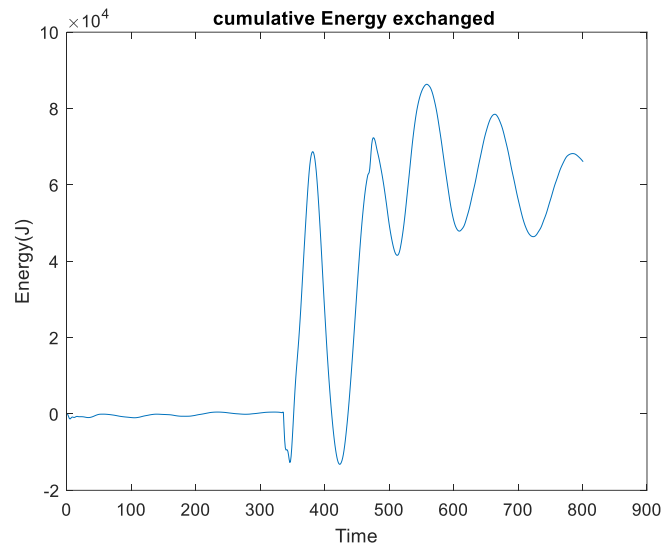


Figure 79 Sliding door,  $\Delta T=42$  °C, cumulative Energy exchanged

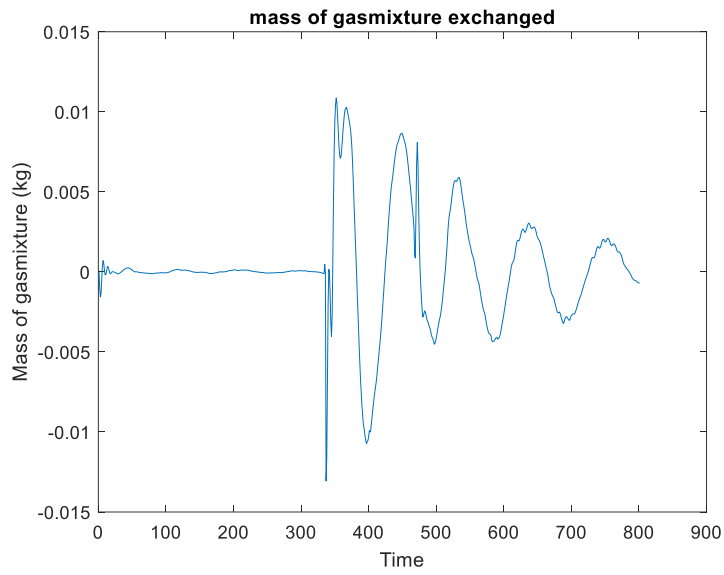


Figure 80 Sliding door,  $\Delta T=42$  °C, mass of gasmixture exchanged

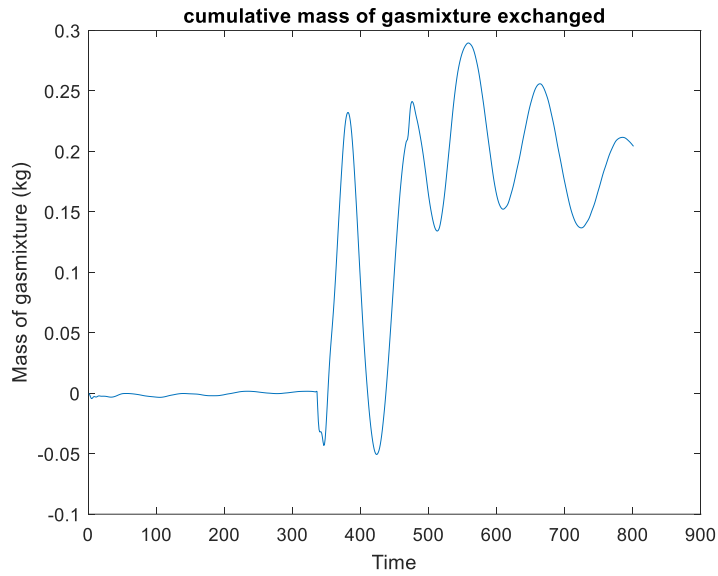


Figure 81 Sliding door,  $\Delta T=42\text{ }^{\circ}\text{C}$ , cumulative mass of gasmixture exchanged

Figure 77 shows that the cumulative mass of SF6 is varying but is positive which means that the mass of SF6 is mostly entering. Figure 79 shows that the cumulative energy is also varying but is positive which means that energy is entering the room. Figure 81 shows the cumulative mass of gasmixture exchanged is also positive. It is noticeable that the cumulative mass of SF6 is larger than for the non-thermal. The effect of the temperature difference can also clearly be seen when comparing the plot for the cumulative mass of SF6.

Table 11 Cumulative values Sliding door thermal

	Sliding door
Cumulative mass of SF6 (kg)	2.0144e-04 (0.2 g)
Cumulative Energy (J)	6.6066e+04
Cumulative mass of gass mixture (kg)	0.2042 (204 g)

### 5.2.3 Elevator door

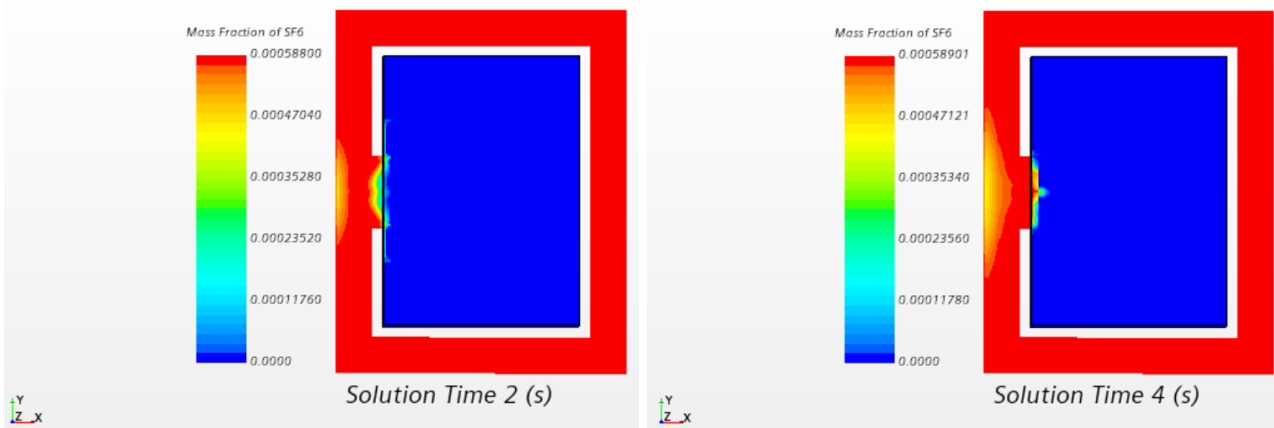


Figure 82 Elevator door 4 s opening time,  $\Delta T=42$  °C, mass fraction of SF6 at  $z=1$  m

Figure 82 show the mass fraction of SF6 at  $z=1$ m with a temperature difference of 42 °C. At  $t=2$ s the elevator door is fully opened and at  $t = 4$  the door is fully closed.

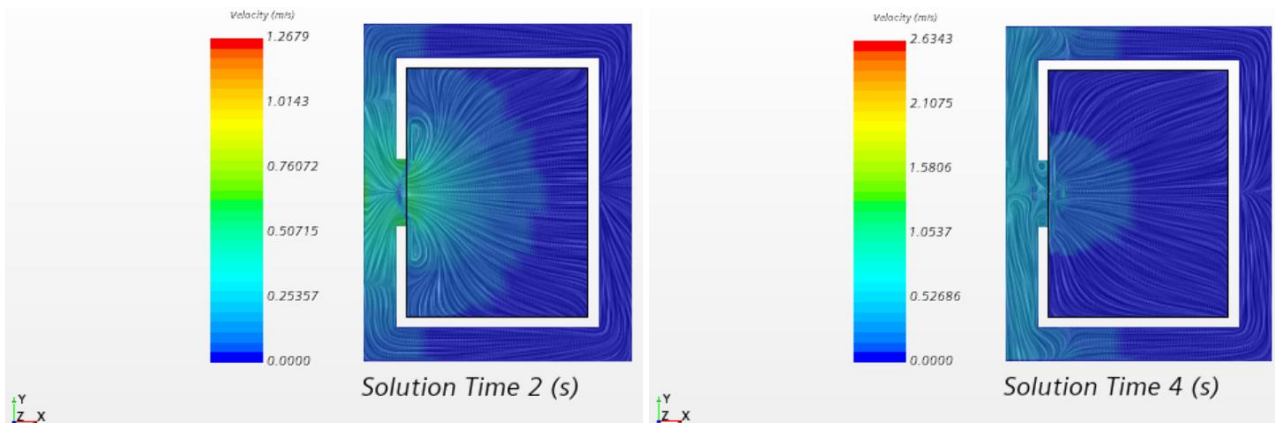


Figure 83 Elevator door 4 s opening time,  $\Delta T=42$  °C, velocity at  $z=1$



Figure 83 show the velocity at  $z=1\text{m}$  with a temperature difference of  $42\text{ }^\circ\text{C}$ . At  $t=2\text{s}$  the sliding door is fully opened and at  $t = 4$  the door is fully closed.

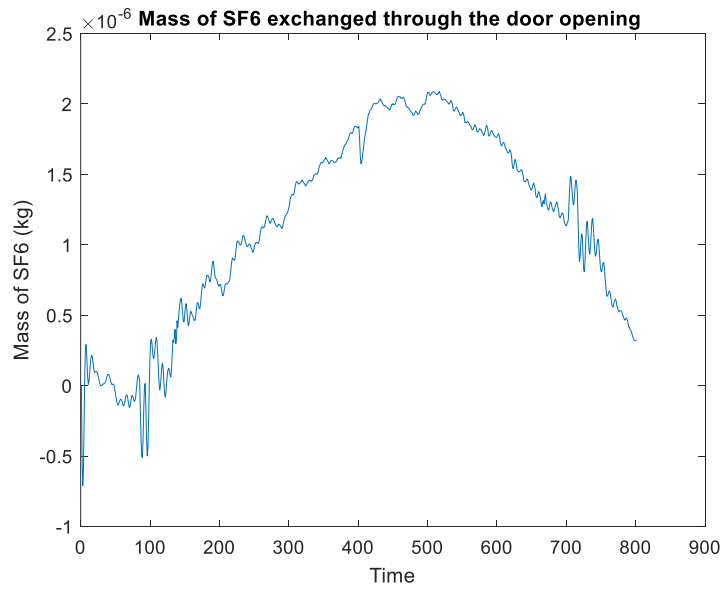


Figure 84 Elevator door,  $\Delta T=42\text{ }^\circ\text{C}$ , mass of SF6 exchanged

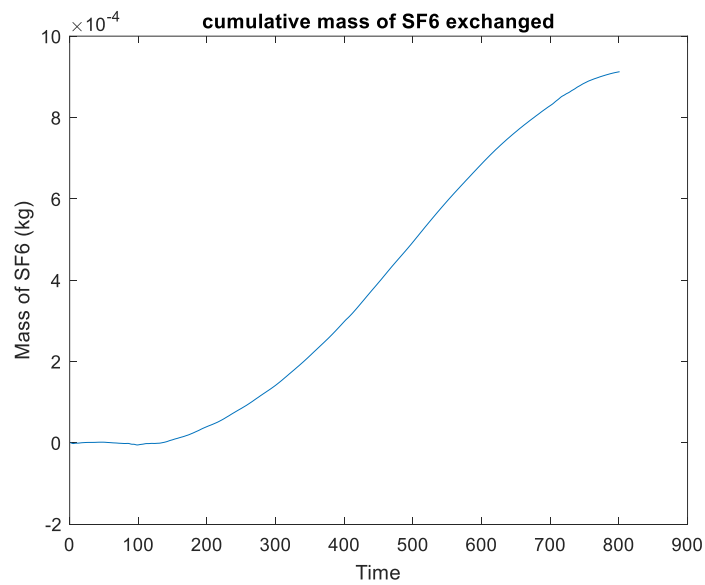


Figure 85 Elevator door,  $\Delta T=42\text{ }^\circ\text{C}$ , cumulative mass of SF6 exchanged

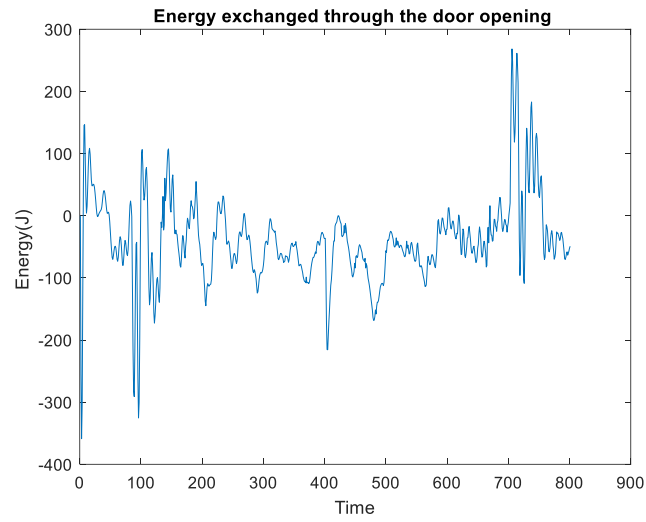


Figure 86 Elevator door,  $\Delta T=42\text{ }^{\circ}\text{C}$ , Energy exchanged

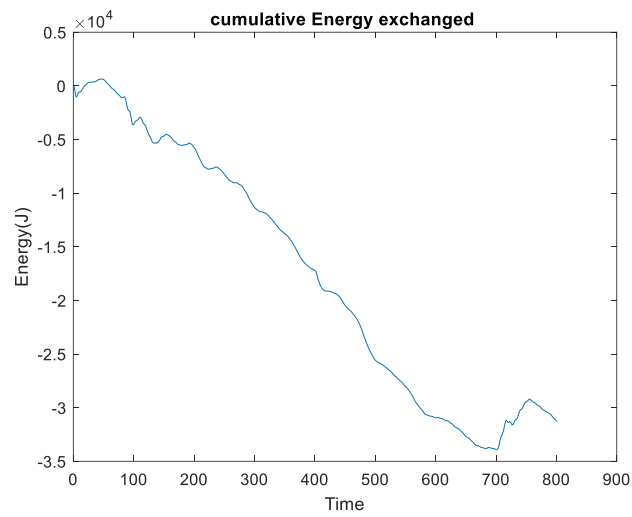


Figure 87 Elevator door,  $\Delta T=42\text{ }^{\circ}\text{C}$ , cumulative Energy exchanged

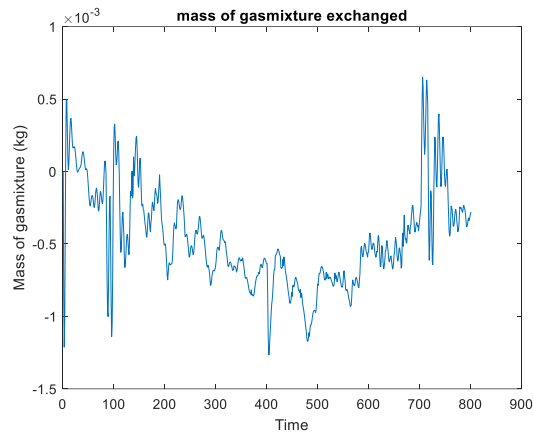


Figure 88 Elevator door,  $\Delta T=42$  °C, mass of gasmixture exchanged

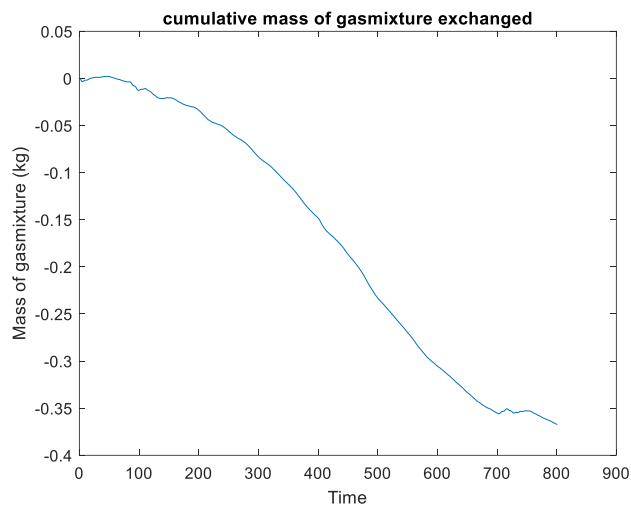


Figure 89 Elevator door,  $\Delta T=42$  °C, cumulative mass of gasmixture exchanged

Figure 85 shows that the cumulative mass of SF6 is positive which means that the mass of SF6 is mostly entering. Figure 87 shows that the cumulative energy is negative which means that energy is leaving the room. Figure 89 shows the cumulative mass of gasmixture exchanged is also negative. When comparing the cumulative mass of SF6 with the non-thermal case it is clear that the temperature difference have a big effect. This is seen both when comparing the cumulative mass and by reviewing the plot.

Table 12 Cumulative values Elevator door thermal

	Elevator door
Cumulative mass of SF6 (kg)	9.13E-04 (0.9g)
Cumulative Energy (J)	-3.1268e+04
Cumulative mass of gass mixture (kg)	-0.3674 ( 367 g)

## 5.2.4 Comparison of velocity, mass flux and temperature

### 5.2.4.1 Velocity

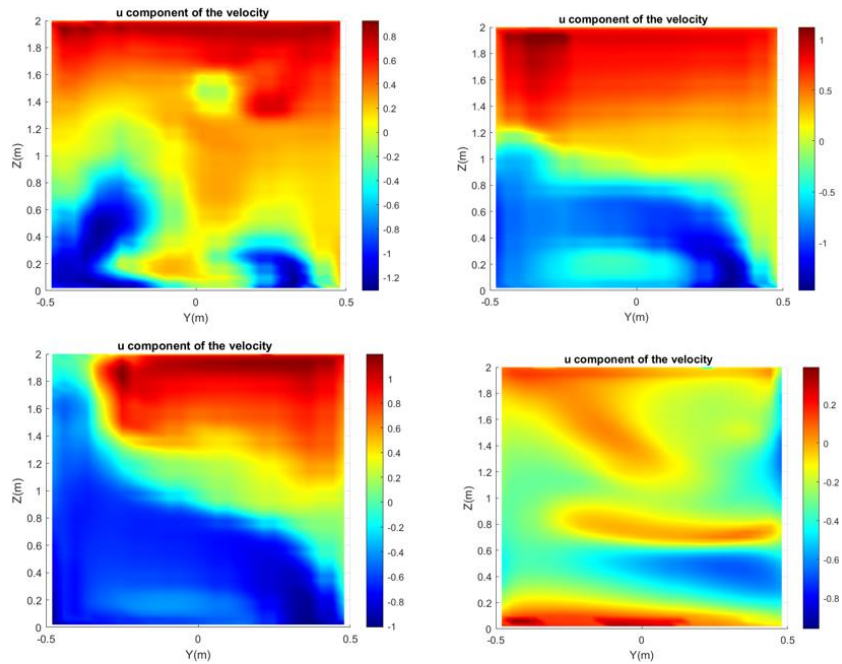


Figure 90 Thermal, Hinged 4s motion, u component of the velocity at t=1,2,3, 4 s

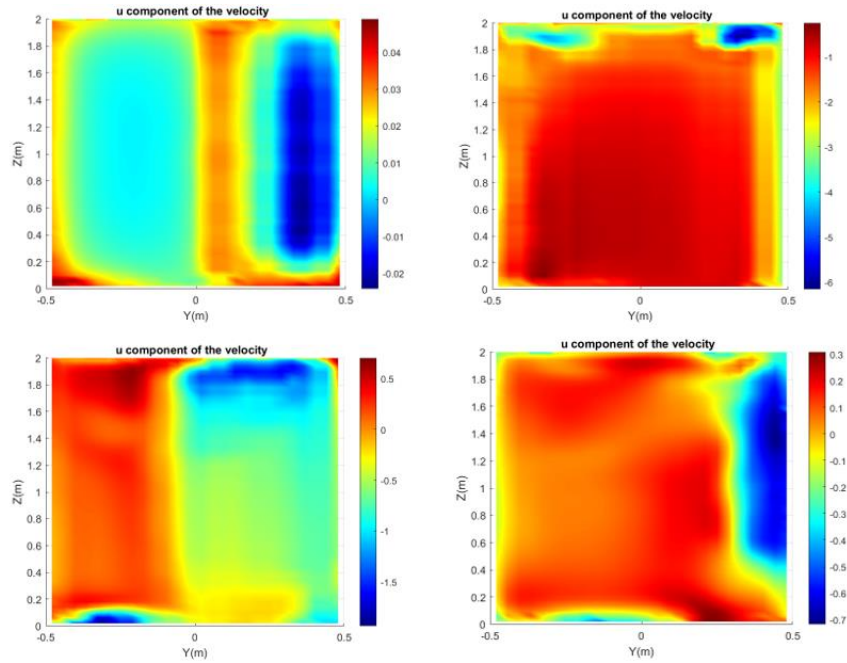


Figure 91 Thermal, Sliding 4s motion, u component of the velocity at t=1,2,3, 4 s

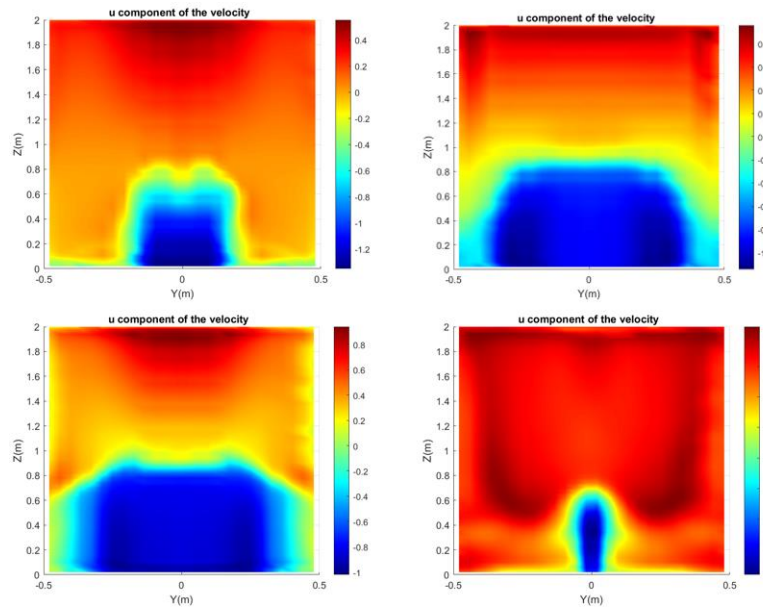


Figure 92 Thermal, Elevator 4s motion. u component of the velocity at t=1,2,3, 4 s

The figures above show the u component of the velocity in m/s. It is seen that velocity is higher and more chaotic in the case of the hinged door also in the thermal case. It is also seen that at  $t=3s$  the velocity is mostly negative but it is seen that the temperature difference still makes the velocity positive in the upper part. A general thing that is noticeable in comparison to the non-thermal cases is that it is much more mixing of the air even from the start of the simulations. For the elevator door it is seen clearly at  $t = 2s$  in Figure 92 that the cold air is leaving the room near the ground and the hot air is entering at the top. For the elevator door and the sliding door it is seen a bigger variation in the velocity compared to the non-thermal simulations. It is still seen that hinged door still creates most velocity and turbulence, but the effect of the temperature is best seen in the elevator door.

#### 5.2.4.2 Mass flux

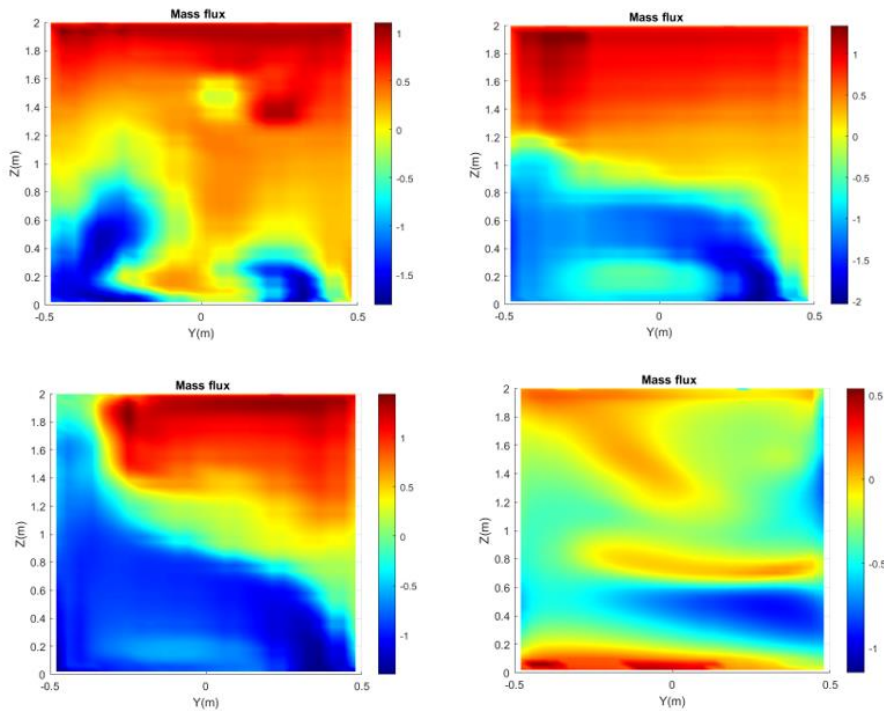


Figure 93 Thermal, Hinged 4s motion. Mass flux at  $t=1,2,3, 4 s$

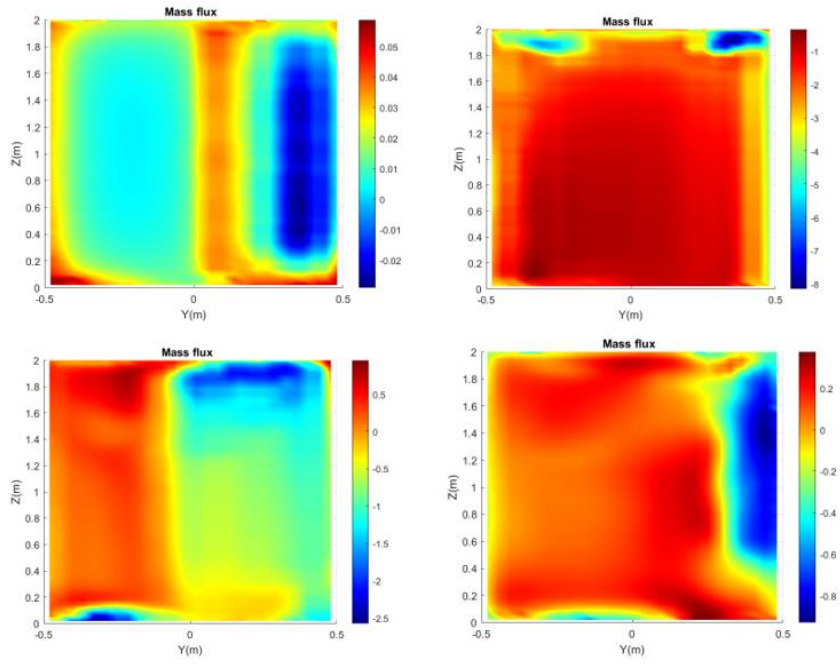


Figure 94 Thermal, Sliding 4s motion. Mass flux at t=1,2,3, 4 s

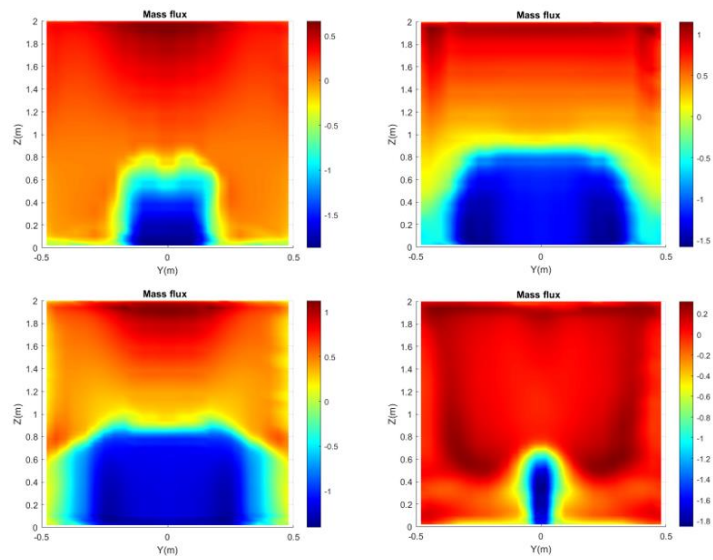


Figure 95 Thermal, Elevator 4s motion. Mass flux at t=1,2,3, 4 s

The figures above show the mass flux in x direction in  $\text{kg}/\text{m}^2 \cdot \text{s}$ . Like in the non-thermal case it is also in the thermal case seen a very similar trend like in the case of the velocity. The mass flux is higher and more chaotic in the case of the hinged door. At  $t=3\text{s}$  the velocity is mostly negative, but it is seen that the temperature difference still makes the mass flux in the upper part. Generally, the mass flux naturally shows the same patterns as the velocity.

### 5.2.4.3 Temperature

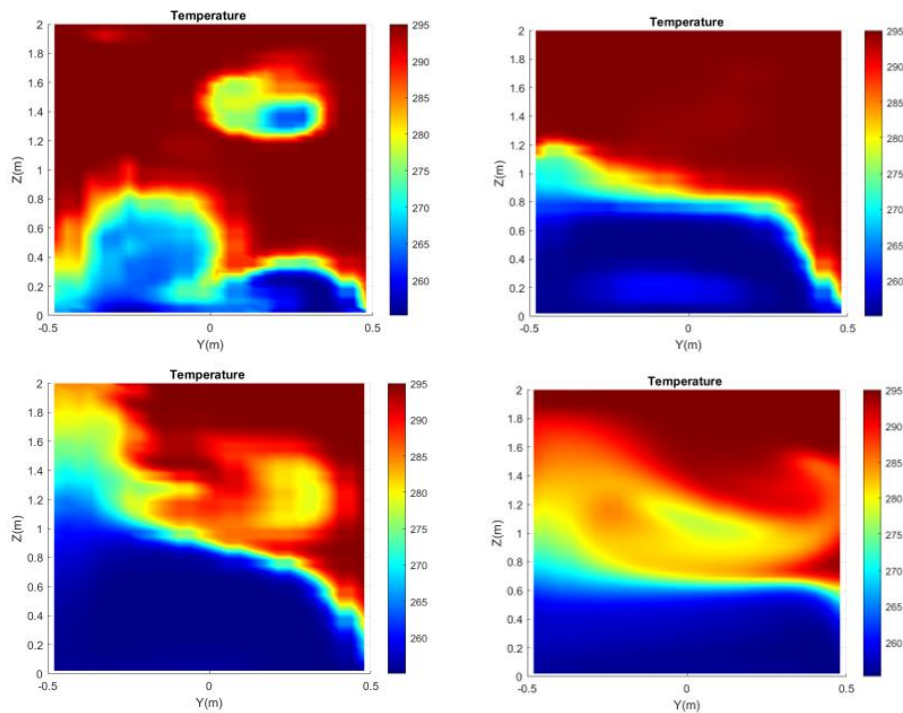


Figure 96 Thermal, Hinged 4s motion. Temperature at  $t=1,2,3, 4\text{ s}$



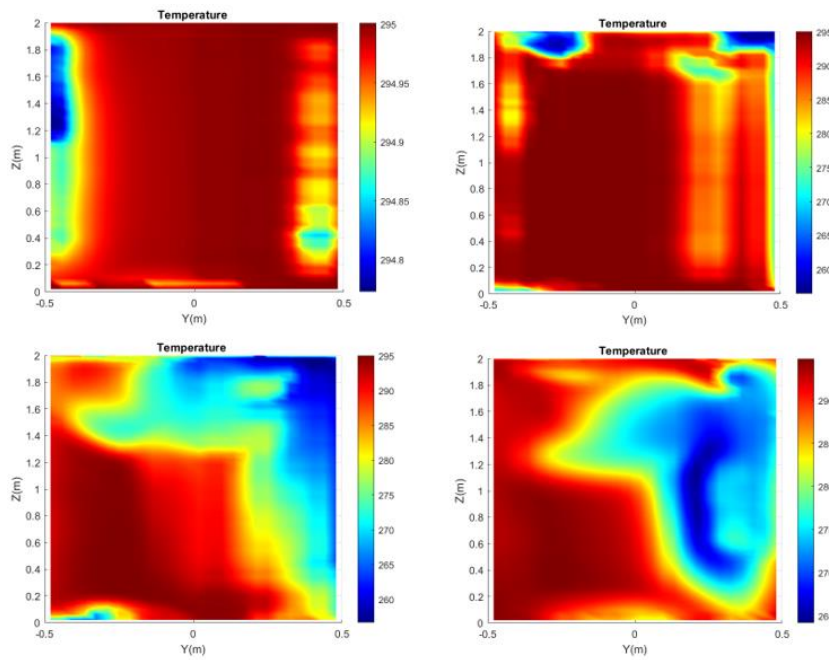


Figure 97 Thermal, Sliding 4s motion. Temperature at t=1,2,3, 4 s

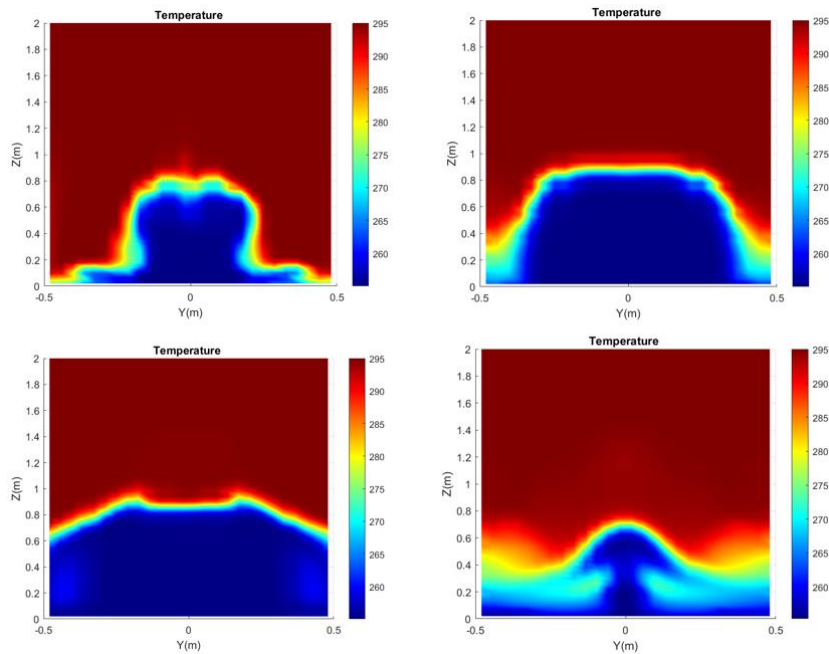


Figure 98 Thermal, Elevator 4s motion. Temperature at t=1,2,3, 4 s

The figures above show the temperature in Kelvin. Especially for the hinged and the elevator door it is clearly seen how the hot air enters in top and the cold air exits in the bottom. This looks as expected in terms of the trend seen when looking at the velocity and the mass flux. For the sliding door it is more mixed and it cannot be seen as clearly. Generally, the exchange of the hot and cold air looks reasonable compared to the other results.

### 5.2.5 Summary thermal simulations

The visual comparison by monitoring the mass fraction of SF6 in a scalar scene and the velocity with the use of The Line Integral Convolution (LIC) in the vector scene still shows that the hinged door creates most exchange of SF6 and creates the most velocity in the airflow. Still the sliding door and the elevator door seems to be most affected by the temperature. Meaning that these cases show a clearer difference compared to the non- thermal case. This can especially be seen with higher velocities in the vector scene. The cumulative mass of SF6 exchanged through the door opening is also closer to hinged door. The time snaps at different timesteps shows the same trend with the most change in velocity and mass flux for the elevator and the sliding door. The hinged door is still the dominant force, but it is seen clearly that the temperature difference effects the airflow. The mass of SF6 at the different timesteps is shown in Appendix D.

*Table 13 Cumulative values thermal case*

	HINGED	ELEVATOR	SLIDING
Cumulative mass of SF6 (kg)	9.4035e-04	9.13E-04	2.0144e-04
Cumulative Energy (J)	-8.16E+04	-3.1268e+04	6.6066e+04
Cumulative mass of the gas mixture (kg)	-0.5707	-0.3674	0.2042

## 6 Conclusions

The aim and objective of this work was to get a better understanding of air flow and mass exchange by the opening and closing motion of different type of doors. The effect of temperature difference and different opening motions was also going to be investigated. For this task the overset mesh in STAR CCM+ was used to move rigid boundaries and two-equation turbulence models to better understand the effects of door opening speed and time, thermal effects, and turbulence models.

The comparison of the opening and closing door motions times for the hinged and the sliding door shows that the total time of the motion affects the airflow. Lower opening time creates a higher velocity and more exchange between the two rooms.

The results from the non-thermal simulations show from visualizations that the hinged door creates the most exchange of air between the two rooms and creates the most velocity in the airflow. This is also shown with the cumulative mass of SF6 through the door opening which was -0.2 g for the hinged door and -0.0043 g and 0.0165 g for the elevator and the sliding door. For the non-thermal cases it can be concluded that the sliding door and the elevator door creates a lower speed in the airflow and less exchange of air between the two rooms. If the goal is to avoid exchange of potential pollutants between two rooms the hinged door is not recommended.

The results from the thermal simulations also show that the hinged door creates most exchange of SF6 and creates the most velocity in the airflow. For all the three doors higher velocities is achieved and more air and SF6 is exchanged between the two rooms. A The biggest difference is seen in the sliding door and the elevator door compared to the non-thermal case. The cumulative mass of SF6 exchanged through the door opening is 0.94g for the hinged and 0.91 g and 0.2 g for the elevator and the sliding door. It is concluded that the temperature difference effects the airflow and has the biggest effect for the hinged door and the elevator door.

It can be concluded that the overset mesh works well for the purpose of simulating solid movements. Using the overset mesh is a demanding process in the start-up phase, but this type of CFD simulations provide valuable information for estimation of pollutant transport and prediction of desired indoor environment. The results are also relevant for energy use, the thermal simulations of the cold storage room in particular.

### Future work

For future work a detailed mesh sensitivity analysis can be done. Comparison of the results of the simulation with more experimental data will enhance the credibility of numerical methodology. Scale resolved turbulence models like Large Eddy Simulations (LES) or Detached Eddy Simulation could be adopted compared to the two-equations turbulence model that has been used in this study. Since the door motion is an integral part of an indoor built environment more realistic indoor setup involving furniture, heat sources and human motion could be simulated based on the present methodology.



## 7 References [17]

- [1] . J.W. Tang, I. Eames, Y. Li, Y.A. Taha, P. Wilson, G. Bellingan, K.N. Ward, J. Breuer,, "Door-opening motion can potentially lead to a transient breakdown in negative-pressure isolation conditions: the importance of vorticity and buoyancy airflows," *Journa of Hospital Infection* , vol. 61 , no. 4 , pp. 283-286 , 2005 .
- [2] Tang, Julian W., et al., "Different types of door-opening motions as contributing factors to containment failures in hospital isolation rooms," *PLoS one* 8.6, 2013.
- [3] L. Fontana, A. Quintino,, "Experimental analysis of the transport of airborne contaminants between adjacent rooms at different pressure due to the door opening," *Building and Environmen*, vol. 81 , pp. 81-91, 2014 .
- [4] A. s. D. V. Nancy Rice, "An Evaluation of Hospital Special-Ventilation-Room Pressures," *Infection Control & Hospital Epidemiology*, vol. 22 , no. 1 , pp. 19-23 , 2015 .
- [5] Ayarmal, Azada, Ole Melhus, and Arnab Chaudhuri., "The effects of fan and door opening on a cold storage room: a numerical study.," 2018.
- [6] Hathway, Abigail, et al., "Experimental and modelling investigations of air exchange and infection transfer due to hinged-door motion in office and hospital settings," *International Journal of Ventilation* , vol. 14, no. 2 , pp. 127-140, 2015.
- [7] Papakonstantis, Ilias G., Elizabeth Abigail Hathway, and Wernher Brevis, "An Experimental study of the flow induced by the motion of a hinged door seperating two rooms," *Building and Enviroment* , vol. 131 , pp. 220-230, 2018.
- [8] Chang, Le, et al., "Control room contaminant inleakage produced by door opening and closing: Dynamic simulation and experiments.," *Building and Environment* , vol. 98 , pp. 11-20, 2016.
- [9] Petri Kalliomäki, Pekka Saarinen, Julian W.Tang, Hannu Koskela, "Airflow patterns through single hinged and sliding doors in hospital isolation rooms – Effect of ventilation, flow differential and passage," *Building and Environment*, vol. 107, pp. 154-168, 2016.
- [10] Petri Kalliomäki, Pekka Saarinen, Julian W Tang & Hannu Koskela , "Airflow Patterns through Single Hinged and Sliding Doors in Hospital Isolation Rooms," *International Journal of Ventilation*, vol. 14, no. 2, pp. 111-126, 2015 .
- [11] Yun-ChunTung, Yang-ChengShih, Shih-ChengHu, "Numerical study on the dispersion of airborne contaminants from an isolation room in the case of door opening," *Applied Thermal Engineering* , vol. 29 , no. 8-9 , pp. 1544-1551, 2009.
- [12] N.J. Adams, D.L. Johnson, R.A. Lynch, "The effect of pressure differential and care provider movement on airborne infectious isolation room containment effectiveness," *Am J Infect Control*, vol. 39, no. 2 , p. 91/97, 2011.
- [13] D. W. D.E. Kiel, "Combining door swinging with density driven flow," *ASHRAE Trans* , pp. 590-599, 1989.

- [14] Eames I., Shoaib D., Klettner C. A. and Taban V., "Movement of airborne contaminants in a hospital isolation room," *Airborne transmission of disease in hospitals* , vol. 6 , p. 757–S766, 2009.
- [15] Kalliomäki, Petri, et al., "Effectiveness of directional airflow in reducing containment failures in hospital isolation rooms generated by door opening," *Building and Environment* , vol. 131, pp. 83-93, 2019.
- [16] I. P. Abigail Hathway, "CFD Simulation of airflow due to door motion using a momentum source method," 2016.
- [17] Lee, Sihwan, Beungyong Park, and Takashi Kurabuchi., "Numerical evaluation of influence of door opening on interzonal air exchange.," *Building and Environment* , vol. 102, pp. 230-242, 2016.
- [18] H K Versteeg, W Malalasekera, "An introduction to Computational Fluid Dynamics, The Finite Volume Method", Pearson Education Limited, 2007.
- [19] 2. S. D. I. Software, "Simcenter STAR-CCM+ documentation version 2020.2," pp. 3034-3098.
- [20] J. C. J. R. Edwards, "Large-eddy simulation of human-induced contaminant transport in room compartments," *Indoor Air - International Journal of Indoor Environment and Health* , vol. 22, no. 1 , pp. 77-87 , 2011.



# Figures

Figure 1 Effect of opening a hinged door. ....	4
Figure 2 Airflow across an open doorway induced by door opening motion. ....	5
Figure 3 Mesh scene from initial test case with hinged door ....	9
Figure 4 Draw and extrude ....	19
Figure 5 Boolean operations ....	20
Figure 6 Unite bodies.....	20
Figure 7 Create parts and split by patch.....	21
Figure 8 Creating Blocks ....	21
Figure 9 Boolean subtract.....	22
Figure 10 Intersect working as the overset region.....	22
Figure 11 Setting Boundary Conditions.....	23
Figure 12 Meshing models ....	24
Figure 13 Mesh shown with plane sections ....	25
Figure 14 Volume control for the hinged door.....	27
Figure 15 Volume controll for the elevator door ....	27
Figure 16 Physics Continua.....	28
Figure 17 Multi-Component Gas ....	29
Figure 18 Rotation and Translation ....	30
Figure 19 Motion Specification in the Region ....	31
Figure 20 Rotation and Translation Properties ....	31
Figure 21 Cartesian Coordinate system.....	32
Figure 22 Field function: Rotation Rate.....	33
Figure 23 Field function: Slide ....	33
Figure 24 Field function for fixing the mass fraction of SF6 and a scalar scene showing the Mass Fraction of SF6 ....	34
Figure 25 Species mass fraction ....	34
Figure 26 Drawing of the grid.....	35



Figure 27 Presentation Grid properties.....	36
Figure 28 Presentation Grid.....	36
Figure 29 Velocity through the grid at t=4s for a non-thermal case and thermal case .....	37
Figure 30 Extracting information with XYZ Internal Table .....	37
Figure 31 Matlab script for presenting cumulative mass and Energy .....	38
Figure 32 Geometry test case.....	40
Figure 33 Mesh scene showing the geometry in STAR CCM+ .....	41
Figure 34 Comparison of Mass fraction of SF6 at z=1m, t=1.5 s .....	42
Figure 35 Comparison of Mass fraction of SF6 at z=1m, t=3.5 s .....	43
Figure 36 Comparison of Mass fraction of SF6 at z=1m, t=7.9s .....	43
Figure 37 visualized airflow at different times .....	44
Figure 38 Comparison of velocity at z=1m, t=1.5s .....	44
Figure 39 Comparison of velocity at z=1m, t=3.5s .....	45
Figure 40 Comparison of velocity at z=1m, t=7.9s .....	45
Figure 41 Elevator door, Hinged door and Sliding door .....	46
Figure 42 Mesh scene displaying the mesh.....	47
Figure 43 Hinged door 4 s opening time, Mass fraction of SF6 at z=1 m .....	51
Figure 44 Hinged door 8 s opening time, Mass fraction of SF6 at z=1 m .....	51
Figure 45 Hinged door 4 s opening time, velocity at z=1 .....	52
Figure 46 Hinged door 8 s opening time, velocity at z=1 .....	52
Figure 47 Residuals hinged door 4 s opening time.....	53
Figure 48 Hinged door, mass of SF6 exchanged through the door opening.....	53
Figure 49 Hinged door, cumulative mass of SF6 exchanged through the door opening .....	54
Figure 50 Sliding door 4 s opening time, Mass fraction of SF6 at z=1 m.....	55
Figure 51 Sliding door 8 s opening time, Mass fraction of SF6 at z=1 m.....	55
Figure 52 Sliding door 4 s opening time, velocity at z=1 .....	56
Figure 53 Sliding door 8 s opening time, velocity at z=1 .....	56
Figure 54 Sliding door 4 s opening time, mass of SF6 exchanged.....	57

Figure 55 Sliding door 4 s opening time, cumulative mass of SF6 exchanged .....	57
Figure 56 Elevator door 4 s opening time, Mass fraction of SF6 at z=1 m .....	58
Figure 57 Elevator door 4 s opening time, velocity at z=1 .....	58
Figure 58 Elevator door 4 s opening time, mass of SF6 exchanged .....	59
Figure 59 Elevator door 4 s opening time, cumulative mass of SF6 exchanged .....	59
Figure 60 Hinged 4s motion, u component of the velocity at t=1,2,3, 4 s .....	60
Figure 61 sliding 4s motion, u component of the velocity at t=1,2,3, 4 s .....	60
Figure 62 Elevator 4s motion, u component of the velocity at t=1,2,3, 4 s .....	61
Figure 63 Hinged 4s motion, Mass flux at t=1,2,3, 4 s.....	62
Figure 64 Sliding 4s motion, Mass flux at t=1,2,3, 4 s .....	62
Figure 65 Elevator 4s motion, Mass flux at t=1,2,3, 4 s.....	63
Figure 66 Hinged door 4 s opening time, $\Delta T=42$ °C, mass fraction of SF6 at z=1 m .....	64
Figure 67 Hinged door 4 s opening time, $\Delta T=42$ °C, velocity at z=1.....	65
Figure 68 Hinged door, $\Delta T=42$ °C, mass of SF6 exchanged .....	65
Figure 69 Hinged door, $\Delta T=42$ °C, mass of SF6 exchanged .....	66
Figure 70 Hinged door, $\Delta T=42$ °C, Energy exchanged.....	66
Figure 71 Hinged door, $\Delta T=42$ °C, cumulative Energy exchanged .....	66
Figure 72 Hinged door, $\Delta T=42$ °C, mass of gasmixture exchanged.....	67
Figure 73 Hinged door, $\Delta T=42$ °C, cumulative mass of gasmixture exchanged .....	67
Figure 74 Sliding door 4 s opening time, $\Delta T=42$ °C, mass fraction of SF6 at z=1 m .....	68
Figure 75 Sliding door 4 s opening time, $\Delta T=42$ °C, velocity at z=1 .....	69
Figure 76 Sliding door, $\Delta T=42$ °C, mass of SF6 exchanged .....	69
Figure 77 Sliding door, $\Delta T=42$ °C, cumulative mass of SF6 exchanged .....	70
Figure 78 Sliding door, $\Delta T=42$ °C, Energy exchanged.....	70
Figure 79 Sliding door, $\Delta T=42$ °C, cumulative Energy exchanged .....	71
Figure 80 Sliding door, $\Delta T=42$ °C, mass of gasmixture exchanged.....	71
Figure 81 Sliding door, $\Delta T=42$ °C, cumulative mass of gasmixture exchanged.....	72
Figure 82 Elevator door 4 s opening time, $\Delta T=42$ °C, mass fraction of SF6 at z=1 m.....	73

Figure 83 Elevator door 4 s opening time, $\Delta T=42$ °C, velocity at $z=1$ .....	73
Figure 84 Elevator door, $\Delta T=42$ °C, mass of SF6 exchanged .....	74
Figure 85 Elevator door, $\Delta T=42$ °C, cumulative mass of SF6 exchanged .....	74
Figure 86 Elevator door, $\Delta T=42$ °C, Energy exchanged .....	75
Figure 87 Elevator door, $\Delta T=42$ °C, cumulative Energy exchanged .....	75
Figure 88 Elevator door, $\Delta T=42$ °C, mass of gasmixture exchanged .....	76
Figure 89 Elevator door, $\Delta T=42$ °C, cumulative mass of gasmixture exchanged .....	76
Figure 90 Thermal, Hinged 4s motion, u component of the velocity at $t=1,2,3, 4$ s.....	77
Figure 91 Thermal, Sliding 4s motion, u component of the velocity at $t=1,2,3, 4$ s.....	78
Figure 92 Thermal, Elevator 4s motion. u component of the velocity at $t=1,2,3, 4$ s .....	78
Figure 93 Thermal, Hinged 4s motion. Mass flux at $t=1,2,3, 4$ s .....	79
Figure 94 Thermal, Sliding 4s motion. Mass flux at $t=1,2,3, 4$ s .....	80
Figure 95 Thermal, Elevator 4s motion. Mass flux at $t=1,2,3, 4$ s .....	80
Figure 96 Thermal, Hinged 4s motion. Temperature at $t=1,2,3, 4$ s .....	81
Figure 97 Thermal, Sliding 4s motion. Temperature at $t=1,2,3, 4$ s .....	82
Figure 98 Thermal, Elevator 4s motion. Temperature at $t=1,2,3, 4$ s .....	82
Figure 99 Residuals hinged door 8 s opening time.....	95
Figure 100 Residuals sliding door 8 s opening time .....	95
Figure 101 Residuals sliding door 4 s opening time .....	96
Figure 102 Residuals Elevator door 4 s opening time .....	96
Figure 103 Residuals hinged door 4 s opening time, $\Delta T=42$ °C.....	96
Figure 104 Hinged flux of SF6 .....	104
Figure 105 Elevator.....	104
Figure 106 sliding flux of SF6 .....	105
Figure 107 Elevator thermal 4s motion. Flux of SF6 at the door opening at $t=1,2,3, 4$ s.....	106
Figure 108 sliding thermal.....	106
Figure 109 Hinged thermal.....	107
Figure 110 Elevator thermal 4s motion. Heat flux at the door opening at $t=1,2,3, 4$ s .....	107

Figure 111 sliding thermal ..... 108  
Figure 112 Hinged thermal ..... 108

# Appendices

# Appendix A Residuals

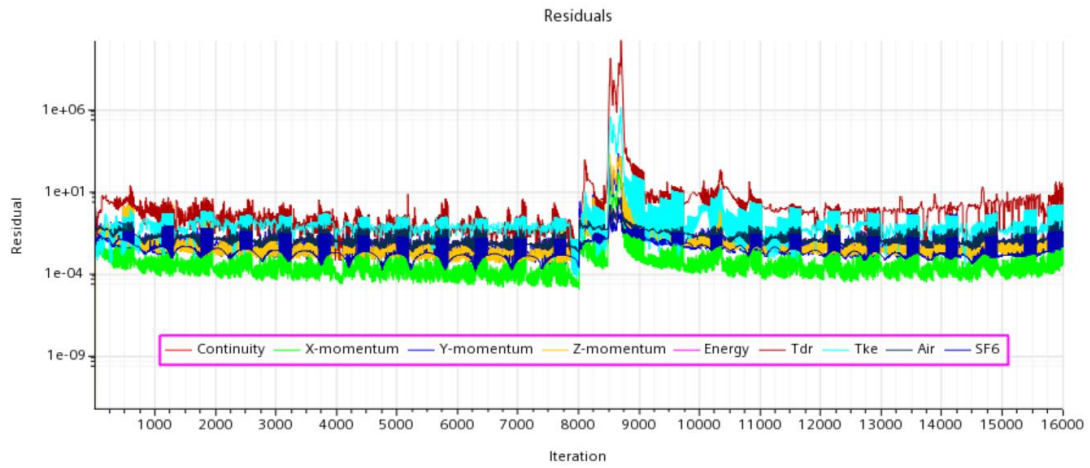


Figure 99 Residuals hinged door 8 s opening time

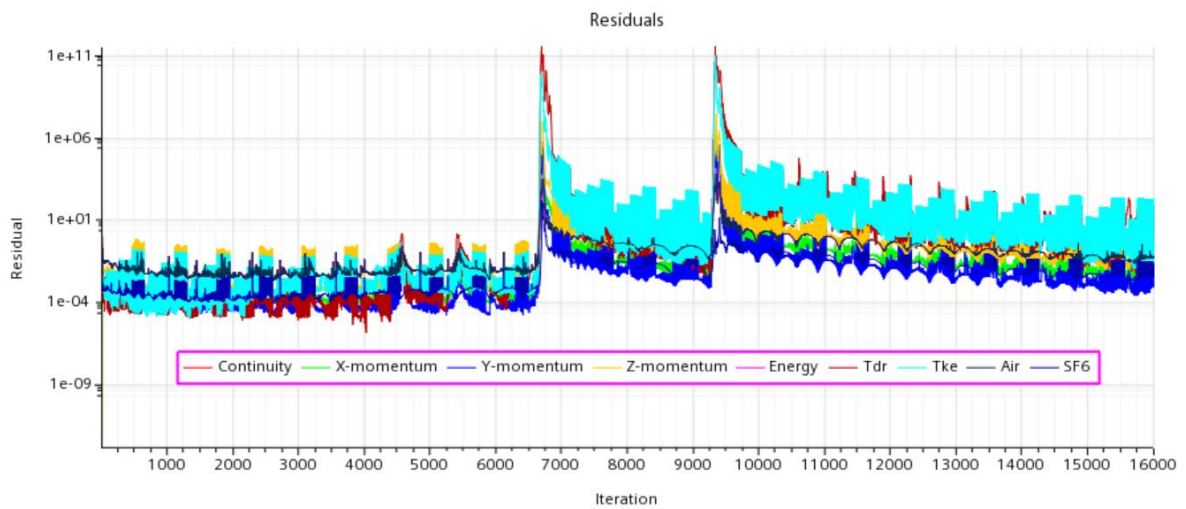


Figure 100 Residuals sliding door 8 s opening time

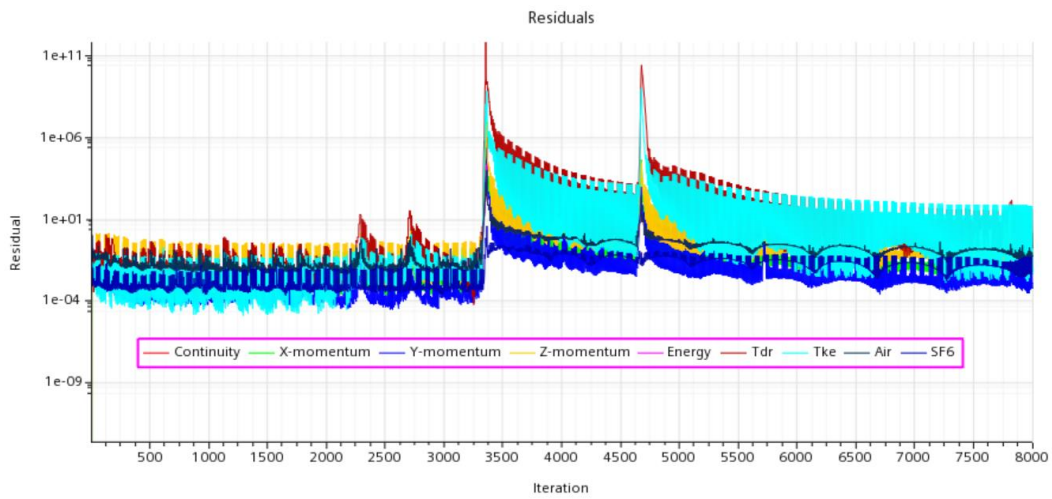


Figure 101 Residuals sliding door 4 s opening time

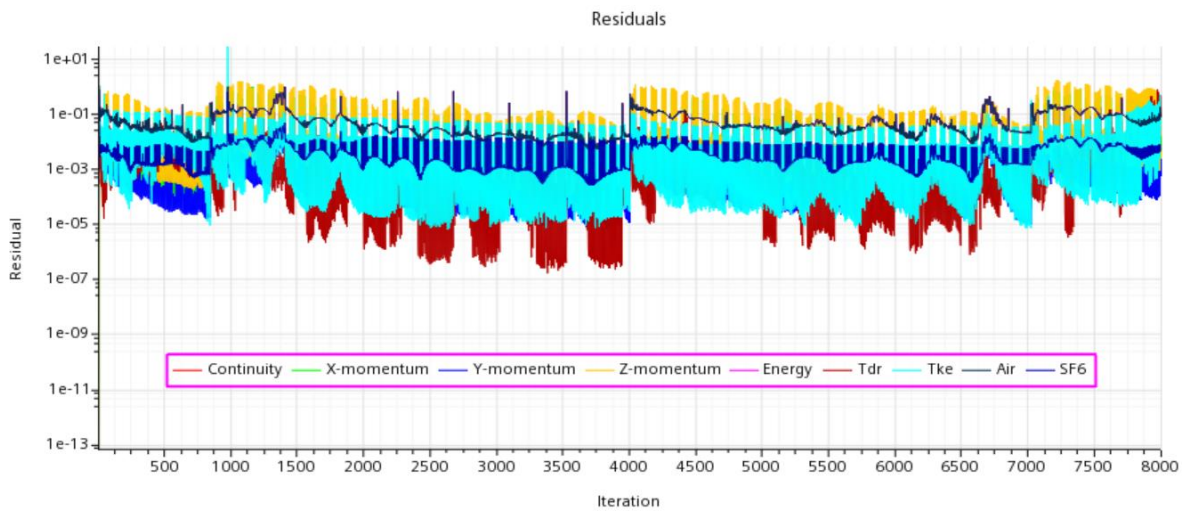


Figure 102 Residuals Elevator door 4 s opening time

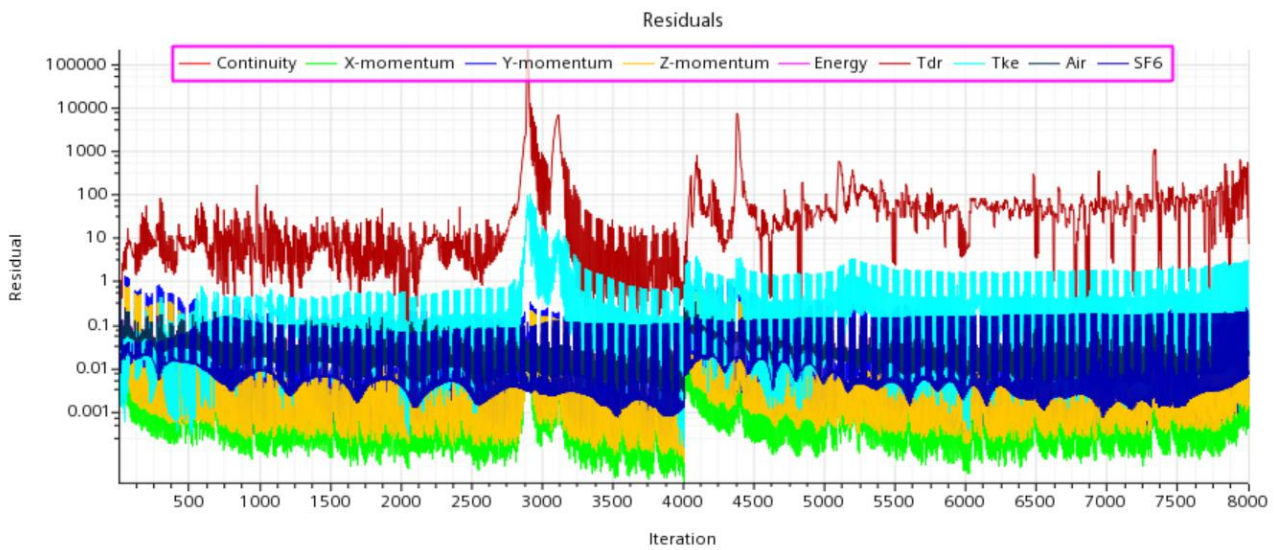


Figure 103 Residuals hinged door 4 s opening time,  $\Delta T=42\text{ }^{\circ}\text{C}$

## Appendix B Matlab

```
post_processing_script_headings.m x +
1 - clear all; close all; clc;
2
3 - dt = 0.005; % time step (s)
4 - dx = 0.04; % length of the presentation grid (m)
5 - dy = 0.04; % length of the presentation grid (m)
6 - A = dx * dy; %Area m^2 of the presentation grid
7 - % corresponding to each grid point
8
9 - n = 800; % Total number of files (800 timesteps for 4 s simulation)
10 - m = n+1;
11
12 - M = zeros(m,1);
13 - part1 = 'XYZ_Internal_Table_table_';
14 - part3 = '.csv';
15 - count = 1;
16
17
18 - for i = 1:n
19 -     part2 = num2str(i,'%d');
20 -     filename = [part1 part2 part3 ]
21 -     Data = readtable(filename);
22 -     mydata = table2array(Data);
23 -     mdot = A * mydata(:,1) .* mydata(:,2) .* mydata(:,3); %kg/s of SF6
24 -     totalm = mdot * dt; %kg of SF6
25 -     count = count + 1;
26 -     M(count) = sum(totalm)
27 - end
28
29 - figure
30 - plot(M);
31 - title('Mass of SF6 exchanged through the door opening ')
32 - xlabel('Time')
33 - ylabel('Mass of SF6 (kg)')
34 - %mass ;
35 - figure
36 - plot(cumsum(M));
37 - title('cumulative mass of SF6 exchanged')
38 - xlabel('Time')
39 - ylabel('Mass of SF6 (kg)')
40 - %cumulative mass;
```


Command Window  
fx >>



```

PPTThermal.m x +
1 - clear all; close all; clc;
2
3 - dt = 0.005; % time step (s)
4 - dx = 0.04; % length of the presentation grid (m)
5 - dy = 0.04; % length of the presentation grid (m)
6 - A = dx * dy; %Area m^2 of the presentation grid
7 - % corresponding to each grid point
8
9 - n = 800; % Total number of files
10 - m = n+1;
11
12 - E = zeros(m,1);
13 - Mmix = zeros(m,1);
14 - M = zeros(m,1);
15 - part1 = 'XYZ_Internal_Table_table_';
16 - part3 = '.csv';
17 - count = 1;
18 - cp = 1003.5 ; %J/kg*K
19
20
21 - for i = 1:n
22 -     part2 = num2str(i, '%d');
23 -     filename = [part1 part2 part3 ]
24 -     Data = readtable(filename);
25 -     mydata = table2array(Data);
26 -     mdot = A * mydata(:,1) .* mydata(:,2) .* mydata(:,3); %kg/s of SF6
27 -     totalm = mdot * dt; %kg of SF6
28 -     count = count + 1;
29 -     M(count) = sum(totalm);
30 -     totale = cp * A * mydata(:,2) .* mydata(:,3) .* mydata(:,6)* dt %joule
31 -     E(count) = sum(totale);
32 -     mdotmix = A * mydata(:,2) .* mydata(:,3); %kg/s of SF6
33 -     totalmmix = mdotmix * dt;
34 -     Mmix(count)=sum(totalmmix);
35 - end
36
37 - figure
38 - plot(M);
39 - title('Mass of SF6 exchanged through the door opening ')
40 - xlabel('Time')

```

Command Window  
 >>

```

pp_delaunay_door_Adiabatic.m x +
1 - clear all; close all; clc;
2
3
4 - n = 500;          % number of files|
5
6
7 - part1 = 'XYZ_Internal_Table_table_';
8 - part3 = '.csv';
9 - part2 = num2str(n, '%d');
10 - filename = [part1 part2 part3 ]
11 - Data = readtable(filename);
12 - mydata = table2array(Data);
13 - cp = 1003.5 ; %J/kg*K
14
15 - tri = delaunay([mydata(:,6), mydata(:,7)] );
16
17 % Mass fraction of SF6
18 - figure
19 - h = trisurf(tri, mydata(:,6), mydata(:,7),mydata(:,1));
20 - axis([-0.5 0.5 0 2]);
21 - view([0,90])
22 - colormap jet
23 - shading interp
24 - colorbar EastOutside
25 - title('Mass fraction of SF6 ')
26 - xlabel('Y(m)')
27 - ylabel('Z(m)')
28
29 % u component of the velocity
30 - figure
31 - h = trisurf(tri, mydata(:,6), mydata(:,7),mydata(:,2));
32 - axis([-0.5 0.5 0 2]);
33 - view([0,90])
34 - colormap jet
35 - shading interp
36 - colorbar EastOutside
37 - title('u component of the velocity ')
38 - xlabel('Y(m)')
39 - ylabel('Z(m)')
40

```

Command Window


**fx** >>

```

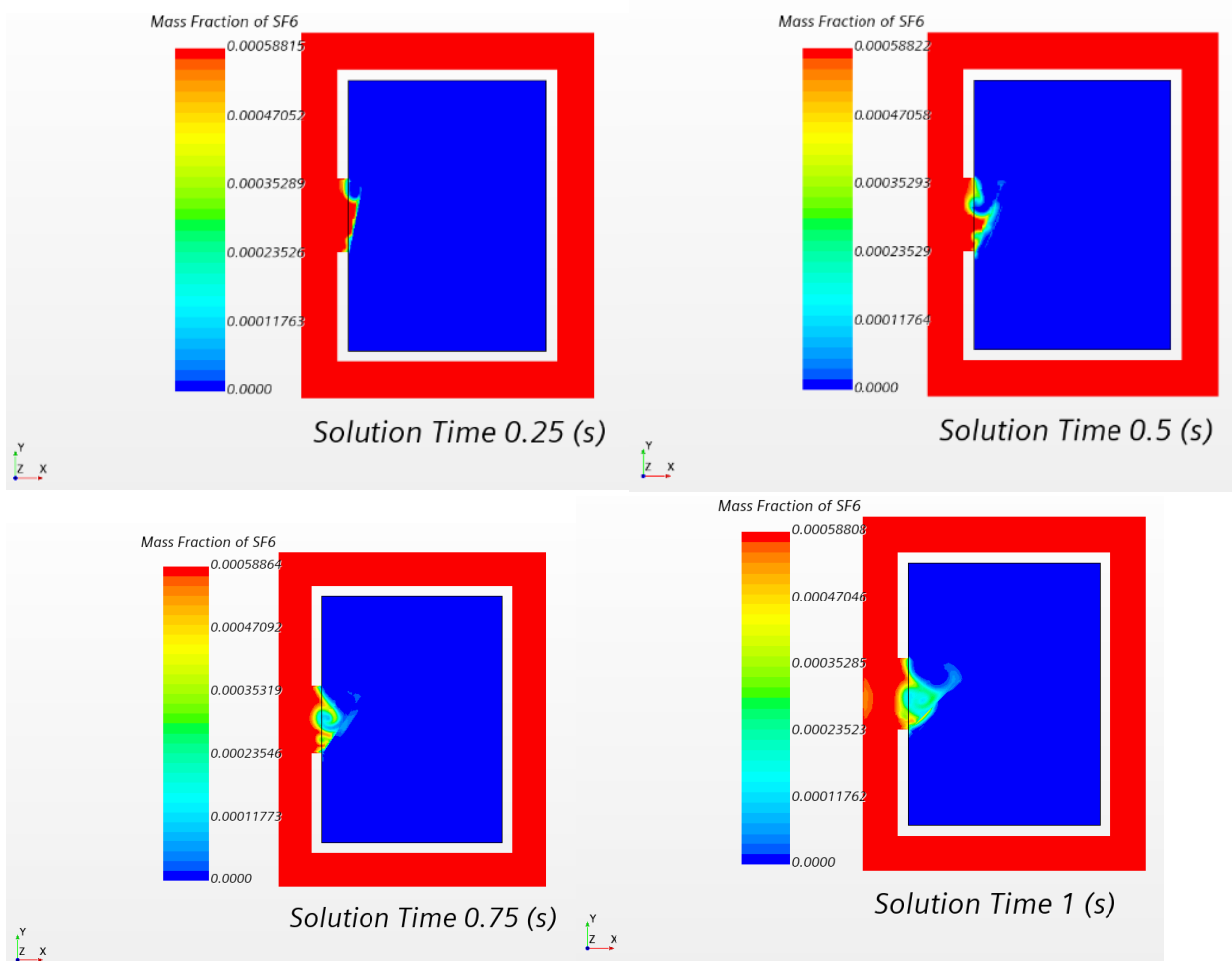
pp_delaunay_door_Temperatur.m x +
1 - clear all; close all; clc;
2
3
4 - n = 500;          % number of file
5
6
7 - part1 = 'XYZ_Internal_Table_table_';
8 - part3 = '.csv';
9 - part2 = num2str(n, '%d');
10 - filename = [part1 part2 part3 ]
11 - Data = readtable(filename);
12 - mydata = table2array(Data);
13 - cp = 1003.5 ; %J/kg*K
14
15
16
17 - tri = delaunay([mydata(:,8), mydata(:,9)] );
18
19 % Mass fraction of SF6
20 - figure
21 - h = trisurf(tri, mydata(:,8), mydata(:,9),mydata(:,1));
22 - axis([-0.5 0.5 0 2]);
23 - view([0,90])
24 - colormap jet
25 - shading interp
26 - colorbar EastOutside
27 - title('Mass fraction of SF6 ')
28 - xlabel('Y(m)')
29 - ylabel('Z(m)')
30
31 % u component of the velocity
32 - figure
33 - h = trisurf(tri, mydata(:,8), mydata(:,9),mydata(:,2));
34 - axis([-0.5 0.5 0 2]);
35 - view([0,90])
36 - colormap jet
37 - shading interp
38 - colorbar EastOutside
39 - title('u component of the velocity ')
40 - xlabel('Y(m)')
41 - ylabel('Z(m)')

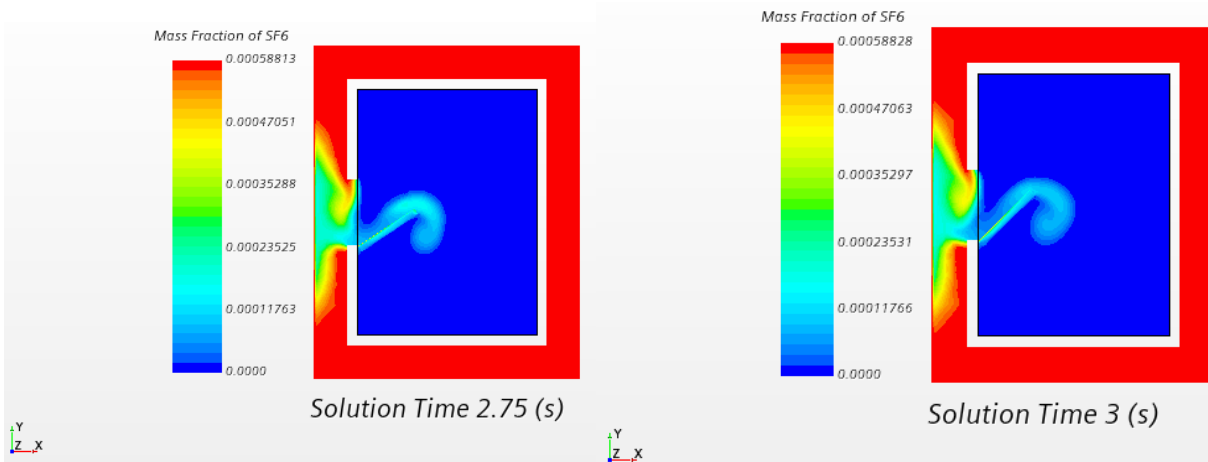
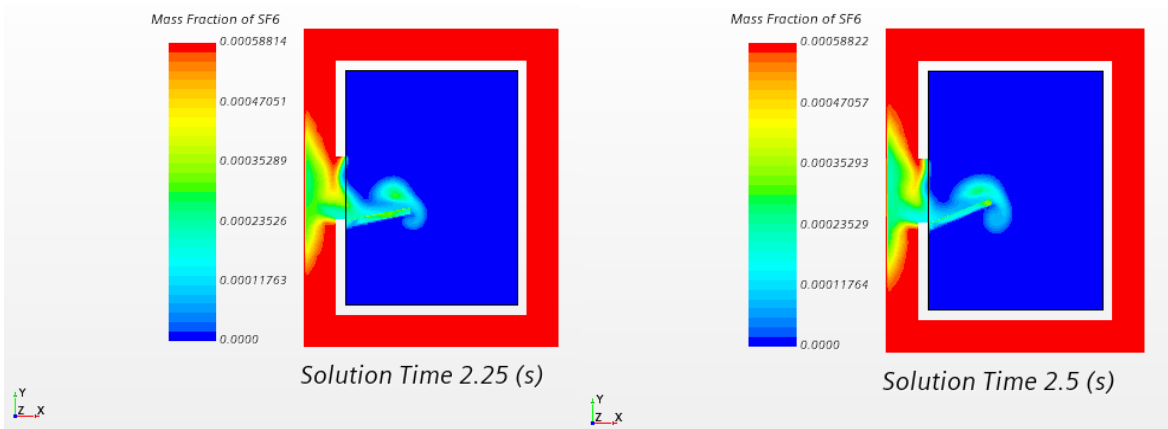
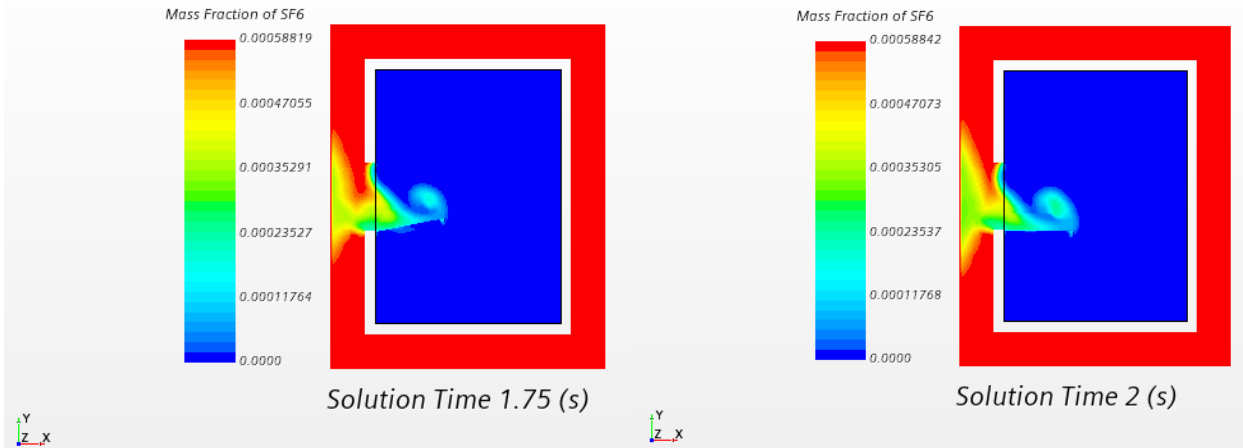
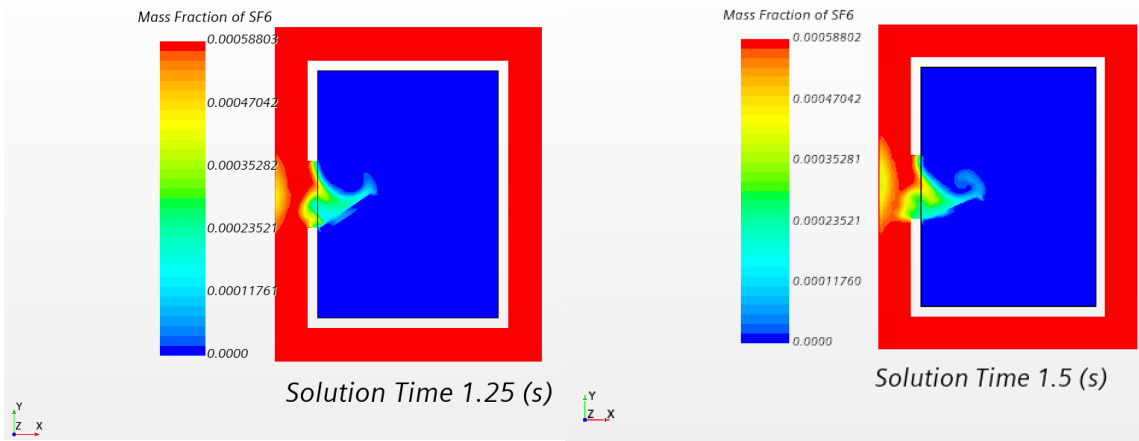
```

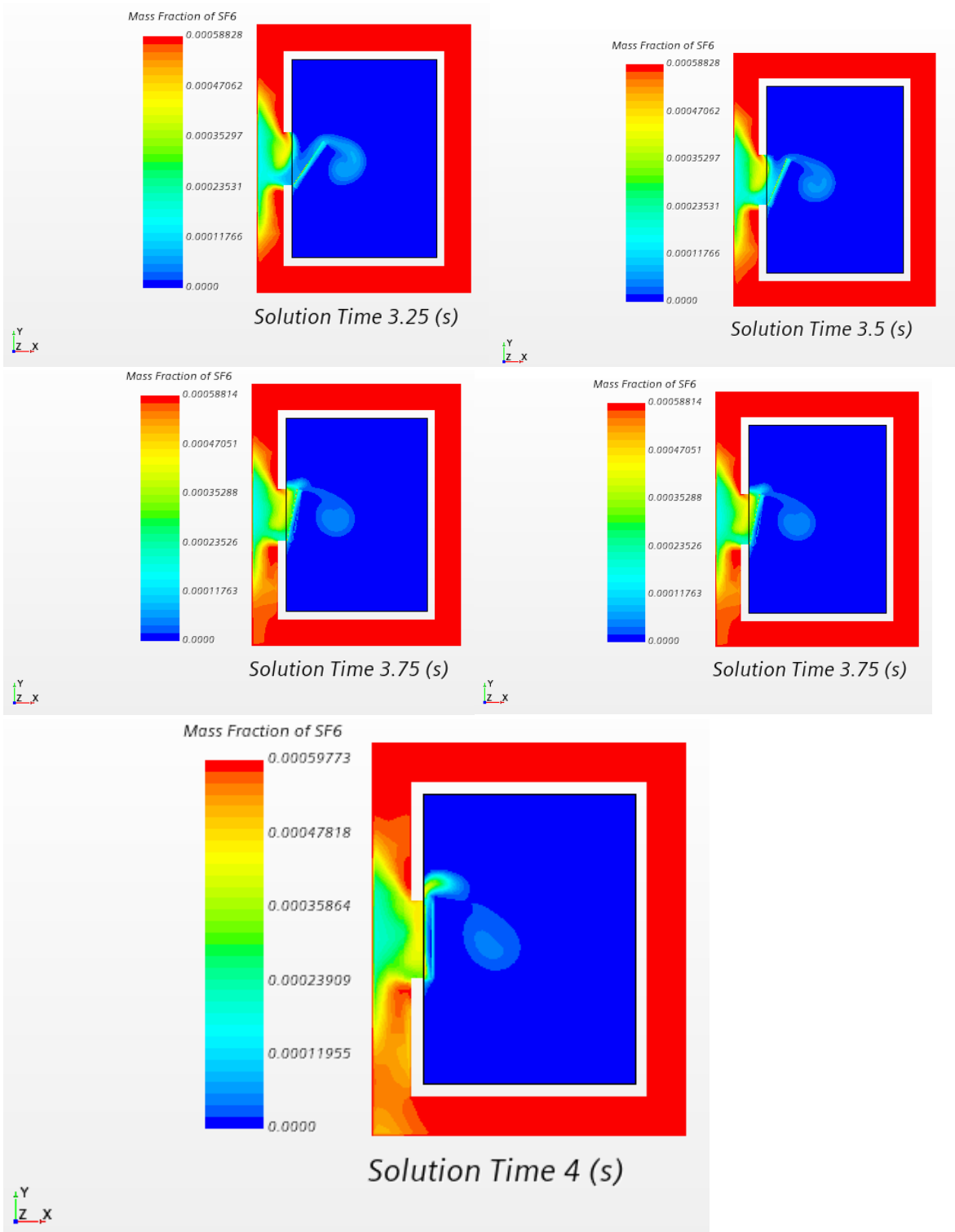
Command Window

 >>

## Appendix C Hinged 4s temperature







## Appendix D Flux of SF6 non thermal

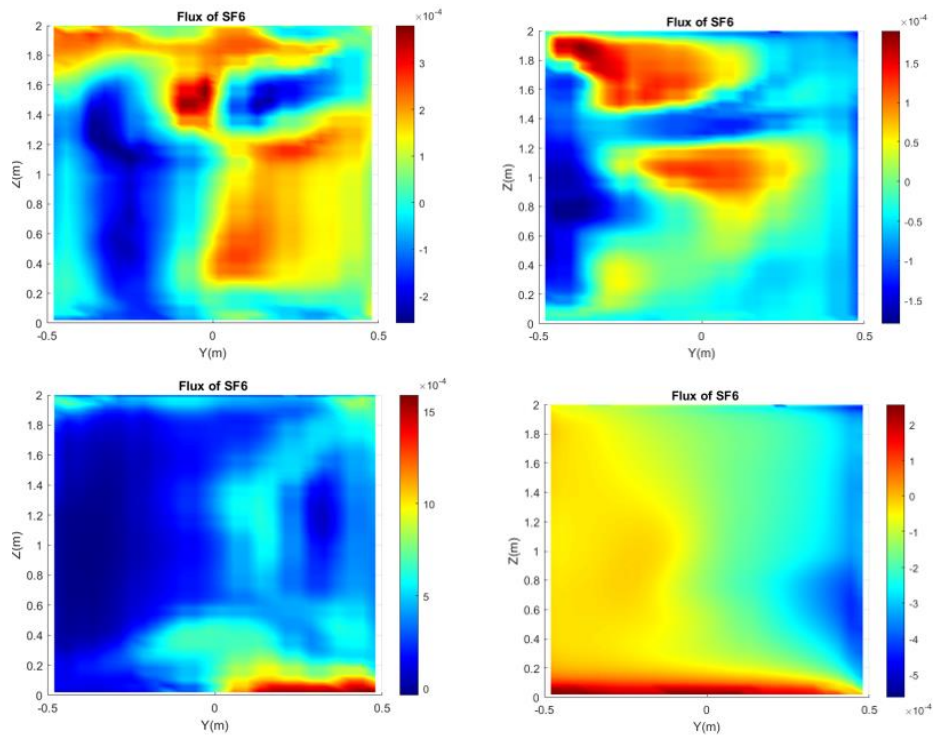


Figure 104 Hinged flux of SF6

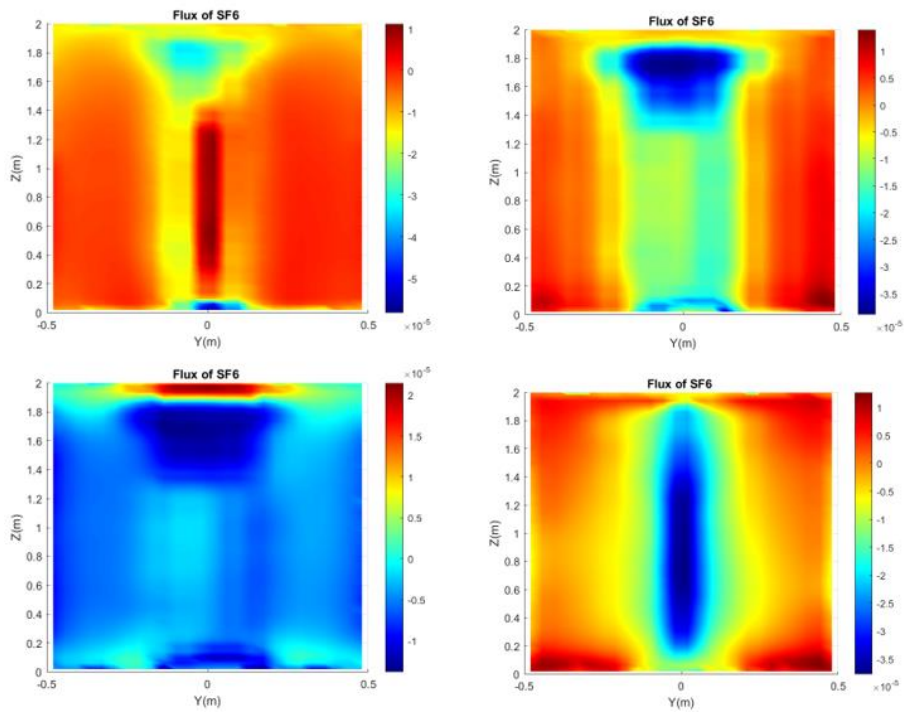


Figure 105 Elevator

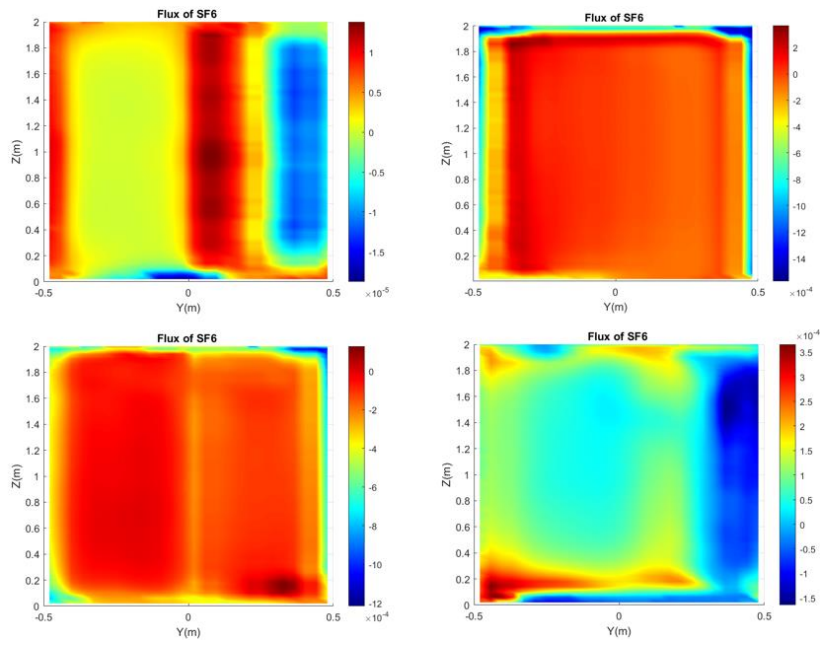


Figure 106 sliding flux of SF6



## Appendix E Thermal flux of SF6 and heat flux

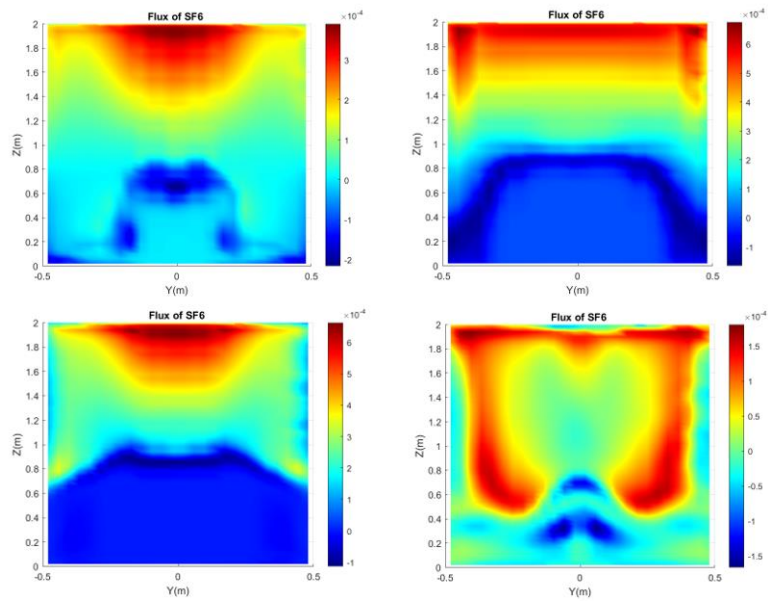


Figure 107 Elevator thermal 4s motion. Flux of SF6 at the door opening at t=1,2,3, 4 s

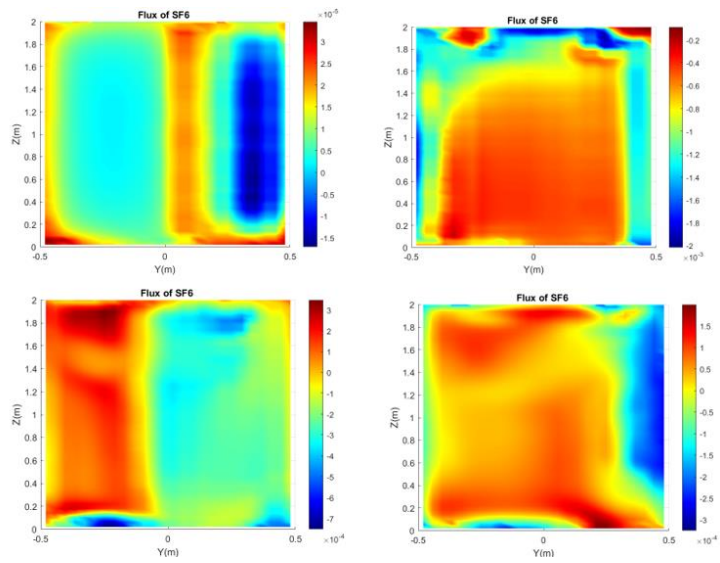


Figure 108 sliding thermal

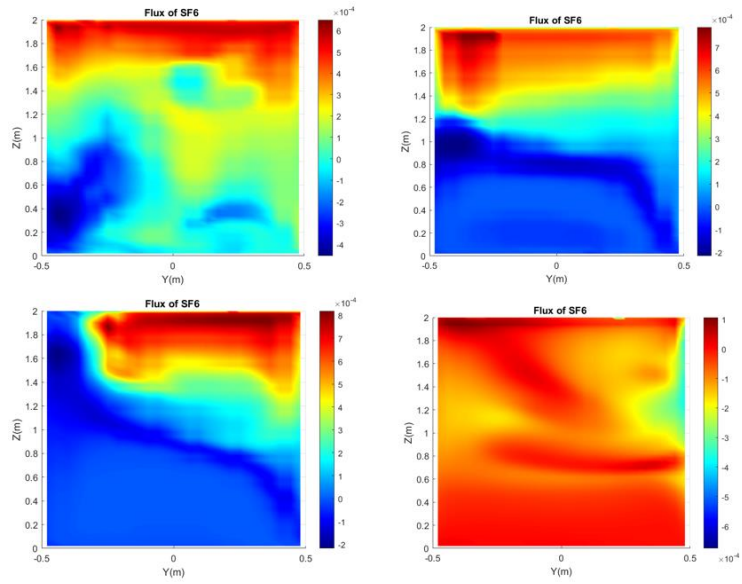


Figure 109 Hinged thermal

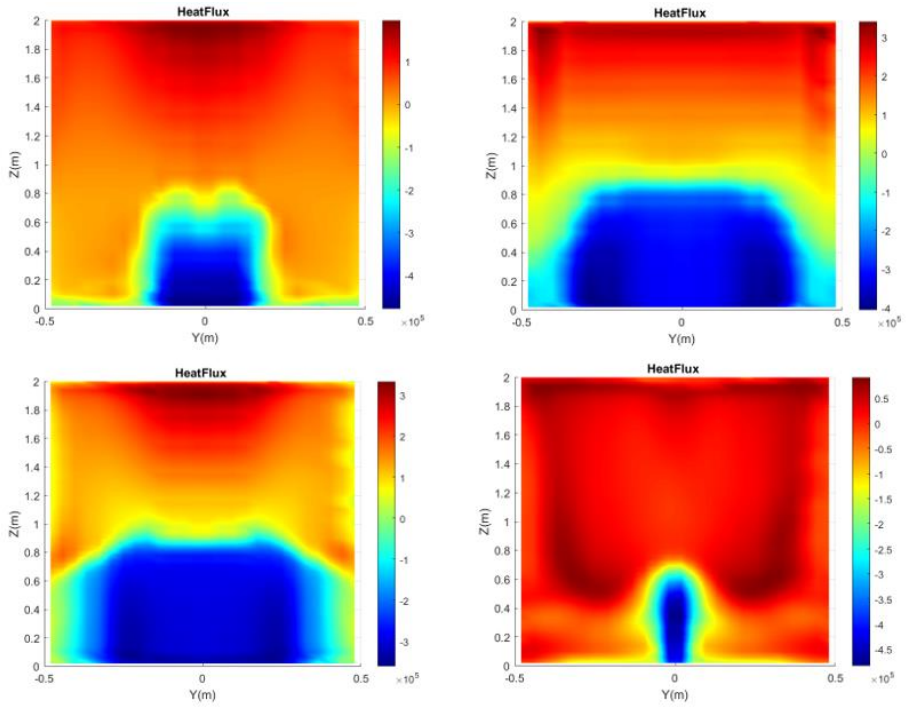


Figure 110 Elevator thermal 4s motion. Heat flux at the door opening at  $t=1,2,3,4$  s

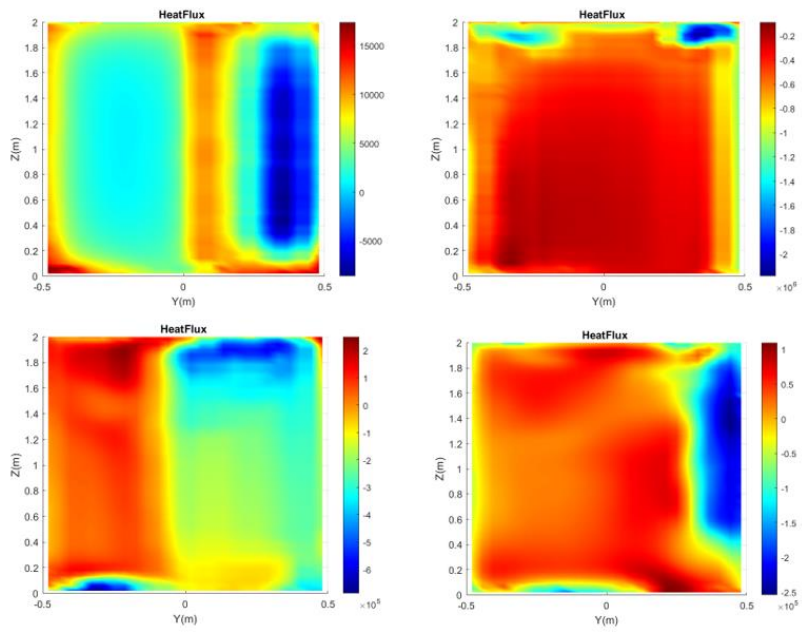


Figure 111 sliding thermal

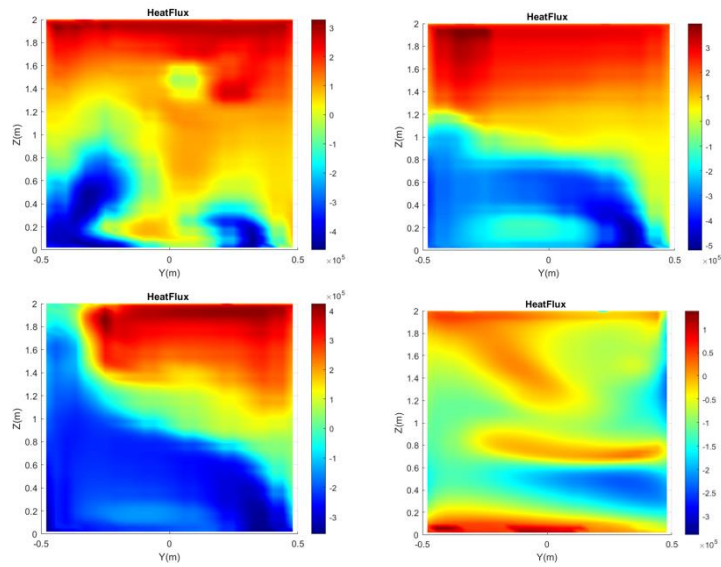


Figure 112 Hinged thermal

# Appendix F Excel

XYZ_Internal_Table_table_800.csv ☆									
	A	B	C	D	E	F	G	H	I
1	Mass Fraction of SF6	Velocity [i] (m/s)	Density (kg/m³)	Area: Magnitude (m²)	Pressure (Pa)	Temperature (K)	X (m)	Y (m)	Z (m)
2	0.000442143161737142	-0.359560257310086	1.24103960674368	1.79769313486232e+308	-37.9683776572543	284.434670275521	-1.5	0.48	0.02
3	0.000442143161737142	-0.359560257310086	1.24103960674368	1.79769313486232e+308	-37.9683776572543	284.434670275521	-1.5	0.4416	0.02
4	0.000469967311402207	-0.317256685205407	1.23125482441267	1.79769313486232e+308	-38.0269554927026	286.701304213769	-1.5	0.4032	0.02
5	0.000469544688155156	-0.331163499002682	1.23182181373954	1.79769313486232e+308	-38.0045569139967	286.569306087205	-1.5	0.3648	0.02
6	0.000485543060243275	-0.30263925511651	1.22630758612564	1.79769313486232e+308	-38.0467978825559	287.861469957358	-1.5	0.3264	0.02
7	0.000495986480850736	-0.28158191869271	1.22313298211404	1.79769313486232e+308	-38.0669458026617	288.610965393128	-1.5	0.288	0.02
8	0.000501055198654042	-0.264319303971428	1.22159746845852	1.79769313486232e+308	-38.0819764033665	288.974873085016	-1.5	0.2496	0.02
9	0.000501055198654042	-0.264319303971428	1.22159746845852	1.79769313486232e+308	-38.0819764033665	288.974873085016	-1.5	0.2112	0.02
10	0.000498111977993365	-0.254075522673241	1.22240662347243	1.79769313486232e+308	-38.0877868372107	288.782891978194	-1.5	0.1728	0.02
11	0.000483172413162391	-0.247348418026072	1.22675036146885	1.79769313486232e+308	-38.0899480675093	287.756901435232	-1.5	0.1344	0.02
12	0.000429778380570651	-0.193463356151403	1.2427250667669	1.79769313486232e+308	-37.9703456717983	284.046080379425	-1.5	0.096	0.02
13	0.000429778380570651	-0.193463356151403	1.2427250667669	1.79769313486232e+308	-37.9703456717983	284.046080379425	-1.5	0.0576	0.02
14	0.000382883736092202	-0.213415236643285	1.25731242143396	1.79769313486232e+308	-37.9801023850056	280.73998927657	-1.5	0.0192	0.02
15	0.00033796803538702	-0.245931077254896	1.27165408562066	1.79769313486232e+308	-37.9915179800799	277.56378605239	-1.5	-0.0192	0.02
16	0.000308907569509785	-0.285253764447125	1.28092182312391	1.79769313486232e+308	-38.0033550748869	275.549100544226	-1.5	-0.0576000000000001	0.02
17	0.000308907569509785	-0.285253764447125	1.28092182312391	1.79769313486232e+308	-38.0033550748869	275.549100544226	-1.5	-0.096	0.02
18	0.000279113991587596	-0.353693810420314	1.29153635385529	1.79769313486232e+308	-38.134687028039	273.277608782397	-1.5	-0.1344	0.02
19	0.000274273165133349	-0.376709469265109	1.29268215983327	1.79769313486232e+308	-38.1380969754464	273.034312296281	-1.5	-0.1728	0.02
20	0.000294175580206101	-0.372201228482121	1.28541676732714	1.79769313486232e+308	-38.144543939865	274.58191280157	-1.5	-0.2112	0.02
21	0.000294175580206101	-0.372201228482121	1.28541676732714	1.79769313486232e+308	-38.144543939865	274.58191280157	-1.5	-0.2496	0.02
22	0.000345734915367474	-0.333528489591815	1.26915110255812	1.79769313486232e+308	-38.1487959707598	278.112489600385	-1.5	-0.288	0.02
23	0.000422203921536254	-0.289770971341793	1.24626627977262	1.79769313486232e+308	-38.1457823764172	283.236764415147	-1.5	-0.3264	0.02
24	0.00049535307539607	-0.298493430336986	1.22523405480723	1.79769313486232e+308	-38.1406550441615	288.115689619285	-1.5	-0.3648	0.02
25	0.000503585899305605	-0.267030269422557	1.22194503760433	1.79769313486232e+308	-38.1559357161786	288.893052759335	-1.5	-0.4032	0.02
26	0.000545343489051733	-0.353618497279699	1.21009283258878	1.79769313486232e+308	-38.1642822258746	291.732349886979	-1.5	-0.4416	0.02

Thermal

XYZ_Internal_Table_table_800.csv							
	A	B	C	D	E	F	G
1	Mass Fraction of SF6	Velocity[i] (m/s)	Density (kg/m <sup>3</sup> )	Area: Magnitude (m <sup>2</sup> )	X (m)	Y (m)	Z (m)
2	0.000457708938263442	-0.192841129281103	1.19727772889463	1.79769313486232e+308	-1.5	0.48	1.18
3	0.000201404467489875	-0.363182816251287	1.19702858832237	1.79769313486232e+308	-1.5	0.4416	1.18
4	0.000108942150347624	-0.544347191255214	1.19693170919944	1.79769313486232e+308	-1.5	0.4032	1.18
5	0.000151012775050206	-0.466048713301847	1.19695898799274	1.79769313486232e+308	-1.5	0.3648	1.18
6	0.000150750555420404	-0.158343492321527	1.19695555753193	1.79769313486232e+308	-1.5	0.3264	1.18
7	0.000106610773739894	0.126970030489067	1.19692747454559	1.79769313486232e+308	-1.5	0.288	1.18
8	0.000176533701184699	0.225558585103219	1.19699667980045	1.79769313486232e+308	-1.5	0.2496	1.18
9	0.000453663104158822	-0.200113006648812	1.19727410601904	1.79769313486232e+308	-1.5	0.48	1.22
10	0.000195975915218179	-0.383897421210623	1.19702373025662	1.79769313486232e+308	-1.5	0.4416	1.22
11	0.000112849319057042	-0.578340900192606	1.19693413987802	1.79769313486232e+308	-1.5	0.4032	1.22
12	0.000161182389183816	-0.490804607121022	1.1969653198427	1.79769313486232e+308	-1.5	0.3648	1.22
13	0.00016024353765068	-0.165708389573741	1.19696104236224	1.79769313486232e+308	-1.5	0.3264	1.22
14	0.000106608703559602	0.133491453165368	1.19692601806359	1.79769313486232e+308	-1.5	0.288	1.22
15	0.000167475889266074	0.232983681454297	1.19698661254801	1.79769313486232e+308	-1.5	0.2496	1.22
16	0.000241291071056595	0.258927017457248	1.19706234238543	1.79769313486232e+308	-1.5	0.2112	1.22
17	0.000277322063086842	0.248748955138424	1.19710612794154	1.79769313486232e+308	-1.5	0.1728	1.22
18	0.000315984247737993	0.208887205730264	1.19714895779707	1.79769313486232e+308	-1.5	0.1344	1.22
19	0.000335037226077241	0.185078554878028	1.1971683092889	1.79769313486232e+308	-1.5	0.096	1.22
20	0.00038924741353621	0.103543574368977	1.19721890384707	1.79769313486232e+308	-1.5	0.0192	1.22
21	0.000419776485622664	0.0788574380680925	1.19724687972565	1.79769313486232e+308	-1.5	-0.0192	1.22
22	0.000464482156071604	0.0650567414128084	1.19728929733875	1.79769313486232e+308	-1.5	-0.0576000000000001	1.22
23	0.000449505109909807	-0.207898588642904	1.19727013132201	1.79769313486232e+308	-1.5	0.48	1.26
24	0.000198528883657386	-0.407915098258401	1.19702574400912	1.79769313486232e+308	-1.5	0.4416	1.26
25	0.000122325327880813	-0.602898074248245	1.19694065202904	1.79769313486232e+308	-1.5	0.4032	1.26
26	0.000172214824388341	-0.507922719134065	1.19697195556714	1.79769313486232e+308	-1.5	0.3648	1.26
27	0.000169474264241312	-0.169543060781312	1.19696625449953	1.79769313486232e+308	-1.5	0.3264	1.26
28	0.000106653005974316	0.143193887175705	1.19692446130307	1.79769313486232e+308	-1.5	0.288	1.26

Non thermal

## Appendix G Running time

name	timestep	inner iterations	mesh cellcount	processors	tot iterations	order discretization	physical time	solution time	time needed (8s)
Validation_case_proto	0.005s	10	848539	8 ( home pc)	400	2nd	12.10- 13.10 ca 1 h	0,2s	40 hours
Validation_case_proto_fin ermeshtest1.8	0.005s	10	1812256	8 ( home pc)	200	2nd	13.22- 14.22 ca 1 h	0,1s	80 hours
Validation_case_proto_fin ermeshtest1.8	0.005s	10	1323153	8 ( home pc)	200	2nd	14.35- 15.50 ca 1h 15 min	0,2s	50 hours
Validation_case_proto_5it erations	0.005s	5	848539	8 ( home pc)	100	2nd	16.05 - 16.20	0,1 s	20 hours
Validation_case_proto_1st	0.005s	10	848539	8 ( home pc)	200	1st	16.28- 16.55 ca 30min	0,1 s	<40 hours
Validation_case_proto	0.005s	10	848539	4 ( school pc)	400	2nd	12.10-13.30 1 h 20 min	0,2s	ca 53,2 hours
Validation_case_proto_fin ermeshtest1.8	0.005s	10	1812256	4 ( school pc)		2nd	13.40- 17.15	0,075s	ca 300 hours ...

